論文 / 著書情報
Article / Book Information

題目(和文)	
Title(English)	ANALYSIS OF STREAM TEMPERATURE AND HEAT TRANSPORT IN THE TAMA RIVER UNDER STRONG ANTHROPOGENIC INFLUENCES
著者(和文)	XinZhuohang
Author(English)	Zhuohang Xin
出典(和文)	学位:博士(工学), 学位授与機関:東京工業大学, 報告番号:甲第9644号, 授与年月日:2014年9月25日, 学位の種別:課程博士, 審査員:木内　豪,石川　忠晴,田村　哲郎,中村　恭志,浅輪　貴史
Citation(English)	Degree:Doctor (Engineering), Conferring organization: Tokyo Institute of Technology, Report number:甲第9644号, Conferred date:2014/9/25, Degree Type:Course doctor, Examiner:,,,,
学位種別(和文)	博士論文
Type(English)	Doctoral Thesis

ANALYSIS OF STREAM TEMPERATURE AND HEAT TRANSPORT IN THE TAMA RIVER UNDER STRONG ANTHROPOGENIC INFLUENCES

XIN Zhuohang

A dissertation submitted in partial fulfillment of the requirements for the Degree of Doctor of Philosophy in Engineering

Department of Environmental Science and Technology
Interdisciplinary Graduate School of Science and Engineering
Tokyo Institute of Technology

July 2014

Abstract

Water temperature is a key determinant in stream ecology, and changes in temperature can significantly alter fish distribution, growth, mortality, reproduction, and community dynamics. It is therefore important to have a better understanding of the thermal regime of rivers for effective river management and biological protection. For stream that runs through highly urbanized area, water temperature can be affected by complex interaction with diverse thermal inputs, including heat exchanges with atmosphere and with riverbed sediment as well as heat advections from tributary inflows, groundwater recharges/outflows and anthropogenic withdrawals/discharges.

This work studied the Tama River system, which is located in the east of Japan and has been a major river system running through the central Tokyo Metropolitan area. It originates from the western mountainous ranges and flows through the Ogochi reservoir that regulates the hydrologic and thermal regimes of the upper part of the river. In the middle and lower parts of the mainstream, the river water is suffering from considerable anthropogenic influences because of the high levels of urbanization. For example, eight wastewater treatment plants (WWTPs) are located in the middle and lower reaches of the river; a certain volume of water is also diverted from the river at several weirs for drinking, agriculture and industry purposes.

This study integrated data analysis, field measurement and modeling approach, and had a goal to provide insights of how human activities alter the stream temperature and heat budget of an urban river. Specifically, the aims of this study were: (1) to reveal the long-term and longitudinal temperature changes in the main stream of the Tama River; (2) to identify the major factors that influenced these past changes by water and heat budgets method considering different natural and anthropogenic processes; (3) to develop a physical model for predicting water temperature and the corresponding heat fluxes; (4) to apply this model to the mainstream of the Tama River, and (5) to quantify the impacts of each energy component and further provide scientific basis for ecological conservation.

Both long-term (1990 to 2013) and longitudinal (more than 50 km) changes in stream temperature were detected. To clarify the major influencing factors of these past trends, the stream flow rate changes, the temperature and volume of wastewater effluents as well as the relationships between air and stream temperature were investigated. Results suggested that the stream temperature increase in the winter season over the past 20 years is likely

attributable to the intensive and warm effluents from wastewater treatment plants located along the mainstream. In the upstream area, there are two weirs that withdraw relatively larger amounts of water from the stream for drinking and agriculture purposes, because of which, the flow rate downstream weirs was found greatly reduced. The low flow rate at this point was found to result in a larger increasing rate of the stream temperature in the summer season, under the joint effects from intense solar radiation.

Water and heat budget analyses were carried out to clarify the relative impacts from each heat component considering different hydrological conditions and levels of human impacts. Results indicated that the largest contributions to water and heat gains were attributable to wastewater effluents, while other factors such as groundwater recharge and water withdrawal were found to behave as energy sinks, especially in summer.

To predict the water temperature and quantify the underling physical processes, a 1-D deterministic model for river flow and heat transport in the main stream was developed. The model takes all necessary processes that significant in temperature modeling into account, including heat exchanges at the air-water and streambed-water interfaces and advective heat through tributary inflows and wastewater discharge. This model was calibrated using hydrological, meteorological and stream temperature data collected during the intensive periods in summer and winter seasons, and was verified by data obtained during a 2-year course field measurement. Results indicated a satisfactory agreement between the observed and simulated stream temperatures.

Further, this model was applied to simulate the changes in temperature that resulted from changes in controllable factors. The specific factors assessed in this study were wastewater discharges and surface-groundwater interactions. The existence of wastewater was found to contribute to suppress the stream warming in summer seasons; whereas in other colder seasons, it greatly enhanced the stream temperature at the downstream sites. Regardless of seasons, the interactions between surface and groundwater were found to behave as major energy sinks.

Finally, the methods and discussions in this study will provide insights for new studies concerning other urban rivers in the world. Specially, the findings on stream temperature variability in response to changes in natural and anthropogenic factors will provide biological implications towards better ecological protection.

Contents

Chapter 1
Introduction

1.1 Water temperature significances

Water temperature influences many physical, chemical and biological properties of streams and rivers. Changes in temperature can have a significant impact on fish distribution, growth, mortality, reproduction, and habitat use (Caissie, 2006). It is therefore important to understand the thermal regime of rivers for effective river water management and aquatic resources conversation.

Recent studies have concerned the temperature significances mainly from two aspects. On one hand, it affects a number of water quality parameters. The amount of oxygen that can be dissolved in water is partly governed by temperature. For example, gas solubility decreases and mineral solubility increases with increasing water temperature. As cold water can hold more oxygen than warm water, certain species of aquatic invertebrates and fish with high oxygen demands are found only in these waters. In addition, rates of chemical reaction as well as photosynthesis by algae and aquatic plants increase with the stream temperature increases, which can result in adequate amounts of nutrients (Ducharne, 2007). The toxicity of contaminants and the efficacy of water treatment, as well as taste and odor are also related to water temperature.

On the other hand, considerable interests have been shown in the influences of stream water temperature on aquatic organisms. In fact, most aquatic organisms, particularly fish, have specific temperature preferences (Billman et al., 2006). If the stream temperature rises above an upper threshold, biological processes such as growth or reproduction, or even survival itself, are expected to decline or cease (Eaton et al., 1995). Water temperature was found important for fish spawning (Preece and Jones, 2002), growth (Elliott and Hurley, 1997), movement (Jensen et al., 1998) and emergence (Elliott et al., 2000). Ojanguren et al. (2001) related the growth rate of brown trout to their living temperature by thermal performance curves, which exhibit a humped shape, with an optimal temperature associated with the maximum growth rate. In the Snake River basin (US), the emergence timing estimates for salmon within the upper and lower reach were found to differ by 13 to 75 days based on water temperatures of the river and shallow hyporheic zone locations (Hanrahan, 2007).

Recent studies have shown that the high water temperature, especially for streams dominated by cold-water fish species, can significantly influence the distribution, migration patterns, growth rate and even survival of fish species. The extremely high temperatures in summer were found to approach or exceed the tolerable limits for juvenile salmon (Eaton et al., 1995). Depending on its life stage, the larger Atlantic salmon died first under the high temperature conditions, followed by juvenile salmon and then parr (Huntsman, 1942). Chen et al. (1998) suggested that there is a need to restore the riparian vegetation along many headwater streams in the Upper Grande Ronde basin (U.S.), to alleviate the lethal and sublethal stream temperatures during hot days for conserving the salmon habitat. Several studies have noted that the high water temperatures are likely to force the aquatic species to change their behavior by seeking new thermal refuges and by changing their distributions (Caissie, 2006; Elliott, 2000; Torgersen et al., 1999). For example, Ebersole et al. (2001) demonstrated that salmonids tended to aggregate within small, but colder refuge spaces during the high temperature events. Similarly, Kaya et al. (1977) reported that trout within a geo-thermally heated stream at a temperature of 28.8°C, utilized the tributaries which possess a colder water temperature as refuges during the summer season. Therefore, cold water areas or patches are very essential for fish specifics. In addition to the adverse effects of extreme temperature on fish species, the high water temperature has also been found to result in the increase in biological rates and thus associated oxygen consumption, which can become more serious and problematic in rivers that have lower dissolved oxygen due to the high water temperature (Brown and Krygier, 1967).

Depending on its severity, the global warming could modify the thermal regimes of rivers and ultimately affect fish and other aquatic species as pointed out in recent studies (Rahel et al., 1996; Schindler, 2001). Sinokrot et al. (1995) applied a stream temperature model to quantify the impacts of the projected global climate scenario on stream habitats. Results indicated that this impact on stream temperature downstream dams will be more pronounced when the water release is from the reservoir surface rather than deep water. By studying 57 fish species in the U.S., Mohseni et al. (2003) have shown that the number of thermal habitat for cold water fishes could be reduced by 36% under the predicted climate change scenario

In addition to the surface temperature, the substratum water temperature can also influence fish habitat conditions (Crisp, 1990) as stream invertebrates and fish can usually be found in a variety of habitats within stream, including deep within the hyporheic zone. Caissie and Giberson (2003) monitored the surface and intragravel temperatures in

Catamaran Brook (Canada) and found that the intragravel temperatures were less fluctuated, and were lower in summer and higher in winter comparing to the surface water temperatures, suggesting a generally more stable thermal habitat in the substrate.

With these implications of the stream water temperature for biological conservation, it became clear that the thermal regime of rivers plays a fundamental role in the general health of river ecosystems and is therefore worthy of study and understanding. The scientific information will ultimately impel a more effective river water management and a better protection of aquatic resource.

1.2 Factors influencing stream temperature

Temperature of river water is highly dependent on various physical processes of heat energy added or lost to/from the watershed, and fluctuations of water temperature can occur naturally or a result of anthropogenic perturbations.

As illustrated in **Figure 1.1**, natural factors influencing stream temperature can generally be divided into four groups: (1) atmospheric conditions; (2) stream discharge; (3) topography; and (4) streambed (Caissie, 2006). It is recognized that the atmospheric drivers are among the most important factors, which primarily determines the heat exchanges at the air-surface water interface, i.e. solar or short-wave radiation, long-wave radiation, evaporative processes and convective transfer resulting from temperature differences between the stream and the atmosphere. Topography and geographical setting are also important because they can have an impact on the atmospheric conditions as well as the streambed heat transport. Stream flow rate, mostly a function of river hydraulics (e.g. inflows and outflows), mainly influences the heating and/or cooling capacity (volume of water) through mixing of water from various sources. Heat exchange at the water-streambed interface is mainly a function of geothermal heating/cooling through conduction and advective heat transfer through groundwater flows and hyporheic exchanges.

On the other hand, the thermal regime of rivers can also be affected by anthropogenic perturbations, such as climate change, deforestation, thermal effluents, alterations in river flows (water withdrawals/discharges due to irrigation, hydroelectric, etc.) and dam release.

Climate change has been identified as a primary source that causes aquatic disturbance or thermal pollution on a large to global scale in recent years (Caissie, 2006; Mohseni and Stefan, 2001). Data from Europe suggested that the warming of up to 1°C in mean river temperatures has occurred during the 20th century and the rising air temperatures may be

one of the multiple reasons that accounted for the elevated water temperature (Webb, 1996).

Zwieniecki and Newton (1999) studied 14 streams with riparian buffers (8.6 m to 30.5 m wide) in the western Oregon (US). In their study, a higher than normal warming trend in stream temperature was noted when the forest was removed. For stream segments in central Tokyo and its suburbs (Kinouchi et al., 2007), an increase of 0.11-0.21°C/year was recorded in stream temperature for winter and spring seasons between 1978 and 1998, which can be ascribed to the increases in anthropogenic heat input from urban wastewater. Hockey et al. (1982) employed a deterministic model to study the impact of water withdrawal on the surface temperature in the Hurunui River (New Zealand). They found that river water temperature exceeded critical values of 22 °C for over six hours at low flows. Provided that thermal stratification occurs, the water from deep-release reservoir is cooler in summer and warmer in winter than it would be without the reservoir (Webb and Walling, 1993). A long term study (Webb and Walling, 1997) in the U.K. over a 15-year period has revealed a considerable complexity (from day to day, month to month and year to year) in the thermal modification downstream of the reservoir. Therefore, because of the ecological significance of stream temperature, preventing or mitigating anthropogenic thermal degradation has become a common concern for river management and aquatic resource protection.

1.3 Recent advances in stream temperature modeling

Different models have been developed and applied to predict water temperature, which can be categorized into three groups: (1) regression models, (2) stochastic models and (3) deterministic models. Each type of model has its advantages and drawbacks with respect to a specific study.

1.3.1 Regression and stochastic models

Regression and stochastic models utilize the statistical techniques, in which the water temperature is related to the relevant input parameters, such as air temperature, solar radiation and stream flow rate. Mostly, these models have been applied on a daily, weekly or monthly basis (Crisp and Howson, 1982, Webb and Nobilis, 1997). For example, Webb et al. (2003) found that the nature relationship of water-air temperature became more sensitive and less scattered as the time base of data increased from hourly to weekly mean values. Further, by multiplying river flow into the regression analysis, the impact of

discharge in accounting for water temperature variation was isolated and was proved greater at shorter time-scales in larger catchments. Notably, regression and stochastic models are relatively simple and are very efficient in modeling water temperatures, especially for the study region where air temperature is recorded but other data are rarely available.

1.3.2 Deterministic models

Even though the regression and stochastic models are simple and require less data as input, they have the limitation of little explanation on the underling physical processes. In contrast, deterministic models are used to predict river water temperature using a mathematical representation of the underlying physics of heat exchange between the river and surrounding environment. The deterministic models have been applied extensively regarding a variety of problems and issues, such as natural conditions (Caissie, et al., 2007) and anthropogenic perturbations due to reservoirs (Lowney, 2000), deforestation (Chen, et al., 1998), water diversion (Hockey, et al., 1982; Sinokrot and Gulliver, 2000), wastewater effluent (Kinouchi and Jia, 2009) and climate change (Tung, et al., 2006).

The QUAL2K model can simulate temperature variations in the stream, but the flow is assumed steady, and the surface-groundwater interaction is not considered (Chapra, et al., 2006). Early modeling studies have relied on quantifying the energy fluxes at the air-water interface to predict water temperatures, whereas most recent studies have recognized the importance of water-streambed heat fluxes in modeling and an advection-dispersion equation is typically employed to model this process (Hebert et al., 2011; Hondzo and Stefan, 1994). Sinokrot and Stefan (1993) showed that the streambed heat flux is more important to consider when dealing with hourly stream temperature modeling. Evans et al. (1998) investigated river heat budgets with an emphasis on the streambed–water interaction. In their study, over 82% of the total energy transfers occurred at the air–water interface, with 15% at the streambed–water interface. Kim and Chapra (1997) coupled a 1D heat transport model with a simplified hydrodynamic model for unsteady flow. The former further integrated the heat transports in the surface water system and the diffusion in the sediment zone. A sensitivity analysis indicated that an error of approximately 8% in water temperature would arise as a result of the ignorance of sediment heat flux.

Many studies gave special concerns on the longitudinal variations in water temperature due to lateral inflows, e.g. tributary, wastewater and subsurface/groundwater flows, but with consideration in short-term durations (less than one month) or in a specific season of

the year. Chen et al. (1998) demonstrated the effects of riparian vegetation on stream temperature in the Upper Grande Ronde Basin (US), with primary emphasize on two summers during which the high water temperature was already reaching the upper lethal or sublethal limit for Salmon. Lowney (2000) simulated the water temperature downstream a reservoir in Sacramento River (US), taking tributary and groundwater flows into account. It was found that in the summer season, the steady reservoir discharge with relatively constant cooler temperatures, can result in remarkable diurnal variations in downstream temperatures compared to normal conditions. In an upland stream reach of Little Pine Creek (US), the subsurface flow was found on average an energy sink term, which in particular contributed to the heat budget at a magnitude even comparable to the shortwave radiation (Younus et al., 2000).

On the other hand, there are several studies that have looked at the changing nature of heat budget from a long-term prospect, e.g. more than an annual cycle. Webb and Zhang (2004) presented a perspective on temporal variation (during an annual cycle) of river heat budgets for four rivers that possessing different natural characteristics, i.e. moorland, deciduous, regulated, coniferous reaches (Devon, UK). Over their study period as a whole, the water temperature trend generally followed the net non-advective heat energy, whereas the unsatisfied agreements were attributable to the fact that the advective sources were not quantified and considered in their study. Benyahya et al. (2010) studied water temperature and corresponding heat fluxes in different seasons within one year. Moreover, Caissie et al. (2007) dealt with the modeling of river water temperature for two watercourses that possess different size and thermal characteristics (New Brunswick, Canada). The data accounted for model calibration and validation were relatively longer: from 1992 to 1999.

Although previous studies provided valuable perspectives on temporal and spatial variations in river water temperature and heat budgets, few have covered all the necessary natural and anthropogenic processes in modeling stream temperature. Besides, as reviewed above, most of them have limitations either by short-term duration, i.e. data collected in a specific season of the year, or by site-specific location that the water temperature varied only with time as a result of heat exchanges through air-water and streambed-water interface.

Therefore, the originality of the deterministic model used in this study lies in our design of the whole model system, which integrated the effects from atmosphere, wastewater, tributary and groundwater, etc. These are not easy to be found in other studies although the equations applied for explaining the processes might be conventional. Our model applied in

Chapters 3 and 4 takes all the processes that significant in modeling stream temperature into account. The longitudinal variations of water temperature and corresponding heat fluxes due to natural (i.e. heat exchanges at air-water and streambed-water interfaces and through tributary) and anthropogenic impacts (wastewater effluents) were considered. Additionally, the seasonal and diurnal variations of stream temperature were able to be investigated owing to the continuous field measurement throughout a 2-year cycle.

1.4 Study site

We studied the Tama River system, which is located in the east of Japan and has been a major river system running through the central Tokyo Metropolis (**Figure 1.2**). It has been officially classified as a first class river by the Japanese government. The 138 km of its mainstream originates from the western forested mountain ranges in Yamanashi Prefecture, and flows eastward through the Ogochi reservoir into Tokyo Bay. The Ogochi reservoir was created by the construction of Ogochi Dam as shown in **Figure 1.2**.

The total basin area spans 1240 km^2 with the upper portion of the watershed mostly in a forest and grass, whereas the middle and lower portions of the reach in a highly urbanized area. The forest and urban areas accounted for 60% and 22.5% of the watershed in 1991, and 59% and 28.9% in 2009, respectively. An example of land use distribution in 2009 is shown in **Figure 1.3**.

It was reported that decades ago, this river used to be very notorious in terms of its bad water quality as a result of anomalous discharge from residential, commercial and industrial sections (Tsutaya, 1970). Fortunately, this deteriorative situation was greatly improved owing to the establishment and expansion of sewer networks since 1970s. Even though the BOD concentration decreased in recent years (report of Ministry of Land, Infrastructure, Transport and Tourism, Kanto Regional Development Bureau) as illustrated in **Figure 1.4**, there are unseen problems remained, such as nutrients (e.g. nitrogen and phosphorus) and thermal pollution.

The study reach has two major features. On one hand, the hydrologic and thermal regimes of the upper parts of the mainstream are to some extent regulated by the Ogochi reservoir that locates in the most upstream ranges. Along the mainstream, there are several weirs that divert a certain volume of water for drinking, agriculture and industry purposes. In the middle and lower parts of the watershed, the high levels of urbanization as well as the high population density (3400 person/km^2) have resulted in considerable anthropogenic influences on the streams. For example, eight wastewater treatment plants (WWTPs) are

located in the middle and lower reaches of the river; this sewer network has gradually expanded from 78% coverage of the total population in 1990 to 99% in 2013. The banks of the stream are lined with parks and sports fields, making the river a popular recreation zone.

One the other hand, the alluvial reach of the Tama River is characterized by strong surface-groundwater interaction; therefore the stream thermal regime is greatly influenced by this process. This was further confirmed by our field observation that the sediment material comprises predominantly of coarse gravel and sand.

1.5 Fish assemblages in the Tama River

Changes in fish assemblages of the Tama River in recent years were characterized by three community parameters: fish species, distributions and individual numbers. These information were collected based on mark-recapture method and were available for one or two days in spring and autumn seasons from the Ministry of Land, Infrastructure, Transport and Tourism (MLIT), Japan.

Suffered from poor data availability, comparisons were made between the years 1995 and 2001 at 14 stations along the mainstream (**Figure 1.5**). The selection of fish species for analysis was based on the following two aspects: (1) native and exotic species, and (2) cold water (<19 °C), cool water (19-25 °C) and warm water (>25 °C) species.

As shown in **Figure 1.5 (a)** and **(b)**, Ayu (genus: Plecoglossus) and Gin-buna (Cyprinidae) are both native species that widely existed in the domestic Japanese rivers. The former prefers a cooler water environment from 15 °C to 25 °C, whereas Gin-buna can tolerate a wider temperature range from 0 °C to 30 °C. Although these two species were detected in both years, the individual numbers were found to decrease in 2001 compared to 1995. Besides, it should be noted that the distribution of habitat spread throughout the river from the upstream to downstream areas in 1995, whereas in the year 2001, it narrowed and congregated in the middle and lower reaches.

An example of exotic species was presented in **Figure 1.5 (c)**, showing the distributions and individual numbers for rainbow trout (cool water fish) and tilapia (warm water fish). Notably, they were both newly detected in the year 2001 with nothing recorded in 1995. The advent of exotic species in more recent years was probably due to the alteration of water environment which benefited their spawning, growth and propagation.

On the contrary, as illustrated in **Figure 1.5 (d)**, some cold water species (e.g. seema and cottus pollux) were found to disappear in 2001 compared to the large numbers recorded in

1995. In particular, they showed a significant spatial distribution preference on the upstream region, i.e. from 44 km to 62 km, which was probably in response to the cooler upstream water temperature in spring and autumn seasons.

Moreover, the numbers of total fish species that detected in the Tama River were reported at 77 and 71 for the years 1995 and 2001, respectively, with 38 species in common. Although it may be not sufficient to conclude from the intensive surveys in two years, the findings of advent of exotic species and changes in behaviors of native species can somewhat reflect the transformation of their living environment, such as the changes of water temperature, water quality, habitat structure, hydrology condition and geomorphology. For this reason, further studies are needed to quantify the impacts of water environment changes on biological behaviors.

1.6 Purpose and structure of this study

In general, river water temperature is a very determinant variable in ecological studies, and changes in temperature can significantly modify the distribution, growth rate, mortality, reproduction, habitat of aquatic life. With the implications of the stream water temperature for biological conservation, it became clear that the thermal regime of rivers plays a determinant role in stream ecology and is therefore worthy of study and understanding. This study integrated data analysis, field measurement and modeling approach, and had a goal to provide insights of how human activities alter the stream temperature and heat budget of an urban river.

The contents of this study have been divided into 5 chapters outlined as below.

Chapter 1 includes the general background, introduction of the study site, and outline of the thesis.

Chapter 2 revealed the long-term (from 1990 to 2013) and longitudinal (more than 50 km) variations of stream temperature in the mainstream of the Tama River. Regarding these past changes, different types of natural and anthropogenic processes, i.e. atmosphere, wastewater effluents, dam release and water withdrawals, were analyzed and discussed. Water and heat budgets analysis were also conducted to quantify the contribution from each energy component.

Chapter 3 introduced a 1D deterministic model for simulating unsteady river flow and heat transports interacted with the atmosphere, sediment and anthropogenic process by wastewater effluents. This model was applied to the middle to downstream reach of the Tama River and was calibrated using the detailed data collected during intensive field

measurements in summer and winter seasons. In addition, the accuracy and reliability of historical analysis introduced in Chapter 2 were verified by conducting the present-day field measurements.

Chapter 4 dealt with the modeling of stream temperature throughout a 2-year course by applying the 1D physical model introduced in Chapter 3. Observed data on weather conditions, stream temperature and hydrodynamic variables were used to run and to verify the model. With satisfactory simulation results obtained, this model was further applied to assess the impacts of wastewater and surface-groundwater interactions on stream temperature, thereby providing implications for ecosystem conservation in our study reach.

Chapter 5 summarized this thesis and suggested several points that could be improved in the further study.

Although the analysis and discussion in this thesis focused on the Tama River, Japan, the basic ideas and approaches are applicable to other urban rivers that have similar characteristics to the Tama River in general.

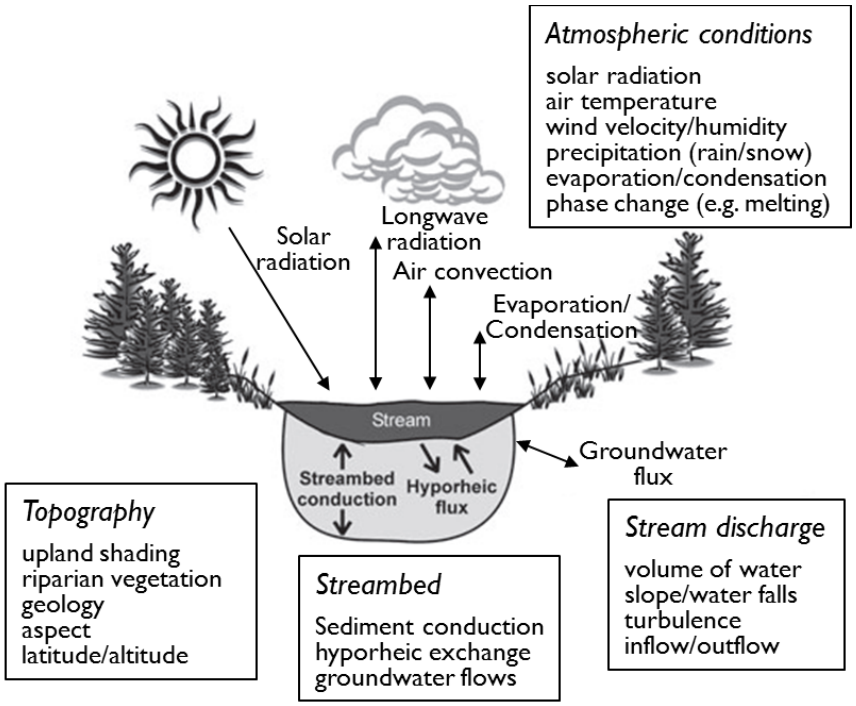

Figure 1.1 Natural processes responsible for variability in water temperature.

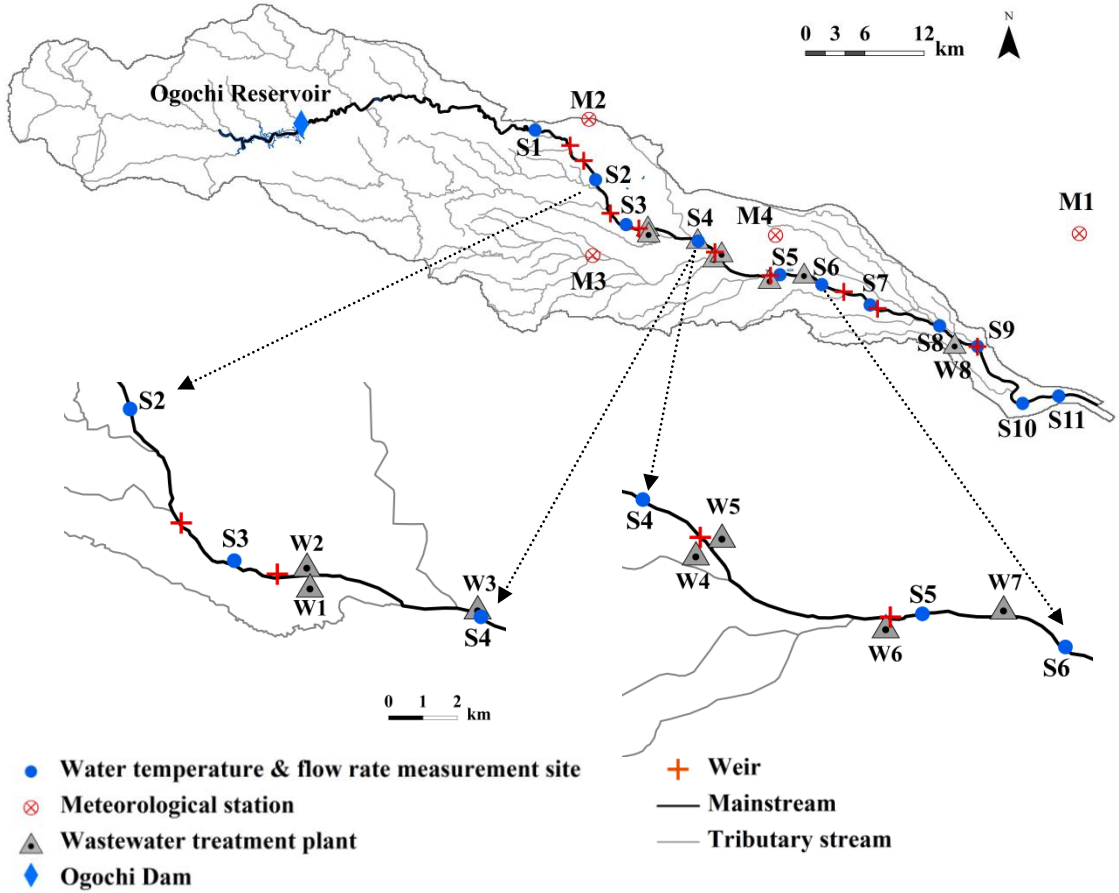

Figure 1.2 Study map showing the Tama River system, mainstream, tributary stream and locations of Ogochi reservoir, stream flow and temperature measurements, wastewater treatment plant and weir.

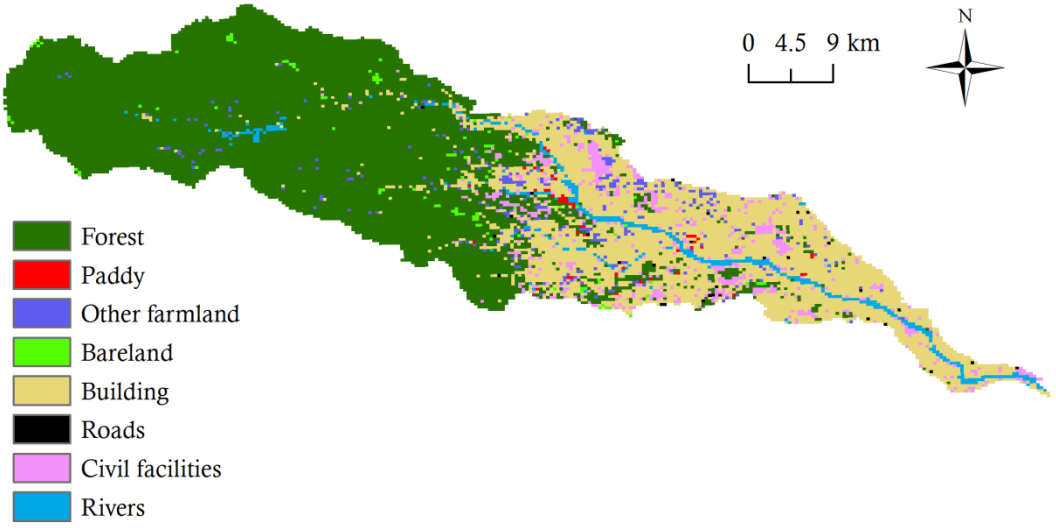

Figure 1.3 Land use distribution in the Tama River Watershed (2009).

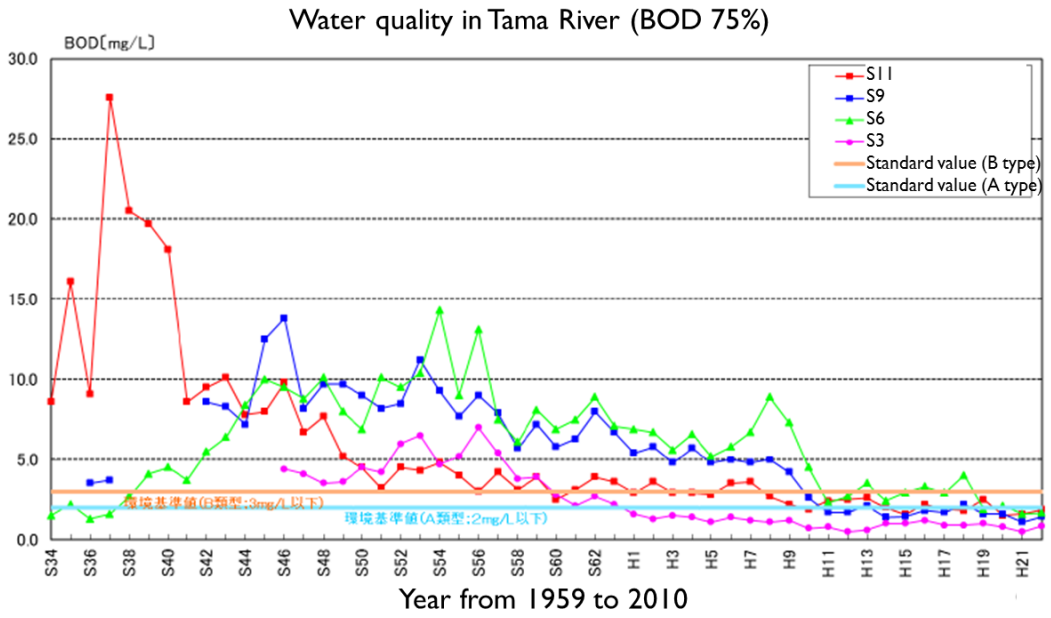

Figure 1.4 Water quality (BOD 75%) changes from 1959 to 2010 at S3, S6, S9 and S11 (see Figure 1.2 for site information)

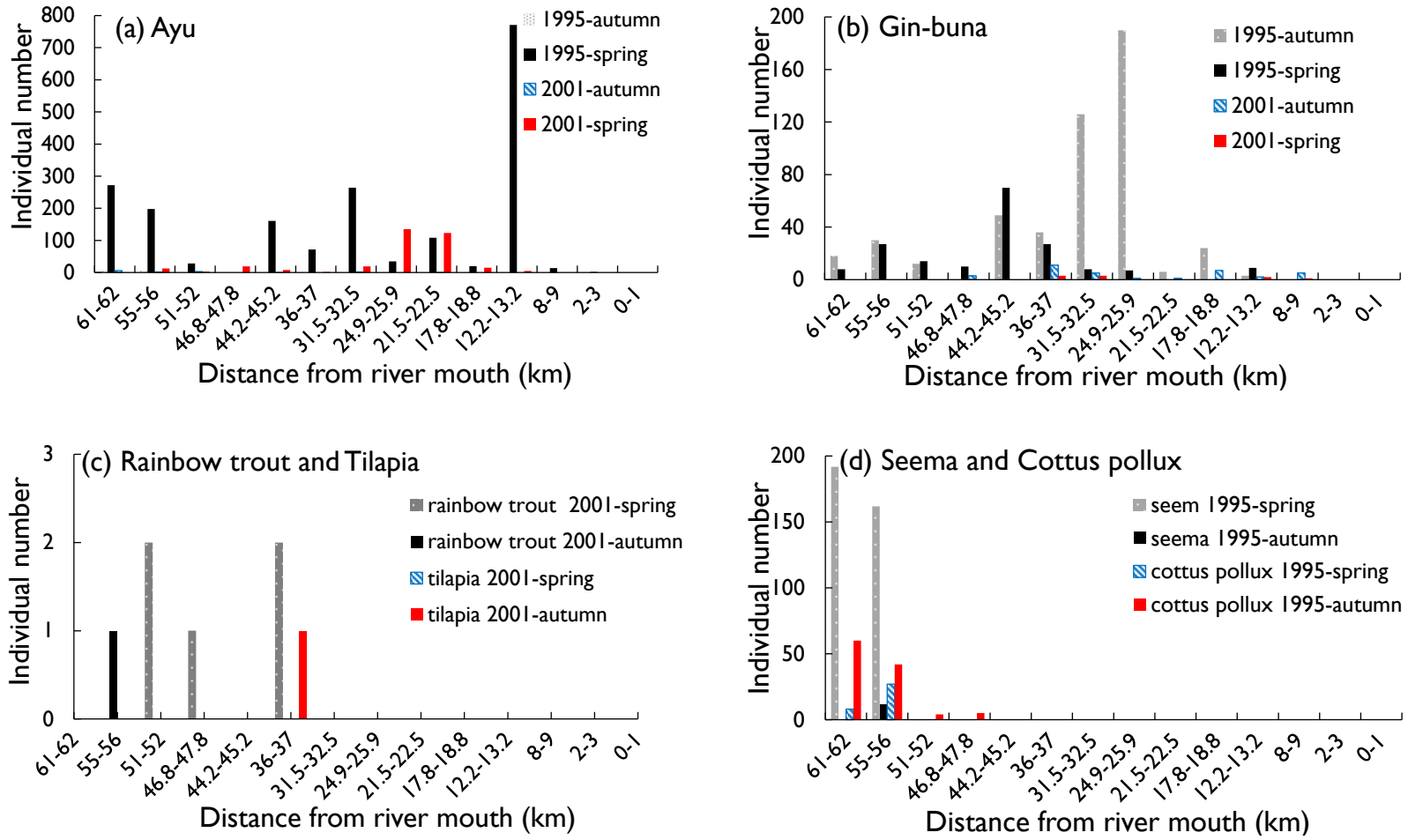

Figure 1.5 Distributions and individual numbers for six selected fish species along the main stream of the Tama River in 1995 and 2001.

References

Arnell, N.W., 2004. Climate-change impacts on river flows in Britain: the UKCIP02 scenarios. Water and Environment Journal, 18, 112–117.

Benyahya, L., Caissie, D., EI-Jabi, N., Satish, M.G., 2010. Comparison of microclimate vs. remote meteorological data and results applied to a water temperature model (Miramichi River, Canada). Journal of Hydrology, 380, 247-259.

Billman, E.J., Wagner, E.J., Arndt, R.E., 2006. Effects of temperature on the survival and growth of age-0 least chub (iotichthys phlegethontis). Western North American Naturalist, 66, 434-440.

Brown G.W., Krygier J.T., 1967. Changing water temperatures in small mountain streams, Journal of Soil and Water Conservation, 22, 242–244.

Caissie, D., 2006. The thermal regime of river: a review, Freshwater Biology, 51, 1389-1406.

Caissie, D., Giberson, D.J., 2003. Temporal variation of stream and intragravel water temperatures in an Atlantic salmon (Salmo salar) spawning area in Catamaran Brook (New Brunswick). Canadian Technical Report of Fisheries and Aquatic Sciences, 2464, 26 p.

Caissie, D., Satish, M.G., EI-Jabi, N., 2007. Predicting water temperatures using a deterministic model: application on Miramichi River catchments (New Brunswick, Canada). Journal of Hydrology, 336, 303-315.

Chapra, S.C., Pelletier, G.J., Tao, H., 2006. QUAL2K: A modeling framework for simulating river and stream water quality, version 2.04: Documentation and Users Manual. Civil and Environmental Engineering Department, Tufts University, Medford, MA.

Chen Y.D., McCutcheon S.C., Norton D.J., and Nutter W.L., 1998. Stream temperature simulation of forested riparian areas: 2. Model application. ASCE, Journal of Environmental Engineering, 124, 316–328.

Cunjak, R.A., Caissie, D., EI-Jabi, N., Hardie, P., Conlon, J.H., Pollock, T.L., Giverson, D.J. Komadina-Douth-wright, S., 1993. The Catamaran Brook habitat research project: biological, physical and chemical conditions. Canadian Technical Report of Fisheries and Aquatic Sciences, 1914, 81p.

Crisp, D.T., 1990. Water temperature in a stream gravel bed and implication for salmonid incubation. Freshwater Biology, 23, 601–612.

Crisp, D.T., Howson, G., 1982. Effect of air temperature upon mean water temperature in streams in the north Pennines and English Lake District. Freshwater Biology, 12, 359-367.

Ducharne, A., 2007. Importance of stream temperature to climate change impact on water quality, Hydrology and Earth System Sciences Discussions, 2425-2460.

Durance, I., Ormerod, S.J., 2007. Climate change effects on upland stream macroinvertebrates over a 25-year period. Global Change Biology, 13, 942–957.

Eaton, J.G., McCormick, J.H., Goodno, B.E., Obrien, D.G., Stefany, H.G., Hondzo, M., Scheller, R.M., 1995. A field Information-Based System for estimating fish temperature tolerances. Fisheries, 20, 10-18.

Eaton, J.G., McCormick, J.H., Stefan, H.G., Hondzo, M., 1995. Extreme value analysis of a fish/temperature field database. Ecological Engineering, 4, 289-305.

Eaton, J.G., Scheller, R.M., 1996. Effects of climate warming on fish thermal habitat in streams of the United States. Limnology and Oceanography, 41, 1109–1115.

Ebersole, J.L., Liss, W.J. and Frissell, C.A., 2001. Relationship between stream temperature, thermal refugia and rainbow trout Oncorhynchus mykiss abundance in arid-land streams in the northwestern United States. Ecology of Freshwater Fish, 10, 1-10.

Elliott, J.M., Hurleym, M.A., 1997. A functional model for maximum growth of Atlantic salmon parr, Salmo salar, from two populations in northwest England, Functional Ecology, 11, 592-603.

Elliott J.M., Hurley M.A., Maberly S.C., 2000. The emergence period of sea trout fry in a Lake District stream correlates with the North Atlantic Oscillation. Journal of Fish Biology, 56, 208–210.

Evans, E.C., McGregor, G.R., Petts, G.E., 1998. River energy budgets with special reference to river bed processes. Hydrological Processes, 12, 575–595.

Hanrahan, T.P., 2007. Large-scale spatial variability of riverbed temperature gradients in Snake River fall Chinook salmon spawning areas. River Research and Application, 23, 323-341.

Hembre, B., Arnekleiv J.V., L'Abe´e-Lund J.H, 2001. Effects of water discharge and temperature on the seaward migration of anadromous brown trout, Salmo trutta, smolts. Ecology of Freshwater Fish, 10, 61–64.

Hebert, C., Cassie, D., Satish, M.G., EI-Jabi, N., 2011. Study of stream temperature dynamics and corresponding heat fluxes within Miramichi River catchments (New Brunswick, Canada). Hydrological Processes, 25, 2439-2455.

Hockey, J.B., Owens, I.F., Tapper, N.J., 1982. Empirical and theoretical models to isolate the effect of discharge on summer water temperatures in the Hurunui River. Journal of Hydrology (New Zealand), 21, 1–12.

Hondzo, M., Stefan, H.G., 1994. Riverbed heat conduction prediction. Water Resources Research, 30, 1503-1513.

Huntsman, A.G., 1942. Death of salmon and trout with high temperature. Journal of the Fisheries Research Board of Canada, 5, 485-501.

Jensen, A.J., Hvidsten, N.A., Johnsen, B.O., 1998. Effects of temperature and flow on the upstream migration of adult salmon in two Norwegian Rivers. In: Fish Migration and Fish Bypasses. Fishing New Books, Oxford.

Kim, K.S., Chapra, S.C., 1997. Temperature model for highly transient shallow streams. ASCE, Journal of Hydraulic Engineering, 123, 30-40.

Kinouchi, T., Jia, Y.W., 2009. Hydrologic cycle and heat transport modeling and its application to the Kanda River watershed, Tokyo. Journal of Hydroscience and Hydraulic Engineering, 27, 121-137.

Kaya C.M., Kaeding L.R., Burkhalter D.E., 1977. Use of a cold-water refuge by rainbow and brown trout in a geothermally heated stream. The Progressive Fish-Culturist, 39, 37–39.

Kinouchi, T., Yagi, H., Miyamato, M., 2007. Increase in stream temperature related to anthropogenic heat input from urban wastewater. Journal of Hydrology, 335, 78-88.

Lowney, C.L., 2000. Stream temperature variation in regulated rivers: evidence for a spatial pattern in daily minimum and maximum magnitudes, Water Resources Research, 36, 2947-2955.

Lund, S.G., Caissie, D., Cunjak, R.A., Vijayan, M.M., Tufts, B.L., 2002. The effects of environmental heat stress on heat-shock mRNA and protein expression in Miramichi Atlantic salmon parr. Canadian Journal of Fisheries and Aquatic Sciences, 59, 1553-1562.

Mohseni O., Stefan H.G., 2001. Water budgets of two watersheds in different climatic zones under projected climate warming. Climate Change, 49, 77–104.

Mohseni, O., Stefan, H.G. Eaton, J.G., 2003. Global warming and potential changes in fish habitat in U.S. streams. Climatic Change, 59, 389-409.

Ojanguren, A.F., Reyes-Gavilan, F.G., Brana, F., 2001. Thermal sensitivity of growth, food intake and activity of juvenile brown trout. Journal of Thermal Biology, 26, 165-170.

Preece, R.M., Jones, H.A., 2002. The effect of keepit dam on the temperature regime of the Namoi River, Australia. River Research and Application, 18, 397-414.

Rahel, F.G., Keleher, C.J., Anderson, J.L., 1996. Potential habitat loss and population fragmentation for cold water fish in the North Platte River Drainage of the Rocky Mountains: response to climate warming. Limnology and Oceanography, 41, 1116–1123.

Schindler D.W., 2001. The cumulative effects of climate warming and other human stresses on Canadian freshwaters in the new millennium. Canadian Journal of Fisheries and Aquatic Sciences, 58, 18–29.

Sinokrot, B.A., Gulliver, J.S., 2000. In-stream flow impact on river water temperatures. Journal of Hydraulic Research, 38, 339–349.

Sinokrot, B.A., Stefan, H.G., McCormick, J.H. and Eaton, J.G., 1995. Modeling of climate change effects on stream temperatures and fish habitats below dams and near groundwater inputs. Climatic Change, 30, 181-200.

Sinokrot, B.A., Stefan, H.G., 1993. Stream temperature dynamics: measurements and modeling. Water Resources Research, 29, 2299-2312.

Torgersen, C.E., Price, D.M., Li, H.W. and McIntosh, B.A., 1999. Multiscale thermal refuge and stream habitat associations of Chinook salmon in Northeastern Oregon, Ecological Applications, 9, 301-319.

Tsutaya, T., 1970. Surveys on the Tama River. Journal of Water and Waste, 12, 46-60 (in Japanese).

Tung, C.P., Lee, T.Y., Yang, Y.C., 2006. Modeling climate-change impacts on stream temperature of Formosan landlocked salmon habitat. Hydrological Processes, 20, 1629-1649.

Webb B.W., 1996. Trends in stream and water temperatures. Hydrological Processes, 10, 205–226.

Webb, B.W., Clack, P.D., Walling, D.E., 2003. Water-air temperature relationships in a Devon river system and the role of flow. Hydrological Processes, 17, 3069–3084.

Webb, B.W., Nobilis, F., 1997. A long-term perspective on the nature of the air-water temperature relationship: a case study. Hydrological Processes, 11, 137-147.

Webb, B.W., Walling, D.E., 1993. Temporal variability in the impact of river regulation on thermal regime and some biological implications. Freshwater Biology, 29, 167–182.

Webb, B.W., Walling, D.E., 1997. Complex summer water temperature behaviour below a UK regulating reservoir. Regulated Rivers: Research and Management, 13, 463–477.

Webb, B.W., Zhang, Y., 2004. Intra-annual variability in the non-advective heat energy budget of Devon streams and rivers. Hydrological Processes, 18, 2117-2146.

Younus, M., Hondzo, M., Engel, B.A., 2000. Stream temperature dynamics in upland agricultural watersheds. Journal of Environmental Engineering, 126, 518-526.

Zwieniecki, M.A., Newton, M., 1999. Influence of streamside cover and stream features on temperature trends in forested streams of Western Oregon. Western Journal of Applied Forestry, 14, 106–113.

Chapter 2
Historical Analysis on Stream Temperature and Heat Budgets

2.1 Review and purpose

The temperature of river water is fundamentally dependent on both natural and anthropogenic energy exchange processes. Natural processes include heat exchanges across the water surface and streambed, as well as heat advection from tributaries and groundwater flows. Several studies have quantified and predicted stream temperature behavior, with particular emphasis on heat exchanges across the water surface and streambed (Caissie et al., 2007; Hebert et al., 2011; Sinokrot and Stefan, 1994; Webb and Zhang, 1997). The relative contributions of each natural process such as solar radiation, net longwave radiation, latent and sensible heat fluxes, streambed heat conduction and advective fluxes have been analyzed. Webb and Zhang (1999) demonstrated that heat budget was dominated by radiative fluxes in the River Piddle tributary and the River Bere (both in UK), which accounted on average for close to 90% of the non-advective heat gain in both the summer and winter seasons. Evans et al. (1998) investigated river heat budgets with an emphasis on the streambed–water interaction. In their study, over 82% of the total energy transfers occurred at the air–water interface, with 15% at the streambed–water interface.

Recent studies regarding stream temperature give particular attention to how human impacts may alter stream and river temperatures (Webb et al., 2008). Kinouchi et al. (2007) found that the stream temperatures increased in winter and early spring at a rate of 0.11–0.21°C/year in the Tokyo area, with the increase being attributed to the thermal effluents of urban wastewater. Prats et al. (2010) showed that the reservoir release and thermal effluent of a nuclear power plant resulted in an increase of 2.3°C of the mean annual water temperature in the lower reach of Ebro River, Spain. Other anthropogenic factors that affect stream temperature have been studied including water diversions (Sinokrot and Gulliver, 2000), regional land-use alteration (LeBlanc et al., 1997; Malcolm et al., 2008) and climate change (Mohseni et al., 1999; Tung et al., 2006).

Although previous studies have investigated the various gains and losses of energy by analyzing the heat budget, few have actually analyzed the long-term and longitudinal changes in stream temperatures and heat budgets for an urban river considering different

types of natural and anthropogenic effects.

Therefore, the main purpose of this chapter is three fold.

Firstly, we revealed both the long-term (from 1990 to 2013) and longitudinal (more than 50 km) temperature changes in the mainstream of the Tama River.

Secondly, to identify the major factors that influenced these changes, we analyzed the flow rate changes, the temperature and volume of wastewater effluents from WWTPs, as well as the relationships between air and stream temperatures.

Thirdly, we conducted the water and heat budget analysis to quantify the important processes that determine the temperature regime.

2.2 Data source

To analyze long-term and longitudinal stream temperature variations and heat budgets in the mainstream, data on stream temperatures and flow rates, wastewater effluents and meteorological conditions, were utilized in this chapter. Stream temperatures and flow rates have been measured at 11 sites (hereafter S1 through S11) and 9 sites (S1 through S9), respectively (**Figure 1.2**). These data consist of monthly measurement records, which were taken two to four times for water temperature and once for flow rate on a particular day each month and are available for the period between 1990 and 2013 from the Ministry of Land, Infrastructure and Transport, Japan. The information relating to effluents from WWTPs (i.e. monthly total discharge volumes from 1990 to 2013 and monthly mean effluent temperatures from 1993 to 2013) was provided by the Bureau of Sewerage, Tokyo Metropolitan Government. The monthly mean of dam-released water temperatures for the periods from 1990 to 1995 and 2005 to 2010 were available from the Annual Management Report of Ogochi Reservoir published by the Bureau of Sewerage, Tokyo Metropolitan Government. Data for annual total population and coverage of sewer networks were from the Bureau of Waterworks, Tokyo Metropolitan Government.

We obtained meteorological conditions such as air temperature, global shortwave radiation, sunshine duration, atmospheric pressure, wind velocity and relative humidity on an hourly basis from the Japan Meteorological Agency. The exact locations of the meteorological stations are shown in **Figure 1.2**. Although M1 (Tokyo) is located several kilometers away from the river we studied, it is the closest station that measures shortwave radiation, atmospheric pressure and relative humidity. Other stations, such as M2 (Ome), M3 (Hachioji) and M4 (Fuchu), were accordingly used to obtain data of air temperature, wind velocity and sunshine duration for the nearby stream segments.

2.3 Stream temperature changes and influencing factors

2.3.1 Stream flow rate and temperature

We conventionally divided one year into four seasons: spring is from March to June, summer is from July to September, autumn is from October to November and winter is from December to February in the next year. In historical analysis, particular emphasize has been given on summer and winter seasons as they are considered to be more representative of the extreme hydrological and thermal conditions.

Along the mainstream of the Tama River, stream flow rate and temperature have been measured at 9 sites and 11 sites, respectively. **Figures 2.1 and 2.2** illustrate the 2 to 6- year averages of monthly flow rate and temperature measured under normal flow conditions at each monitoring site. The site-average values of σ/μ (σ and μ represent the standard deviation and average of monthly measured flow rates (**Figure 2.1**) or stream temperatures (**Figure 2.2**), respectively) are also included, which range from 0.18 to 0.42 for flow rate and 0.07 to 0.27 for stream temperature.

In both summer and winter seasons, an abrupt decrease in stream flow was observed between S1 and S2 due to water withdrawals for agriculture and drinking water, which then recovered due to the addition of wastewater effluents and tributary inflows. In the summer season, stream temperatures of the Hurunui River (New Zealand) and Devon River (UK) were found to be more sensitive to heat inputs by shortwave radiation during low flows (Hockey et al., 1982; Webb et al., 2003). Therefore, the decrease in flow rate at this time can strongly affect the stream temperature as the flow generally becomes shallow and the heat capacity is reduced when the flow rate is low. Although the evidence is not clear from **Figure 2.2 (a)**, the averaged stream temperature changes, per unit distance, between S1 and S2 and between S2 and S3 were 0.32 °C/k and 0.40 °C/km, respectively, from which we concluded that the stream water was heated more in segment S2–3 due to the lower flow rate than in segment S1–2.

In the summer season, no apparent long-term trend in temperature was observed (**Figure 2.2 (a)**). However, significant stream temperature changes at both temporal and spatial scales were detected in the winter season (**Figure 2.2 (b)**). In the most recent periods (2006–2010 and 2010–2013), stream temperatures were much higher than those for preceding periods at S4 through S11. The average temperatures (at S4 through S11) were 9.8 °C, 10.8 °C, 10.6 °C, 12.3 °C and 12.0 °C during the periods 1990–1995, 1996–2000,

2001–2005, 2006–2010 and 2011–2013, respectively. Temperature increases were particularly significant at S4, with the maximum difference reaching 4.2 °C between the periods of 1990 to 1995 and 2011 to 2013. Compared to the temperatures at S4 through S11, no obvious temporal changes could be observed at S1 through S3 during the study period, which was likely to be attributable to the absence of wastewater inputs and fewer changes in the land use conditions.

The longitudinal change in stream temperature in winter was characterized by almost constant temperature at S1 through S3, a continuous increase between S3 and S6, with the highest temperature recorded at S6, and a slight decrease at the further downstream sites (S7–S11). In particular, the average increase of 4.3 °C recorded between S3 and S4 was extremely large and occurred over a short distance, which likely occurred because three WWTPs are located in between S3 and S4. At the upstream sites (S1 through S3), unlike the summer season, stream temperatures were relatively stable in the direction of flow even when the flow rate decreased considerably.

2.3.2 Effluents from wastewater treatment plants

Identifying the major factors that generate the marked stream temperature variations in the winter season is of great importance, at both the temporal and spatial scales. Because a large part of the Tama River runs through highly urbanized areas, the volume and temperature of effluents from WWTPs were compared over time to reveal any trend of anthropogenic influences on stream temperature. Among the eight WWTPs (W1–W8) distributed along the mainstream (**Figure 1.2**), W1–W3 and W4–W7 are located between S3 and S4, and S4 and S6, respectively. **Figure 2.3** illustrates the total annual volume and the average temperature of effluents from the WWTPs, and indicates an overall increasing trend of effluent temperature in winter months. Moreover, the increasing volume of effluents from W1 to W3 and W4 to W7 are also relevant, as the total has almost doubled in the last 20 years (a similar trend was identified for both winter and summer seasons). The yearly total discharge volumes in winter and summer seasons from each WWTP (W1 to W7) were given in **Table 2.1**.

The increase in both effluent volume and temperature can likely be associated with the population increase and the expanded sewer network (**Figure 2.4**), which receives larger amounts of warmer wastewater due to increasing water and energy consumption from residential and commercial sectors (Kinouchi, 2007).

The long-term temperature increase at S4 and its downstream sites in winter months is

likely due to the increase in both effluent temperature and volume from WWTPs. Variations in the stream temperature differ between sites, which is probably due to the distribution of WWTPs. For example, the abrupt change found between S3 and S4 is likely to have resulted from heat inputs from the WWTPs (W1–W3) under low flow rate conditions, and the highest stream temperature, which occurred at S6, can be attributed to wastewater inputs from the WWTPs (W4–W7). Although the effluent volume released from W4–W7 was approximately twice that released from W1–W3, the increase in stream temperatures between S4 and S6 was less than that found between S3 and S4 (except for the period of 1990–1995), which was probably due to a larger flow rate and a reduced net impact of warm wastewater.

To clearly identify the effect of wastewater heat inputs on stream temperature changes in the winter season for segments S3–4 and S4–6, the temperature change T_o-T_i (T_i and T_o indicate the stream temperature measured at upstream and downstream sites in each segment, respectively) was plotted against $Q_wT_w/(Q_wT_w+Q_iT_i)$ (**Figure 2.5**). The relative impact of heated effluents from the WWTPs on the mainstream is represented by $Q_wT_w/(Q_wT_w+Q_iT_i)$, in which Q_i is the flow rate at S3 and S4, and Q_w and T_w represent the volume and temperature of effluents from WWTPs in each segment.

Results indicated that stream temperature increases cannot be solely explained by wastewater as the plots produced scattered results. Effluents from W4 to W7 produced relatively small effects compared to those from W1 to W3. This better explains the lower temperature increase between S4 to S6 compared to S3 to S4 in the winter season, especially for the periods 1996–2000, 2001–2005, 2006–2009 and 2010-2011. As reported by Prats et al. (2012), the loss of heat by evaporation, convection and longwave radiation emission increases with the increasing water temperatures. Therefore, another reason of the less temperature increase between S4 to S6 than between S3 to S4 was considered to be the larger heat loss at the air–water interface in the winter season, which was further confirmed by the larger negative values of H_r (heat flux occurred at the air-water interface) in the water and heat budgets analysis for segment S4–6 (**Figure 2.10**).

2.3.3 Relationships between air and stream temperatures

Atmospheric effects due to global and regional warming can also generate long-term and longitudinal changes in stream temperatures. To separate the influences of other factors from those of atmosphere, relationships between air temperature and stream temperature were investigated.

Figure 2.6 shows the relationships between air and stream temperatures at four sites (S1, S3, S4 and S6) from 1990 to 1995, 2005 to 2010 and 2011 to 2013, respectively. In each plot, the monthly stream temperature measured at each site and the weekly average air temperature, recorded on an hourly basis at M2 (for S1), M3 (for S3) and M4 (for S4 and S6), were used. The averaging period for air temperatures was a week prior to the monthly stream temperature measurement because the weekly average has been shown to be more strongly correlated with stream temperature than any other short or long interval average (Bogan et al., 2004). The monthly stream temperature was previously shown to be proportionally correlated with the weekly air temperature (Kinouchi et al., 2007; Mohseni et al., 1999).

At S1, the plots for two periods overlapped and stream temperatures were found to be lower than air temperatures when the air temperature was above approximately 15 °C, probably due to the cold water released from the dam in warmer seasons (monthly mean temperatures ranged from 7.7 °C to 19.0°C during 1990–1995 and 15.2 °C to 18.9 °C during 2005–2010 in the summer months). When the air temperature became lower than approximately 5 °C, stream temperature approached 5 °C because the stream water at S1 was strongly controlled by water released from the dam, with relatively warm and constant temperatures in colder seasons (monthly mean temperatures ranged from 6.0 °C to 11.9 °C during 1990–1995 and 5.6 °C to 10.5 °C during 2005–2010 in the winter months). **Figure 2.7** showed the detailed comparisons of temperatures between the dam-released water and upstream (at S1) water for summer and winter seasons from 1990 to 2012. It is quite clear from Figure 2.7 that the temperatures of dam-released water were warmer than the upstream water in winter seasons most of the cases, whereas the reverse was true for summer seasons. The remarkable increase in summer dam-released temperature after 1991 (**Figure 2.7 (a)**) was mostly linked to the change in operating rules of dams. The water used to be released from the bottom layer of the reservoir before the year 1992, where the temperature is relatively lower; however, after that the water was released from the surface layer, where the water temperature is higher. In addition to temperature, the flow rates of dam release and upstream site were plotted in **Figure 2.7** for the years when data were available. The flow discharged by the Ogochi Dam can be the primary contributor to the stream flow at S1. The larger flow rates at S1 compared with the dam were likely attributable to the inflows from other natural sources over this reach, which may mitigate the effects of dam release. Therefore, we conclude that the stream temperature at S1 was strongly influenced by water released from the dam. Although the evidence is not that

apparent at S3, we can observe the deviation of the plots from the proportional line (with unit slope) during the warmer and colder seasons, which indicates that the effect of dam release still remains to some extent at S3.

The plots of stream temperature against air temperature at both S4 and S6 indicate a shift to higher stream temperature ranges in recent years (2005–2010 and 2011–2013) at air temperatures below approximately 15 °C. This suggests that the stream warming in the past 20 years was likely due to larger heat inputs from the increased effluent emissions from the WWTPs (**Figure 2.3**). When air temperatures were above approximately 15 °C, stream temperatures at S4 and S6 were closer to air temperatures for all periods, which indicates that the stream temperature is insensitive to wastewater effluents in warmer seasons because the effluent temperature is close to that of stream water (**Figures 2.2 (a) and 2.3**).

2.4 Water and heat budgets

2.4.1 Segment selection

To quantify the components that contributed to the water and heat budgets in the mainstream, five segments (S2–3, S3–4, S4–6, S5–6 and S6-8) were selected because they were considered to represent different conditions of natural and human impacts. For example, the upstream section S2-3 was not suffering from any wastewater discharge therefore it is considered to stand for a very natural condition. When it comes to the middle and lower reaches, such as S3-4 and S4-6 where receive large amount of warm wastewater, the impacts of anthropogenic behaviors can be evaluated. S6-8 is a further downstream section where stream temperature decreased in winter (**Figure 2.2 (b)**) and has no wastewater impacts.

Table 2.2 summarizes the number of tributaries, WWTPs and weirs for water withdrawal within the river segments selected for analysis.

2.4.2 Methodology

2.4.2.1 Water budget

In each segment, the outflow through a downstream section was assumed to be equal to the total of water inflows from different sources, i.e.

$$Q_o = Q_i + Q_t + Q_w + Q_{other} \tag{2.1}$$

where Q_o is the outflow at the downstream section and Q_i, Q_t and Q_w are inflows from the

upstream section, tributaries and WWTPs, respectively. Q_{other} indicates the combined effect of other factors that were not directly quantified due to data limitation (i.e. groundwater flow and water withdrawal). In Eq. (1), measured values are given for Q_o, Q_i, Q_t and Q_w, while Q_{other} is calculated as a residual term by $Q_{other} = Q_o - Q_i - Q_t - Q_w$.

2.4.2.2 Heat budget

The heat budget in each segment were calculated using Eq. (2), taking both the natural and human fluxes into account,

$$H_o = H_i + H_t + H_w + H_r + H_{other} \tag{2.2}$$

where H_o is the outflowing heat at the downstream section, H_i, H_t, and H_w are the inflowing heat from the upstream section, tributaries, and WWTPs, respectively, H_r is the heat exchange at the air–water interface and H_{other} is the net heat exchange caused by other factors, e.g. heat exchange at the streambed–water interface by conduction and groundwater inflow/outflow and water withdrawal. Precipitation was neglected as we used data obtained during days with no rainfall. The amount of transported heat (i.e. H_o, H_i, H_t, H_w) is defined by

$$H = C_p \rho Q T \tag{2.3}$$

where $Cp\rho$ is the heat capacity of water (TJ m^{-3} $^oC^{-1}$), Q is the measured river flow (Q_o, Q_i, Q_t) or effluent volume from WWTPs (Q_w) (m^3 day^{-1}) and T is the measured stream or effluent temperature (^oC). The heat exchange at the air–water interface (H_r) is derived from

$$H_r = R_{net} \times A \tag{2.4}$$

where A is the water surface area (m^2) and R_{net} is the net heat flux at the air–water interface (TJ m^{-2} day^{-1}), which is typically expressed as (Brutsaert, 1982)

$$R_{net} = R_{is}(1-\alpha_s) + R_{ld} - R_{lu} - J_s - J_l \tag{2.5}$$

where R_{is} is the incident solar radiation at the water surface, α_s is the albedo of the water surface (0.06), R_{ld} is the downward longwave radiation, R_{lu} is the upward longwave radiation and J_s and J_l are the sensible and latent heat fluxes, respectively. The formulas to calculate each flux in Eq. (2.5) are further described below.

Measured incident solar radiation was used because the shading effect was considered to be negligible due to limited vegetated canopies in the reaches we studied. The daily downward longwave radiation was obtained by the following equations taking the effect of cloudiness into account (Idso and Jackson, 1969; Kondo, 1994),

$$R_{ld} = (1-\beta)[1-(1-\varepsilon_{ac})F_c]\sigma(T_a + 273.2)^4 \tag{2.6}$$

$$\varepsilon_{ac} = 1 - 0.261\exp\left(-7.77\times10^{-4}T_a{}^2\right) \tag{2.7}$$

$$F_c = 0.826N_c{}^3 - 1.234N_c{}^2 + 1.135N_c + 0.298 \tag{2.8}$$

where $N_c = n/N$, is the fraction of sunshine hours, in which n is the actual number of hours of bright sunshine duration throughout a day (h) and N is the number of possible sunshine hours. The theoretically possible sunshine hours for each month in our study area are summarized in **Table 2.4**. F_c is the cloud cover ratio, T_a is the daily mean air temperature (°C), ε_{ac} is the atmospheric emissivity under clear skies, σ is the Stefan–Boltzmann constant (4.9×10^{-15} TJ m^{-}2 day^{-1} K^{-4}) and β is the longwave reflectivity (0.03). Eq. (2.7) is an empirical equation solely in terms of the air temperature, but the effect from water vapor has already been included in this equation. It appears that the formula is valid over a wider temperature range above freezing (Idso and Jackson, 1969). Deacon (1970) subsequently showed that the omission of a humidity term was justified because of the strong correlation between screen temperature and screen humidity.

The upward longwave radiation (R_{lu}) is the radiant flux emitted from the water surface given by

$$R_{lu} = \varepsilon_s\sigma(T_s + 273.2)^4 \tag{2.9}$$

where T_s is the stream temperature (°C), ε_s is the emissivity of the water surface (0.97).

The sensible and latent heat fluxes (J_s and J_l) at the water surface are calculated using the bulk aerodynamic formulas as expressed by Eqs. (2.10) and (2.11), respectively (Sinokrot and Stefan, 1993),

$$J_s = 0.61\rho_w\lambda\frac{P_a}{1000}Wftn(T_s - T_a) \tag{2.10}$$

$$J_l = \rho_w\lambda Wftn(e_s - e_a) \tag{2.11}$$

where ρ_w is the density of water taken to be 998.23 kg m^{-3}(20°C), λ is the latent heat of vaporization of water (TJ kg^{-1}) given by $\lambda = (2499 - 2.36T_s)\times10^{-9}$, P_a is the atmospheric pressure (hPa), e_s is the saturated vapor pressure at the water surface temperature (hPa), e_a is the vapor pressure of the air (hPa) and Wftn is the wind speed function (m hPa^{-1} day^{-1}).

The saturated vapor pressure at the water surface temperature e_s and the vapor pressure of the air e_a are given as

$$e_s = a_* \exp\left(\frac{b_* T_a}{T_a + c_*}\right) \tag{2.12}$$

$$e_a = RH \times e_s \tag{2.13}$$

where the coefficients a_*, b_* and c_* are chosen to fit the equation best to the expected range in temperature, and T_s is the stream temperature in °C. *RH* is the relative humidity. For temperatures above freezing, the coefficients are

$$a_* = 6.108\ mb,\quad b_* = 17.27,\quad c_* = 237.3\ ^\circ\mathrm{C}$$

The wind speed function Wftn is given by (Gulliver and Stefan, 1986),

$$Wftn = 0.0000934(\Delta\theta_v)^{1/3} + 0.0000852u_2 \tag{2.14}$$

where $\Delta\theta_v$ is the difference in a virtual temperature between the air temperature and the water surface temperature and u_2 is the wind speed at 2 m above water surface (m/s).

$\Delta\theta_v$ is expressed as

$$\Delta\theta_v = T_s\left(1 + \frac{0.378e_s}{P_a}\right) - T_a\left(1 + \frac{0.378e_a}{P_a}\right) \tag{2.15}$$

The wind speed recorded at each meteorological station above grassland was converted to that at 2 m above the water surface (Macdonald et al., 1998),

$$u_2 = u_h\left(\frac{\ln\frac{h'}{z_0'}}{\ln\frac{h}{z_0'}}\right) \times \left(\frac{\ln\frac{2}{z_0}}{\ln\frac{h'}{z_0}}\right) \tag{2.16}$$

where u_h is the measured wind speed (m s^{-1}) at height h (m), h' (m) is the height at which the wind speed above the water surface was regarded equal to that above grassland (taken to be 50 m), z_0 is the roughness length above the water surface (m) (taken to be 1.0×10^{-4} m) and z_0' is the roughness length at the sites above grassland (m). The dependency of roughness lengths on the wind direction was taken into account by referring to Kuwagata and Kondo (1990). **Table 2.3** displays the height of wind speed measurement and the roughness length under different wind directions at meteorological stations M2, M3 and M4. Measured atmospheric pressure (P_a) and relative humidity (*RH*) at M1 were used for all segments, other meteorological conditions (i.e. air temperature, global shortwave radiation, wind speed and direction, and sunshine duration) measured at M2, M3 and M4 were accordingly utilized for S2-3, S3-4, and S4-6 and S6-8, respectively.

2.4.2.3 Heat exchange due to groundwater flow and water withdrawal

The heat exchanges caused by groundwater flow and water withdrawal were estimated by

$$H_{estimate} = C_p \rho \times Q_{other} \times T_s \tag{2.17}$$

where Q_{other} is the combination of residual flows derived from Eq. (2.1), which represents the combined amount of groundwater flow and water withdrawal. The average of the water temperatures measured at upstream and downstream sites in each segment was used to represent T_s, which is the temperature of groundwater flow (if groundwater recharge or the stream water outflow into the ground occurs) and water withdrawal. Thus, by comparing $H_{estimate}$ with H_{other}, we can verify the magnitude of groundwater flow and water withdrawal.

2.4.2.4 Stream temperature estimation under conditions of no wastewater impact

To simply estimate the wastewater influence on stream temperature, the amount of water and heat transported through the downstream section in each segment with no wastewater effluent are quantified by (Q_o–Q_w) and (H_o–H_w), respectively, and the stream temperature (T_0') at the downstream section with no wastewater inputs is calculated by

$$H_o - H_w = C_p \rho (Q_o - Q_w) T_o' \tag{2.18}$$

With measured Q_o, Q_w and calculated H_o, H_w, we obtain the stream temperature (T_0') at S4 and S6 without wastewater inputs from segment S3–4 and S4–6, respectively.

In applying this equation, we neglected changes in R_{lu}, which is a function of stream temperature, and changes in Q_{other} and H_{other}, which may be influenced by the water level and stream temperature.

2.4.3 Results and discussion

2.4.3.1 Water and heat budgets

The results of water and heat budget analyses for segments S2–3, S3–4, S4–6, S5–6 and S6-8 are presented in **Figures 2.8–2.12**, respectively, in which the flow rate and heat flux are the average of calculated results over several days of measurement; the numbers of days are indicated in parentheses at the bottom of the figure showing the flow rate. The selected years, as well as measurement events used in the analysis, were based on data availability under normal flow conditions.

In segment S2–3 (**Figure 2.8**), the tributary inflow Q_t was the dominant factor for the

stream flow gain, while Q_{other} was negative (except for winter in 2004 (04-win)), implying that a comparative amount of withdrawal and groundwater recharge occurred over the analyzed periods. Tributary heat input greatly contributed to the net heat gain, resulting in the reduction of dam release impacts, while the heat exchange at the air–water interface H_r was secondary or minor. In most seasons, $H_{estimate}$ was in good agreement with H_{other}, which indicated that the outgoing flows, such as water withdrawal and groundwater recharge, were dominant and contributed to the heat loss.

In segments S3–4 (**Figure 2.9**) and S4–6 (**Figure 2.10**), which receive wastewater effluents, the flow rate Q_w and heat H_w from the WWTPs were the major contributors of water and energy increases in both winter and summer months, while the effects of the tributary (Q_t and H_t) were small, especially in winter. The heat fluxes at the air–water interface (H_r) were comparatively minor, which contributed to a heat loss in winter and a gain in summer. In both segments, values of $H_{estimate}$ were close to those of H_{other} in most seasons, but $H_{estimate}$ was slightly underestimated for several seasons, such as the 94-sum, 03-sum and 04-sum for S3–4, and 94-sum, 12-sum for S4–6. These underestimates can be explained by the groundwater outflow into the stream with relatively lower temperatures, which occurred in some reaches when the groundwater table was higher than the water level in the mainstream.

As segment S5–6 had no weir withdrawing water (**Table 2.2**), the results of the water and heat budgets (**Figure 2.11**) specifically indicated the amounts of groundwater recharge and its accompanied heat transport. Q_{other} for the segment S5–6 was negative in most periods with the exceptions of 10-win and 12-sum, which clearly indicates a certain amount of groundwater recharge that almost reduced the flow volume once increased by the wastewater discharged into this segment. This was further confirmed by the agreement between $H_{estimate}$ and H_{other}, especially in summer seasons, which suggests that the groundwater recharge acts as a major sink of water and energy in this segment.

In the further downstream reach S6-8 (**Figure 2.12**), where has no wastewater influence, the tributary inflow Q_t dominated the water balance. However, unlike other sections, the groundwater outflows into stream were more frequent to occur (reflected by the positive values of Q_{other}), which is likely attributed to the higher groundwater table compared to water level in the downstream reach. The flow rate differences Q_o–Q_i showed negative in recent years (i.e. 10-win, 11-win, 09-sum and 10-sum), implying a flow rate decrease probably resulting from water withdrawal or groundwater recharge. The agreement between $H_{estimate}$ and H_{other} indicated that the groundwater recharge (or water withdrawal) and

groundwater outflow were evenly occurred. In summer season, tributary heat input H_t largely contributed to heat gain while H_{other} worked to reduce heat in several events, such as 02-sum, 09-sum and 10-sum. In winter season, H_t became comparatively small whereas H_r played a very determinant role in heat transport process, which worked to reduce the heat inputs from tributaries.

2.4.3.2 Stream temperature estimation without wastewater impacts

The influence of wastewater on stream temperature was quantified by comparing the measured temperatures with those estimated by Eq. (2.18) (**Figure 2.13**). Results showed that in the winter season, stream temperatures decreased by 3.6–9.3°C at S4 and 2.2–5.4°C at S6 when the wastewater impacts from W1–W3 and W4–W7, respectively, were eliminated. In contrast, in the summer season, no substantial difference was observed between the estimated and measured values at both S4 and S6.

Therefore, we concluded that wastewater contributed significantly to stream warming in the winter seasons, while the effects were insignificant in the summer seasons, which could be attributed to the larger natural flow (**Figure 2.1**) and the similar temperature ranges of stream water and wastewater (**Figures 2.2 (a) and 2.3**). This result was further confirmed in Chapter 4**.**

2.5 Summary

This chapter investigated stream temperature variations in the mainstream of the Tama River, which runs through highly urbanized areas of Tokyo. Long-term and longitudinal temperature changes, as well as the water and heat budgets in the mainstream, were identified using data for stream temperature and flow rate, temperature and volume of wastewater effluents, air temperature and other meteorological conditions.

Our analysis detected long-term stream temperature increases in the winter season at sites where considerable volumes of wastewater effluent were received. The flow rate decreased markedly between S1 and S2, resulting in a larger temperature increase in the following sites between S2 and S3 in the summer seasons. Moreover, the relationships between air temperature and stream temperature at S1, S3, S4 and S6 in three periods indicated that the effects of a dam release have strong influence on S1, whereas the impacts of the wastewater effluents from the WWTPs became dominant at S4 and S6.

Water and energy budgets under different hydrological conditions and levels of human

impact were analyzed. In the upstream segment (S2–3), the heat inflow from the tributary was large enough to reduce the impacts of a dam release, although the effect of heat exchange through the air–water interface was minor. In the middle and downstream segments (S3–4 and S4–6), the largest contributions to the water and heat budgets were from wastewater effluents, while other factors such as groundwater recharge and water withdrawal were found to behave as energy sinks, especially in summer. In the further downstream reach (S6-8), the groundwater outflows into stream were found more frequent to occur among analyzing events and the heat exchange occurred at the air–water interface played a very determinant role in winter seasons that worked to reduce the heat inputs from tributaries. By comparing stream temperatures with and without wastewater effluents, we found that stream temperatures were reduced by 3.6–9.3°C at S4 and 2.2–5.4°C at S6 in the winter season, when wastewater influences were removed.

Table 2.1 Yearly total discharge volumes from each WWTP (W1 to W7) in (a) summer (July through September) and (b) winter (December through February) months.

(a) summer season

10^7 (m^3)	W1	W2	W3	W4	W5	W6	W7
1990	0	1.045	0	0	0.250	0.514	1.675
1991	0	1.431	0	0	0.377	0.630	1.995
1992	0	1.100	0	0	0.354	0.607	1.704
1993	0.148	1.266	0	0.097	0.502	0.714	2.209
1994	0.185	1.252	0.465	0.164	0.420	0.705	1.941
1995	0.250	1.262	0.557	0.207	0.469	0.718	1.847
1996	0.335	1.205	0.460	0.240	0.468	0.838	2.109
1997	0.358	1.313	0.471	0.329	0.462	0.803	2.093
1998	0.481	1.694	0.712	0.428	0.615	0.926	2.408
1999	0.539	1.572	0.685	0.470	0.604	1.036	2.361
2000	0.545	1.527	0.616	0.493	0.556	1.104	2.151
2001	0.608	1.432	0.496	0.543	0.478	0.940	2.044
2002	0.675	1.557	0.598	0.584	0.535	1.024	2.144
2003	0.753	1.671	0.711	0.682	0.624	0.952	2.304
2004	0.687	1.231	0.432	0.606	0.456	1.050	1.936
2005	0.821	1.503	0.648	0.697	0.613	1.039	2.117
2006	0.815	1.385	0.562	0.678	0.532	0.994	2.145
2007	0.909	1.491	0.571	0.741	0.555	1.051	2.202
2008	1.016	1.584	0.690	0.763	0.586	1.089	2.357
2009	0.875	1.245	0.436	0.689	0.422	0.985	1.872
2010	—	—	—	—	—	—	—
2011	1.094	1.586	0.44	0.767	0.510	1.079	2.093
2012	0.916	1.243	0.44	0.719	0.520	1.035	1.959

(b) winter season

10^7 (m^3)	W1	W2	W3	W4	W5	W6	W7
1990	0	0.885	0	0.000	0.206	0.441	1.319
1991	0	0.898	0	0.000	0.273	0.501	1.360
1992	0.047	0.867	0	0.009	0.312	0.543	1.522
1993	0.099	0.890	0	0.058	0.320	0.583	1.454
1994	0.169	1.036	0.194	0.132	0.298	0.600	1.365
1995	0.245	1.025	0.301	0.176	0.309	0.629	1.460
1996	0.303	1.118	0.289	0.208	0.314	0.631	1.423
1997	0.342	1.102	0.367	0.298	0.414	0.701	1.816
1998	0.369	1.034	0.308	0.325	0.338	0.653	1.516
1999	0.422	1.086	0.333	0.368	0.367	0.738	1.593
2000	0.468	1.138	0.332	0.434	0.373	0.785	1.652
2001	0.538	1.154	0.341	0.484	0.444	0.854	1.587
2002	0.580	1.131	0.345	0.525	0.455	0.837	1.635
2003	0.606	1.128	0.349	0.545	0.419	0.795	1.594
2004	0.668	1.201	0.396	0.589	0.441	0.840	1.774
2005	0.698	1.135	0.407	0.607	0.440	0.880	1.691
2006	0.802	1.123	0.372	0.637	0.404	0.907	1.569
2007	0.841	1.153	0.372	0.672	0.428	0.936	1.666
2008	0.839	1.151	0.382	0.662	0.395	0.934	1.737
2009	0.849	1.102	0.358	0.651	0.361	0.931	1.697
2010	—	—	—	—	—	—	—
2011	—	—	—	—	—	—	—
2012	0.901	1.151	0.358	0.684	0.385	0.964	1.631
2013	0.871	1.104	0.358	0.672	0.373	0.948	1.504

Table 2.2 Number of tributaries, WWTPs and weirs in each segment.

Segment	Tributary	WWTP	Weir
S2-3	2	0	1
S3-4	2	3	1
S4-6	2	4	2
S5-6	0	1	0
S6-8	2	0	2

Table 2.3 Wind speed measurement height *h* (m) and roughness length z_0' (m) at meteorological stations.

Site	Height	Roughness length[a)]							
		NNE	ENE	ESE	SSE	SSW	WSW	WNW	NNW
M2	7.9	0.59	0.35	0.75	0.68	0.37	0.24	0.30	0.30
M3	49.8	0.71	0.81	1.21	1.06	1.01	0.79	0.53	0.66
M4	6.5	0.83	0.74	0.69	0.49	0.49	0.56	0.57	0.61

[a)]roughness length varies with wind direction: E, W, S and N stand for east, west, south and north winds, respectively.

Table 2.4 Possible sunshine duration in each month (12h/day).

Month	Jan	Feb	Mar	Apr	May	Jun	Jul	Aug	Sep	Oct	Nov	Dec
Possible sunshine duration	0.830	0.900	0.992	1.087	1.167	1.209	1.191	1.123	1.033	0.938	0.854	0.809

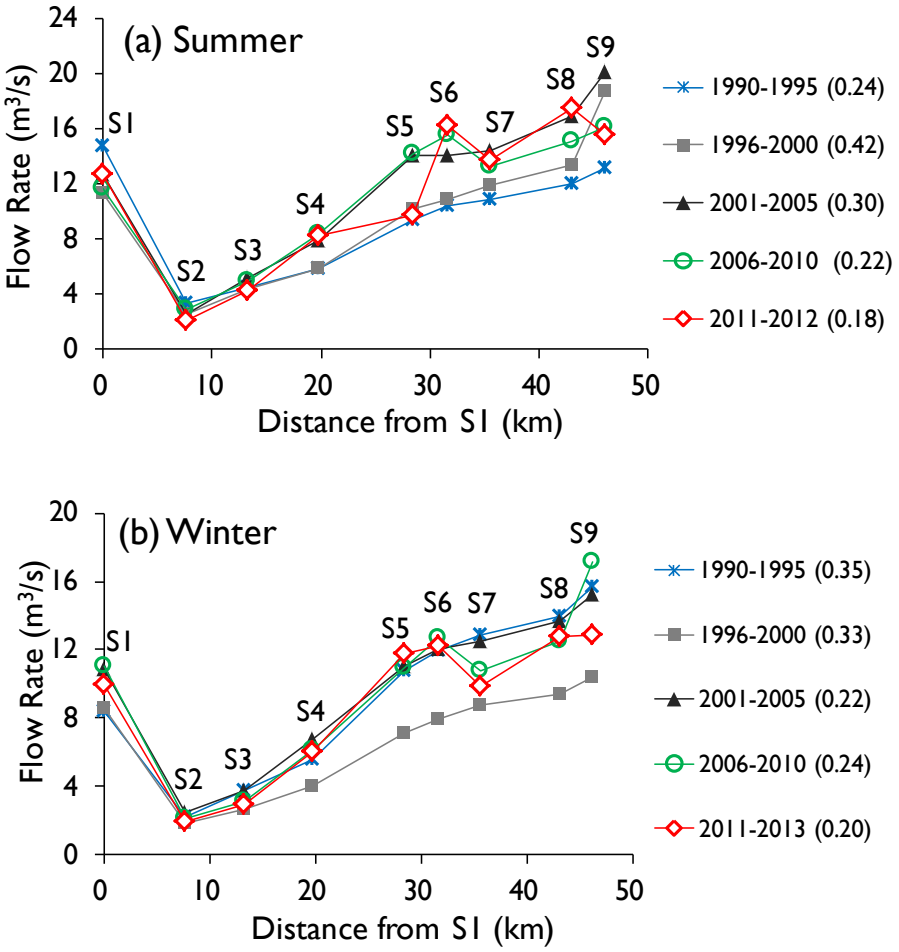

Figure 2.1 Stream flow rate at S1–S9 in (a) summer and (b) winter seasons. Each plot indicates a 2 to 6 − year average of monthly measured data under normal flow conditions. The legends show averages of σ/μ at S1–S9 in each period.

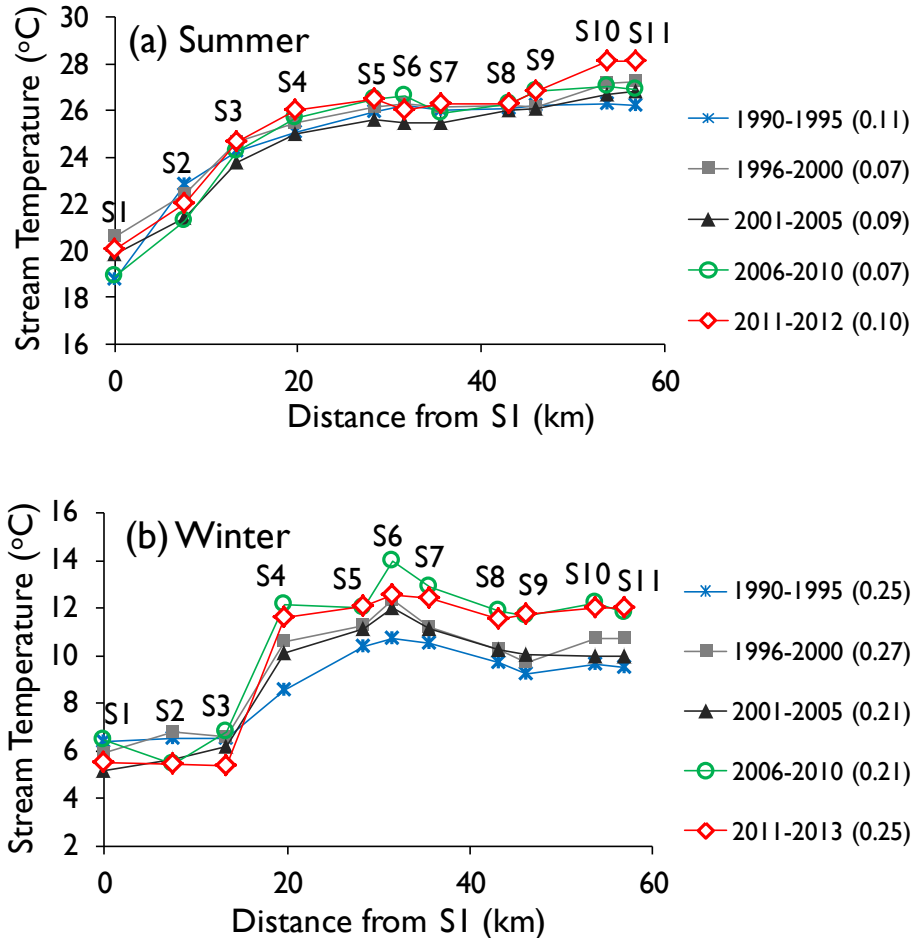

Figure 2.2 Stream temperature at S1–S11 in (a) summer and (b) winter seasons. Each plot indicates a 2 to 6− year average of monthly measured data under normal flow conditions. The legends show averages of σ/μ at S1–S11 in each period

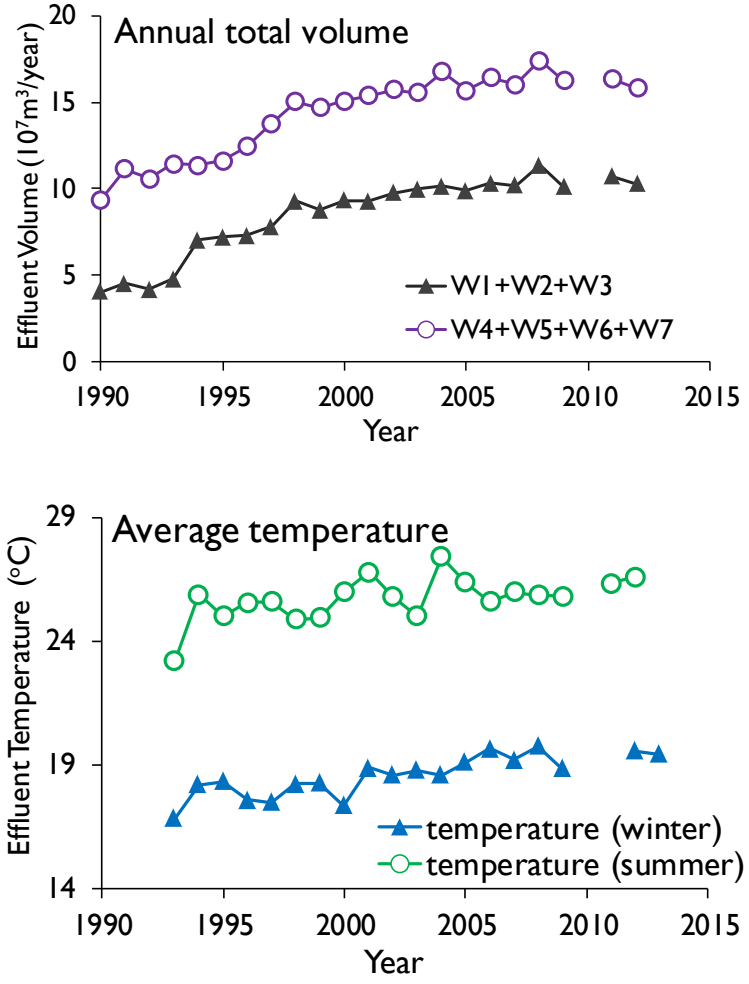

Figure 2.3 Annual total effluent volume (from 1990 to 2012, data in 2010 were absent) and average temperature (from 1993 to 2013, data in 2010 were absent) from WWTPs.

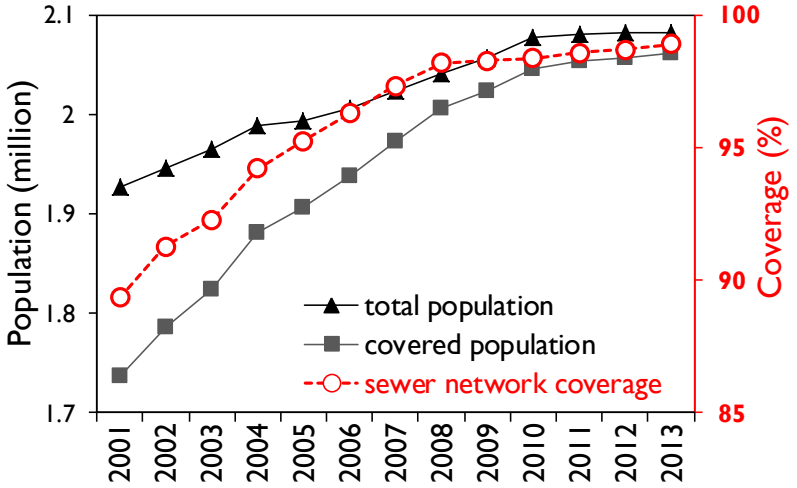

Figure 2.4 Trends in population and coverage of sewer networks from 2011 to 2013.

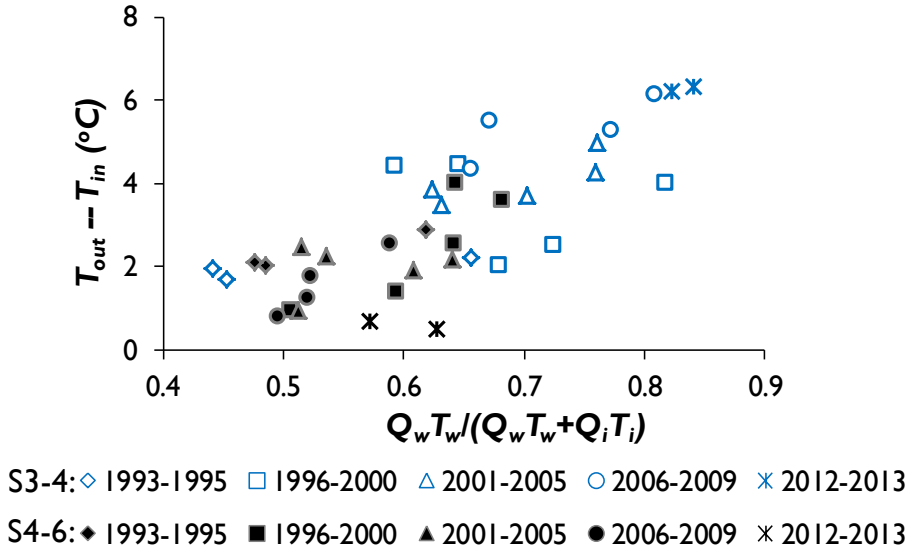

Figure 2.5 Stream temperature differences (To-Ti) versus wastewater effects evaluated by $Q_wT_w/(Q_wT_w+Q_iT_i)$ between segments S3-4 and S4-6. The relationships for the two segments are distinguished by hollow (blue) and solid (black) symbols. Each plot indicates the average values in the winter months of each year under normal flow conditions.

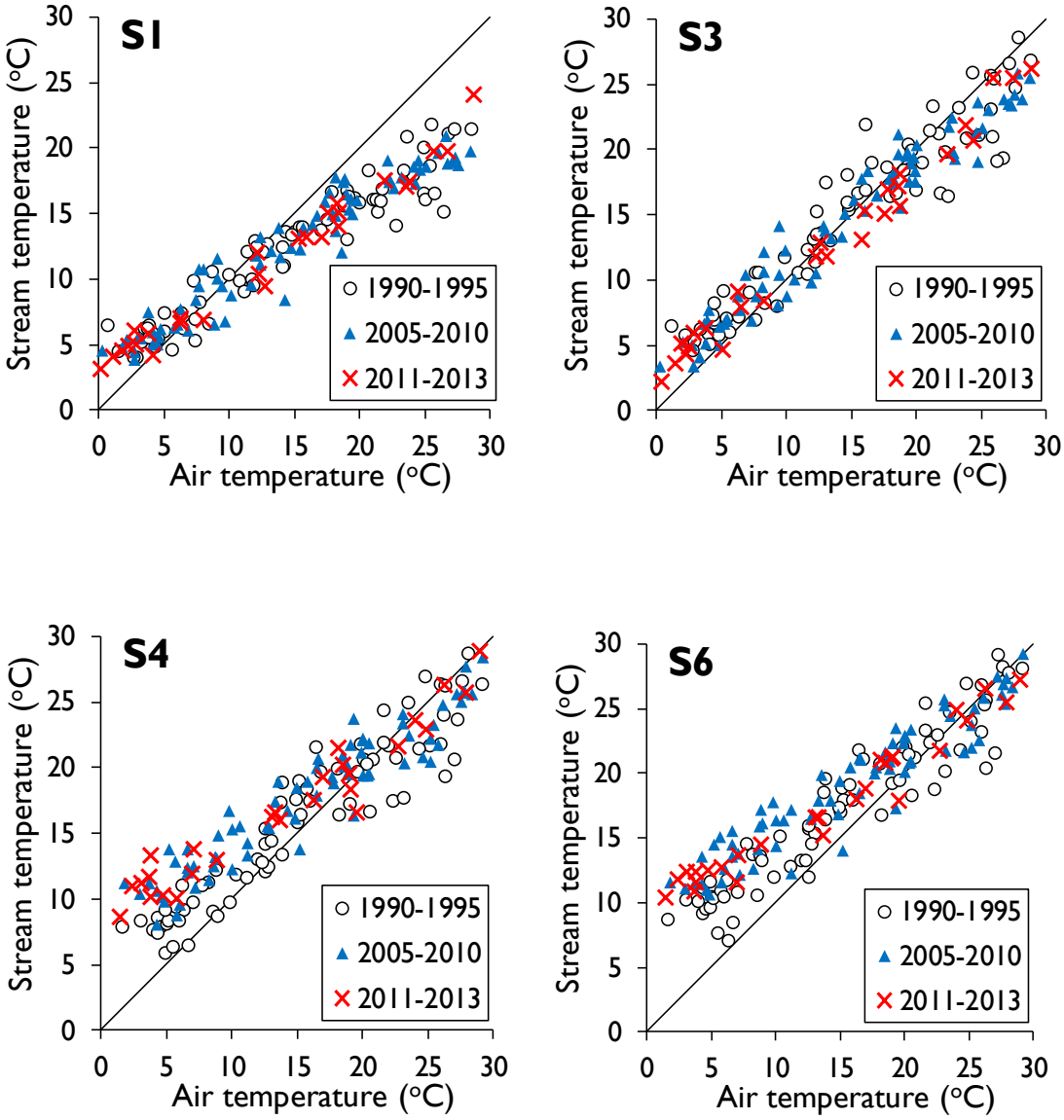

Figure 2.6 Relationships between air and stream temperatures at S1, S3, S4 and S6 during three periods (1990-1995, 2005-2010 and 2011-2013).

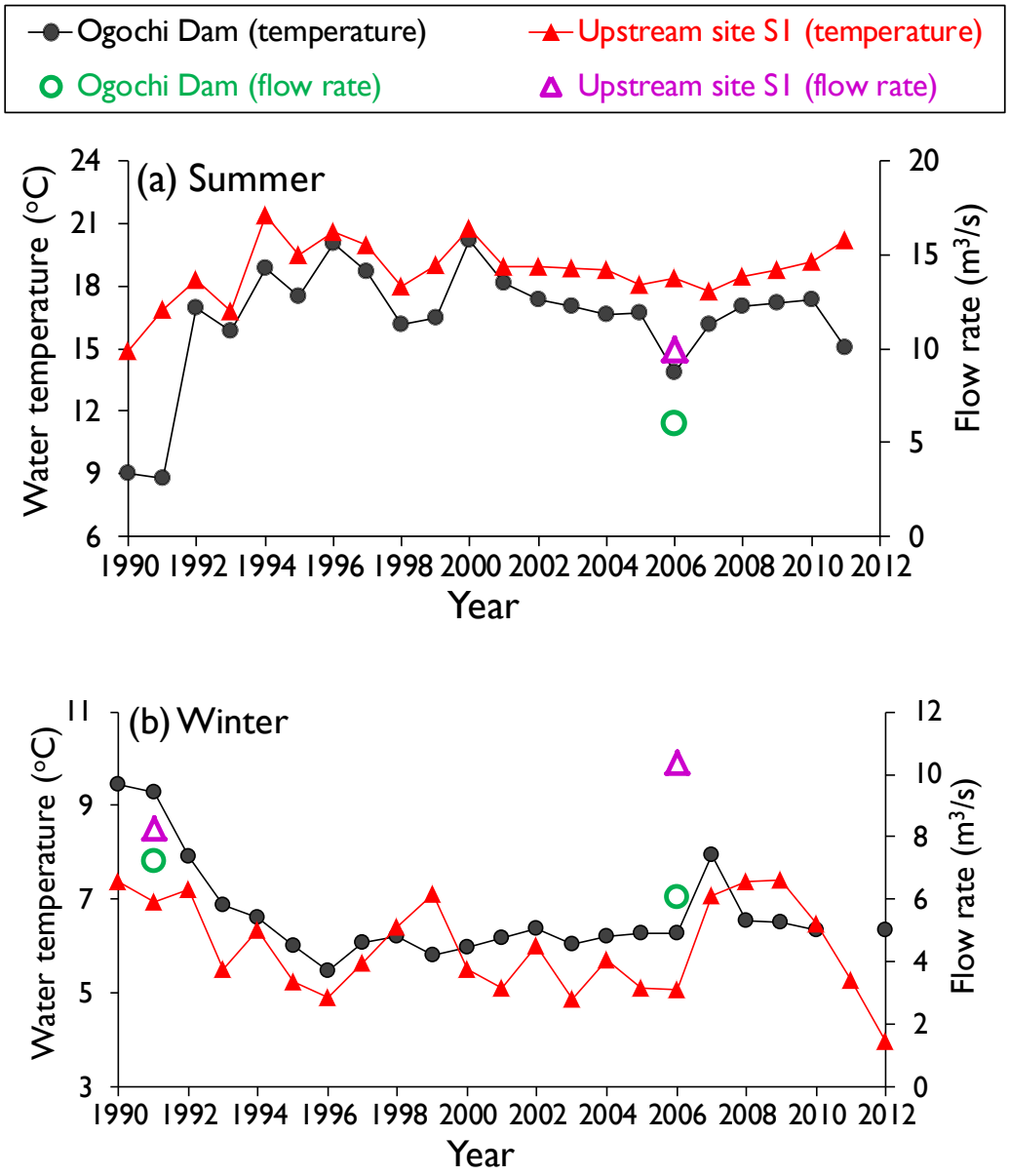

Figure 2.7 Comparison between dam-released temperature and upstream (S1) temperature for (a) summer and (b) winter seasons from 1990 to 2010. Plots of Ogochi Dam and upstream site indicated the summer/winter-averages of monthly means and monthly measurements, respectively. The monthly mean flow rates from Ogochi Dam and monthly measured flow rates at S1 were plotted together as reference.

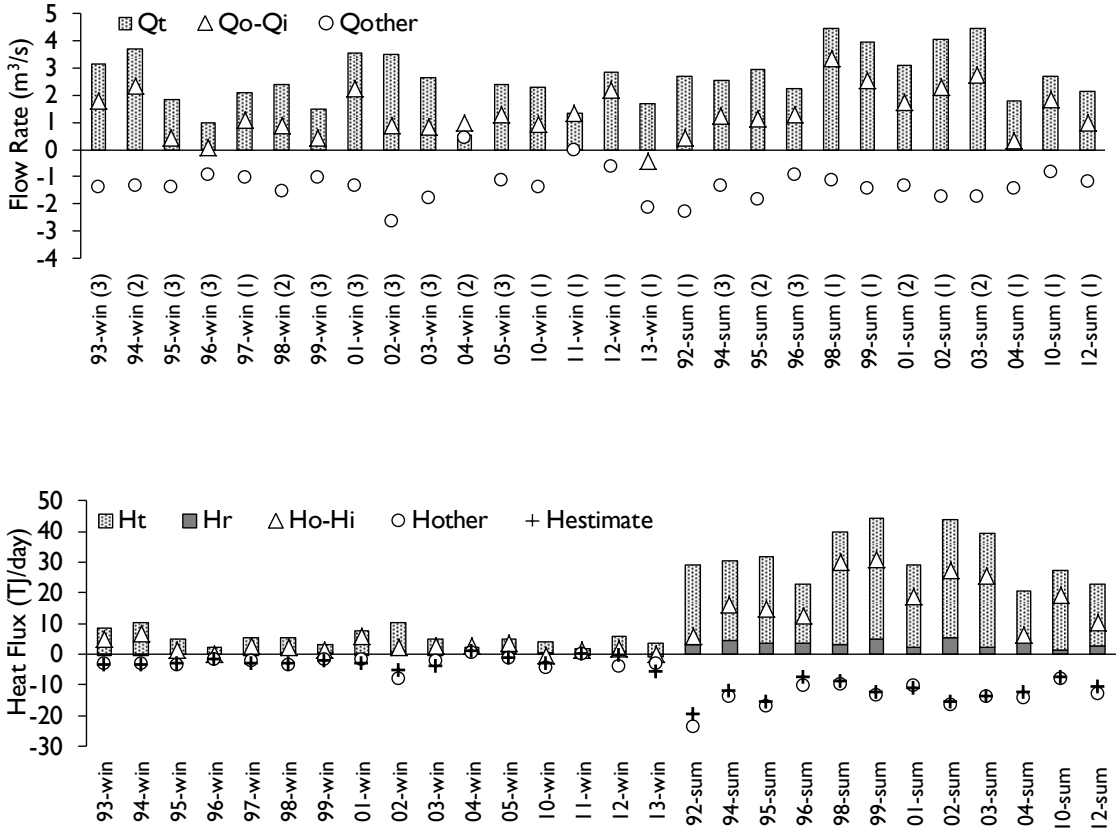

Figure 2.8 Water and heat budgets for segment S2–3 in winter and summer seasons. Q_i, Q_o, Q_w, Q_t, H_i, H_o, H_r, H_w and H_t were calculated using observed data, Q_{other} and H_{other} were derived from Eqs. (2.1) and (2.2) and $H_{estimate}$ is the heat flux calculated by Eq. (2.17). Each term stands for the average of flow rate or heat flux over several days of measurement, with the numbers of days indicated in the parentheses below dates of the figure showing the water budget.

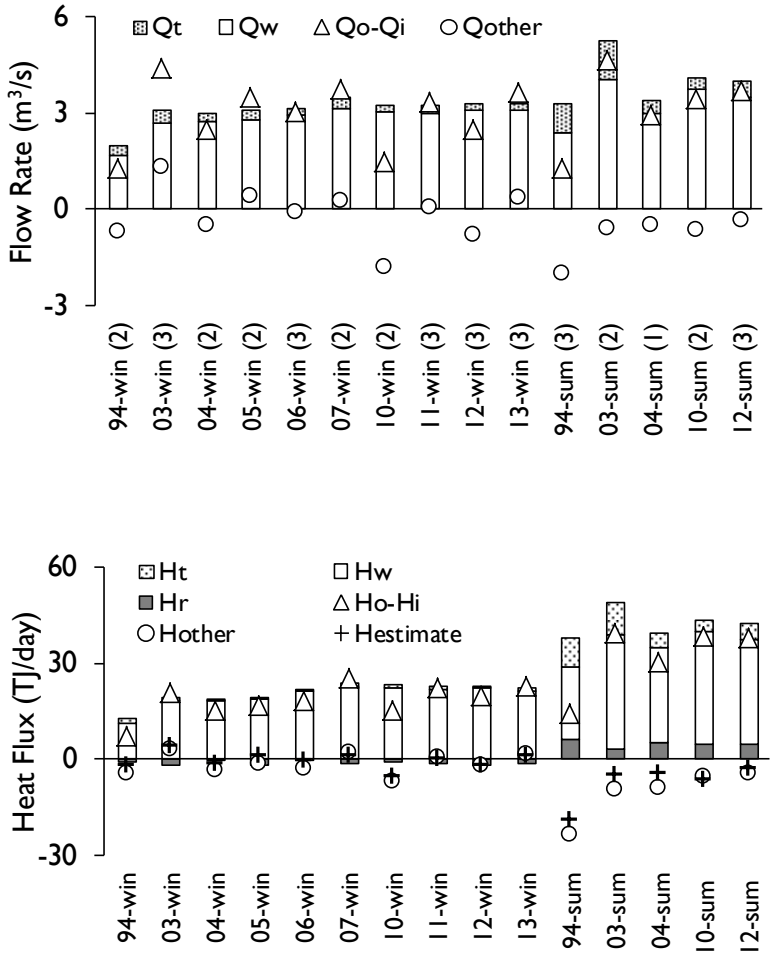

Figure 2.9 Water and heat budgets for segment S3-4 in winter and summer seasons (see Figure 2.8 for the notation of symbols and the meaning of numbers in the parentheses).

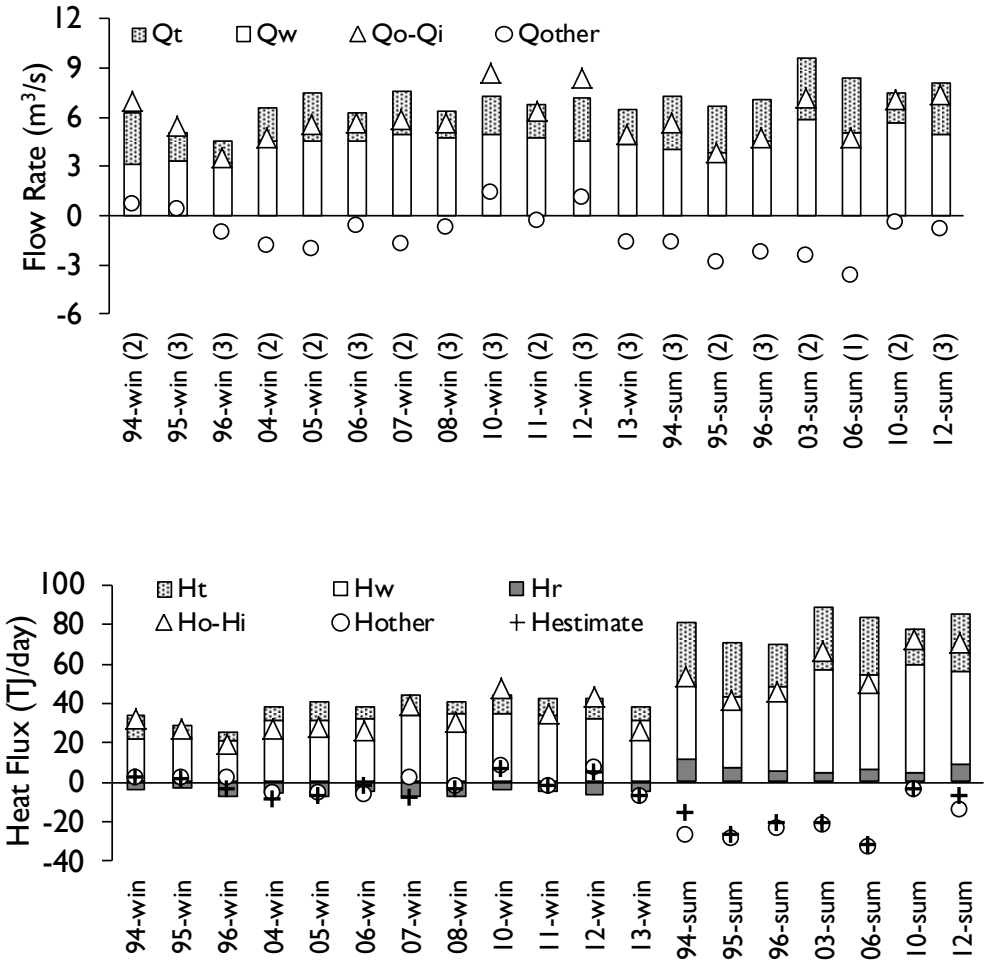

Figure 2.10 Water and heat budgets for segment S4-6 in winter and summer seasons (see Figure 2.8 for the notation of symbols and the meaning of numbers in the parentheses)

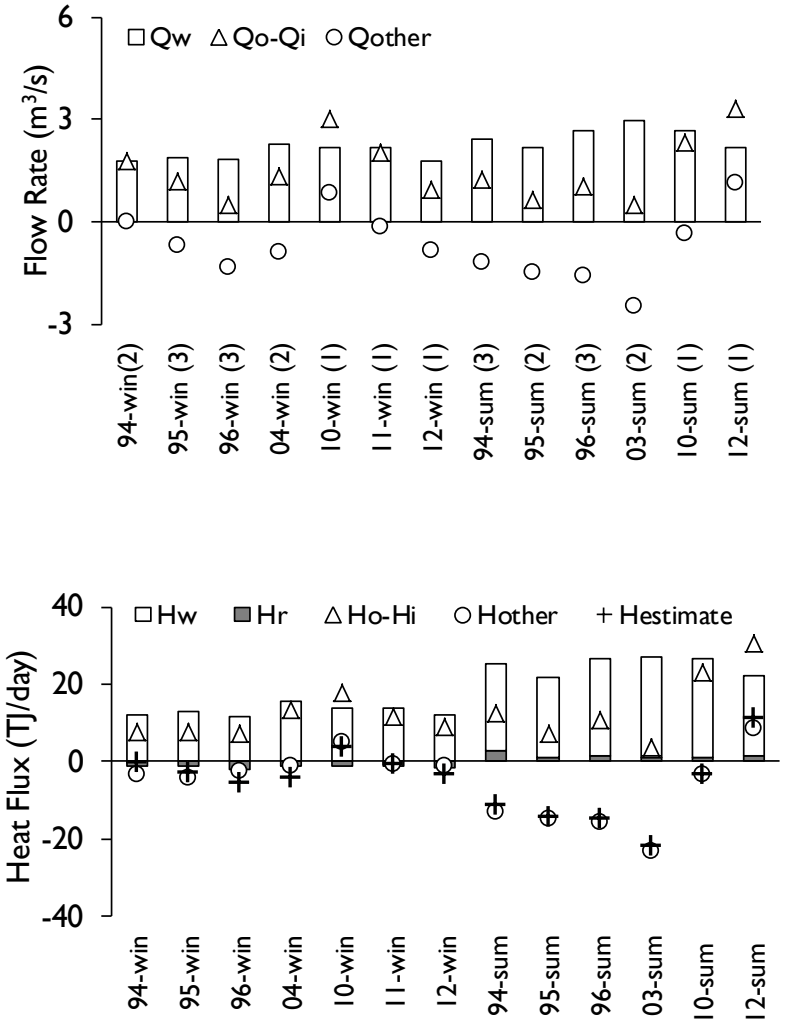

Figure 2.11 Water and heat budgets for segment S5-6 in winter and summer seasons (see Figure 2.8 for the notation of symbols and the meaning of numbers in the parentheses)

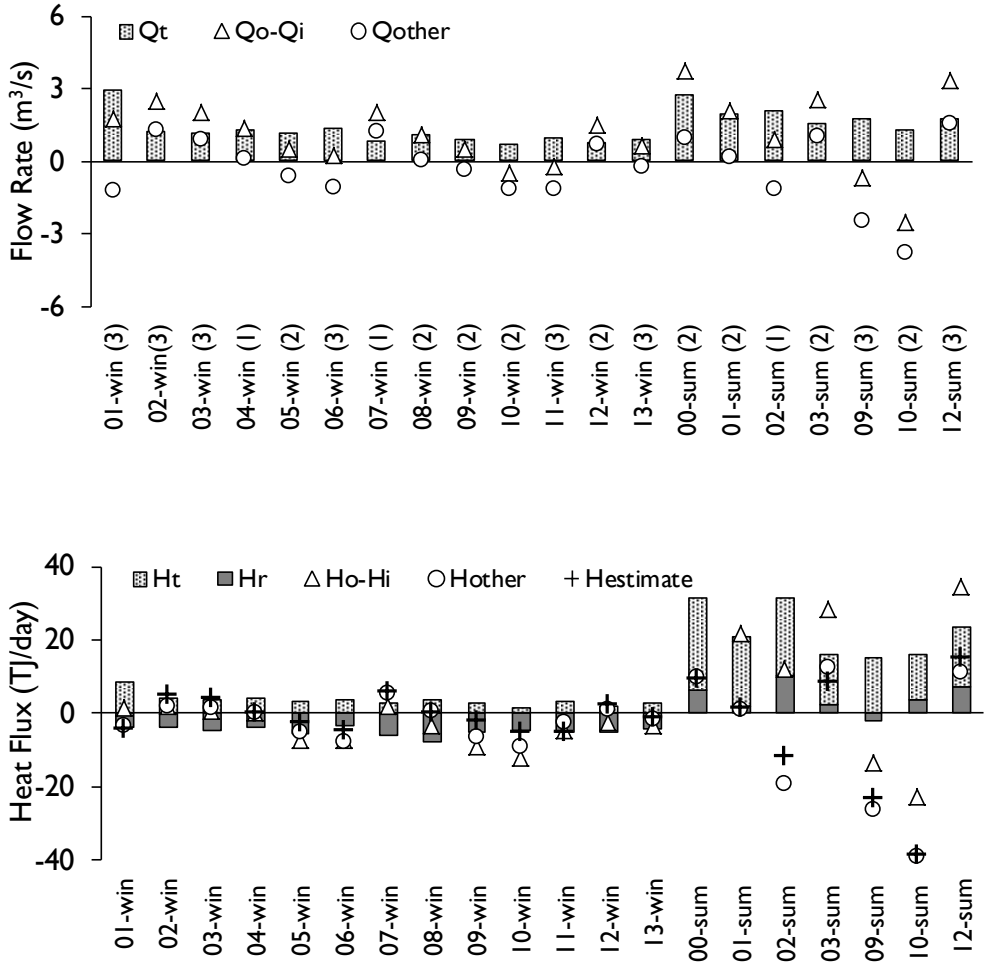

Figure 2.12 Water and heat budgets for segment S6-8 in winter and summer seasons (see Figure 2.8 for the notation of symbols and the meaning of numbers in the parentheses)

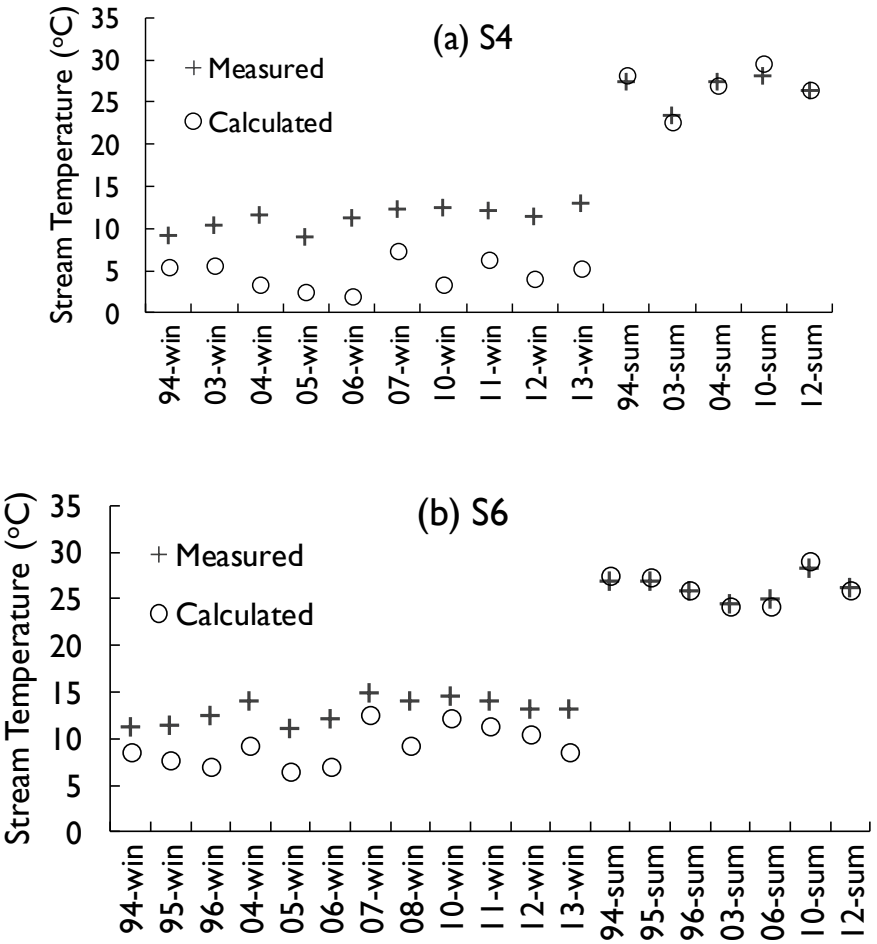

Figure 2.13 Comparison of measured stream temperatures with those calculated by eliminating the impact from WWTPs at (a) S4 and (b) S6.

References

Bogan, T., Stefan, H. G., Mohseni, O., 2003. Imprints of secondary heat sources on the stream temperature/equilibrium temperature relationship, Water Resources Research, 40, W12510, doi:10.1029/2003 WR002733.

Brutsaert, W., 1982. Evaporation into the atmosphere. Kluwer, The Netherlands.

Caissie, D., Satish, M.G., EI-Jabi, N., 2007. Predicting water temperatures using a deterministic model: application on Miramichi River catchments (New Brunswick, Canada). Journal of Hydrology, 336, 303-315.

Evans, E.C., Mcgregor, G.R., Petts, G.E., 1998. River energy budgets with special reference to river bed processes. Hydrological Processes, 12, 575-595.

Gulliver, J.S., Stefan, H.G., 1986. Wind function for a sheltered stream. Journal of Environmental Engineering, 112, 387-398.

Hebert, C., Caissie, D., Satish, M.G., EI-Jabi, N., 2011. Study of stream temperature dynamics and corresponding heat fluxes within Miramichi River catchments (New Brunswick, Canada). Hydrological Processes, 25, 2439-2455.

Hockey, J.B., Owens, I.F., Tapper, N.J., 1982. Empirical and theoretical models to isolate the effect of discharge on summer water temperatures in the Hurunui River. Journal of Hydrology (N.Z.), 21, 1-12.

Idso, S.B., Jackson, R.D., 1969. Thermal radiation from the atmosphere, Journal of Geophysical Research, 74, 5397-5403.

Kinouchi, T., 2007. Impact of long-term water and energy consumption in Tokyo on wastewater effluent: implications for the thermal degradation of urban streams. Hydrological Processes, 21, 1207-1216.

Kinouchi, T., Yagi, H., Miyamato, M., 2007. Increase in stream temperature related to anthropogenic heat input from urban wastewater, Journal of Hydrology, 335, 78-88.

Kondo, J., 1994. Meteorology of the water environment. Asakura, Tokyo (in Japanese).

Kuwagata, T., Kondo, J., 1990. Estimation of aerodynamic roughness at the regional meteorological stations (AMeDAS) in the central part of Japan. Tenki, 37, 55-59 (in Japanese).

LeBlanc, R.T., Brown, R.D., FitaGibbon, J.E., 1997. Modeling the effects of land use change on the water temperature in unregulated urban stream. Journal of Environmental Management, 49, 445-469.

Macdonald, R.W., Griffiths, R.F., Hall, D.J., 1998. An improved method for the estimation of surface roughness of obstacle arrays. Atmospheric Environment, 32, 1857-1864.

Malcolm, I.A., Soulsby, C., Hannah, D.M., Bacon, P.J., Youngson, A.F., Tetzlaff, D., 2008. The influence of riparian woodland on stream temperatures: implications for the performance of

juvenile salmonids. Hydrological Processes, 22, 968-979.

Mohseni, O., Erickson, T.R., Stefan, H.G., 1999. Sensitivity of stream temperature in the United States to air temperatures projected under a global warming scenario. Water Resources Research, 35, 3723-3733.

Mohseni, O., Stefan, H. G., 1999. Stream temperature/air temperature relationship: a physical interpretation, Journal of Hydrology, 218, 128-141.

Prats, J., Val, R., Armengol, J., Dolz, J., 2010. Temporal variability in the thermal regime of the lower Ebro River (Spain) and alteration due to anthropogenic factors. Journal of Hydrology, 387, 105-118.

Prats, J., Val, R., Dolz, J., Armengol, J., 2012. Water temperature modeling in the Lower Ebro River (Spain): Heat fluxes, equilibrium temperature, and magnitude of alteration caused by reservoirs and thermal effluent. Water Resources Research, 48, W05523. doi: 10.1029/2011WR010379.

Sinokrot, B.A., Gulliver, J.S., 2000. In-stream flow impact on river water temperatures. Journal of Hydraulic Research, 38, 339-349.

Sinokrot, B.A., Stefan, H.G., 1993. Stream temperature dynamics: measurements and modeling. Water Resources Research, 29, 2299-2312.

Sinokrot, B.A., Stefan, H.G., 1994. Stream water-temperature sensitivity to weather and bed parameters. Journal of Hydrological Engineering, 120, 722-736.

Tung, C.P., Lee, T.Y., Yang, Y.C., 2006. Modeling climate-change impacts on stream temperature of Formosan landlocked salmon habitat. Hydrological Processes, 20, 1629-1649.

Webb, B.W., Clack, P.D., Walling, D.E., 2003. Water-air temperature relationships in a Devon river system and the role of flow. Hydrological Processes, 17, 3069-3084.

Webb, B.W., Zhang, Y., 1997. Spatial and seasonal variability in the components of the river heat budget. Hydrological Processes, 11, 79-101.

Webb, B.W., Zhang, Y., 1999. Water temperatures and heat budgets in Dorset chalk water courses. Hydrological Processes, 13, 309-321.

Webb, B.W., Hannah, D.M., Moore, R.D., Brown, L.E., Nobilis, F., 2008. Recent advances in stream and river temperature research. Hydrological Processes, 22, 902-918.

Chapter 3
Modeling of Stream Temperature Considering Natural and Anthropogenic Processes

3.1 Review and purpose

The historical analysis in previous chapter was based on the monthly measurements of water temperature and flow rate, and the meteorological stations are located a few kilometers away from the river environment. Therefore, in this chapter, we carried out the intensive field measurements to collect more elaborate and continuous information within the river environment during several days in summer and winter seasons. As such, the accuracy and reliability of the historical analysis can be verified using the present-day measurements.

As biological behaviors are very sensitive to water temperature and changes in temperature can significantly alter fish distribution, growth, mortality, production, and community dynamics (Mahea et al., 2013), there is a necessity to predict the water temperature and quantify the impacts of corresponding energy elements. For this purpose, modeling tools were introduced in this chapter. As reviewed in Chapter 1, among all river temperature models, the deterministic model remains the most efficient tool that underlies physics of heat exchange between river water and its surrounding environment. Although many studies have utilized the deterministic models to predict river water temperatures and to quantify the heat fluxes, few studies cover all of the processes significant in predicting stream temperature variations (e.g. lateral inflows/inflowing heat by tributary, wastewater and groundwater and water-streambed heat exchanges) and consider the longitudinal variability in stream water temperature in response to strong anthropogenic impacts.

Therefore, the other purpose of this chapter was to develop a 1-D dynamic model for river flow and heat transport interacted with the sediment and anthropogenic heat input by wastewater effluents. This model was then applied to the middle and downstream reaches of the Tama River and was calibrated using the intensive field measurement data.

3.2 Intensive field measurement

Intensive field measurements were conducted to obtain the in-stream data for analysis.

Surface and subsurface water temperatures, stream flow rates, radiant fluxes as well as the meteorological conditions were intensively recorded. Water temperature sensors were placed approximately 0.5–1 m (in the middle of the water depth) below the water surface in the main flowing area. A meteorological station was installed at Met. site suited in the downstream reach (**Figure 3.1)**, recording air temperature, relative humidity, wind speed and direction (**Figure 3.2 (a)**). Beside it, a four-component radiometer was placed to monitor radiant fluxes, such as upward and downward shortwave radiations and upward and downward longwave radiations (**Figure 3.2(b)**). A sampling interval of 1 minute was adopted for these weather condition and radiant energy. In addition, water-streambed heat conduction and sediment water temperature (25 cm-depth in summer and 26 cm-depth in winter) were measured at the Met. site as well.

The float method (also known as the cross-sectional method) was applied to measure stream flow rate at several sites. The flow rate was calculated by multiplying a cross sectional area (equal to water depth multiplied by transverse interval) by the velocity of water (at 60% of the water depth) at equal intervals (every 1, 1.5 or 2 meters) transversely at each transection. The details of measurements in summer and winter seasons are summarized in **Table 3.1**. According to the field observation, the sediment material comprises predominantly of gravel and sand at and nearby the monitoring site.

3.3 Observed results

3.3.1 Stream flow rate and temperature

The measured flow rate patterns in summer and winter seasons are given in **Figure 3.3**, showing virtually identical trends with historical analysis (**Figure 2.1**). An abrupt decrease between S1 and S2 was observed due to water withdrawals for drinking and agriculture water (**Figure 3.3 (a)**). From S3, the river flow recovered mainly due to the addition of tributary inflows and wastewater effluents. Moreover, the values of measured flow rate at each site were found lying within the similar range with the historical results (**Figure 2.1**).

The daily mean temperatures at measurement sites over the entire period are displayed in **Figure 3.4**. It was noted that in summer, the averaged stream temperature changes, per unit distance, between S1 and S2 and between S2 and S3 were 0.43 °C/km and 0.73 °C/km, respectively. This consists with the historical analysis (section 2.4.1), which was attributed to the interacted effects of the reduced flow rate between S2 to S3 and the intense solar radiation in summer seasons. In general, the overall temperature trends in spatial scale were

similar to the historical analysis: a gradual increase towards the equilibrium state at downstream sites in summer season; a notable increase between S3 and S4, the highest value at S6 and slight decrease until the further downstream S8 in winter season. However, one point worth noticing was that in summer, a temperature decrease between S3 and S4 was observed, which contradicted with the historical finding showing a temperature increase (**Figure 2.2 (a)**). The reason for this different point will be figured out in later analysis (sections 4.7).

Other than surface temperature, increasing attentions have been given to the monitoring and modeling of temperature patterns within the streambed or hyporheic zone. The interaction of surface and groundwater is dependent on many factors, such as streambed elevation, substrate material and porosity, and water table of surface and groundwater (Caissie and Giberson, 2003). **Figure 3.5** plotted the time series of surface and sediment water temperatures (25cm deep in summer and 26 cm deep in winter) recorded at Met. site during intensive measurements. It should be noted that the sediment temperature varied substantially during the day. This variation was found clearly correlated with the water temperature with a slight shift in phase resulting from travel time and a reduced amplitude owing to conduction (the daily amplitude was calculated at 5.224 °C and 4.490 °C for surface and sediment temperatures in summer, and 2.904 °C and 2.900 °C for surface and sediment temperatures in winter). Normally, surface water temperature was warmer in summer and cooler in winter than intragravel temperatures with cross-over periods in spring and fall (Caissie and Giberson, 2003). However, according to our measurements, the monitored sediment temperatures were at any time below the surface water temperature in both winter and summer seasons.

3.3.2 Meteorological conditions

Figure 3.6 showed the time series of monitored radiant fluxes, i.e. incident solar radiation, upward shortwave radiation, upward and downward longwave radiations, heat conduction through riverbed, as well as the latent and sensible heat fluxes calculated based on measurements using Eqs. (2.10)-(2.16). Daily totals of incoming and outgoing heat energy to the river water (at Met. site) were integrated based on the 10-minute dataset over 2012.8.2 12:00 to 2012.8.3 12:00 for summer and 2013.2.7 12:00 to 2013.2.9 12:00 for winter (**Table 3.2**).

As expected, the solar radiation accounted for most of the energy input with daily total contribution of 23.6 MJ m^2 day^{-1} in summer and 10.8 MJ m^2 day^{-1} in winter. The heat gains

from net long-wave radiation were offset by the loss due to outgoing long-wave radiation, so that the budget was always negative with the daily total heat losses calculated at -4.9 MJ m^2 day^{-1} in summer and -9.1 MJ m^2 day^{-1} in winter. The effects of evaporative heat flux (-3.9 MJ m^2 day^{-1} in summer and -5.7 MJ m^2 day^{-1} in winter) were comparable to the net longwave radiation. The sensible heat transfer depends primarily on the temperature difference between water and air as well as wind velocity. Therefore, normally it transports from the atmosphere to the stream in summer whereas in winter it goes an opposite direction. The sensible heat in summer day was calculated at 0.2 MJ m^2 day^{-1}, contributing to a heat gain of 0.3 MJ m^2 day^{-1} during the daytime and a heat loss of 0.1 MJ m^2 day^{-1} at night. The sensible heat flux was found in a lower magnitude in summer than in winter (-3.4 MJ m^2 day^{-1}) with correspondingly minor differences between the water and air temperatures in summer days. Compared with heat fluxes discussed above, the recorded bed conduction from heat flux plate was of minor importance, with the contribution of -0.08 MJ m^2 day^{-1} in summer and -0.04 MJ m^2 day^{-1} in winter. Similar heat budget analysis has been reported by Evans et al. (1998).

3.3.3 Water and heat budgets

To verify the relative contribution of each energy component to water and heat budgets that concluded from the historical study (section 2.4), and also to quantify the present-day situation, we analyzed the water and heat budgets relying on the same methods in previous chapter (Eqs. (2.1)-(2.16)).

Considering the data availability on flow rate and water temperature, several segments were selected: S2-S3, S3-S4 and S4-Keio in summer and S3-S4 and S4-Keio in winter (see **Figure 3.1** for site information). Results are presented in **Figure 3.7**, in which the flow rate and heat flux are the daily averages of measured and calculated results over 2012.8.2 12:00 to 2012.8.3 12:00 for summer and 2013.2.7 12:00 to 2013.2.9 12:00 for winter (the upstream inflow (Q_i) and downstream outflow (Q_o), as well as the tributary inflow (Q_t) in water balance are based on once measurement). Results indicated a dominant role of tributary in upstream reach S2-3 and of wastewater in middle and downstream reaches of S3-4 and S4-Keio, which agreed with the historical findings in section 2.4.3.1. As the groundwater and water withdrawal behaviors have not been directly quantified with this method, we can observe the negative Q_{other} and H_{other} representing the combined effects of them. This was further supported by the good agreements between H_{other} and $H_{estimate}$. However, the water withdrawals were found of insignificant volume, especially in winter

seasons and were mostly intermittent, in this sense, the Q_{other} and H_{other} might be considered to primarily stand for the groundwater behavior.

3.4 Modeling of stream and sediment temperatures

3.4.1 Model description

To investigate factors affecting stream temperatures, we developed a physical model that simulates unsteady river flows and accompanied heat transports. The heat transport processes considered in the model for a stream reach are summarized schematically in **Figure 3.8**.

For simulating river flow velocity and depth, the continuity equation (Eq. (3.1)) is used with the Saint-Venant momentum equation (Eq. (3.2)).

$$\frac{\partial Q}{\partial x}+\frac{\partial A}{\partial t}-q=0\,, \tag{3.1}$$

$$\frac{\partial Q}{\partial \mathrm{t}}+\frac{\partial(\beta Q^2/A)}{\partial x}+gA\left(\frac{\partial h}{\partial x}-S_o+S_f\right)=0\,, \tag{3.2}$$

where q: lateral inflow per unit length, Q: flow rate, A: cross-sectional area, g: gravitational acceleration, h: water depth, S_o: bottom slope, S_f: energy slope ($=n^2|Q|Q/A^2R^{4/3}$), β: momentum correction coefficient, n: Manning's roughness coefficient, R: hydraulic radius, x: longitudinal distance and t: time. The sinuosity effect of the stream was neglected. The momentum coefficient was set to 1.1 over the stream reaches, although simulation results are not sensitive to this value.

The governing equation for one dimensional heat transfer in a well-mixed stream is expressed as

$$\frac{\partial(AT)}{\partial t}+\frac{\partial(\eta QT)}{\partial x}=\frac{\partial}{\partial x}\left(AD_L\frac{\partial T}{\partial x}\right)+\frac{H_r B}{\rho C_w}+\frac{H_{bed}W}{\rho C_w}+qT_0\,, \tag{3.3}$$

where T: water temperature, η: heat flux correction factor (=1.1), D_L: longitudinal dispersion coefficient, B: river width, W: wetted perimeter of the river, ρ: water density, C_w: heat capacity of water, T_o: water temperature of inflow, H_r: heat exchanges at the air-water interface, H_{bed}: convective heat flux transported from the riverbed surface to the stream. D_L was set by D_L/u_*h= const. (=1000 in our cases) (Fischer et al., 1979). The sun shading was neglected, as there are few riverine vegetation in our study reaches and the river is wide enough to limit shaded area on the water surface.

The total heat exchange at the air-water interface (H_r) is the sum of several components as described in Eqs. (3.4) and (3.5).

$$H_r = R_{net} - H - LE\,, \tag{3.4}$$

$$R_{net} = S_{wat} + S_{wat2} + L_d - L_u = b_{wat}\left[1 + al_{bed}\left(1 - b_{wat}\right)\right]\left(1 - al_{wat}\right)S_d + L_d - L_u\,, \tag{3.5}$$

where R_{net}: net radiation, H: sensible heat flux, LE: latent heat flux, $S_{wat,}$ S_{wat2}: incident solar radiation absorbed by the stream water before and after reaching the streambed, L_d: downward longwave radiation, L_u: upward longwave radiation, S_d: global solar radiation, al_{bed}: albedo of riverbed, al_{wat}: albedo of water surface, b_{wat}: water absorption ratio. Measured incident solar radiation was used because the shading effect was negligible due to the limited vegetated canopies in the reaches we studied. The downward longwave radiation (L_d) and upward longwave radiation (L_u) are calculated using Kondo's (1994) method as described in Eqs. (2.6)-(2.9) in Chapter 2. The albedo of riverbed (al_{bed}) and water surface (al_{wat}) are derived from the field observation as 0.27 and 0.04, respectively. Water absorption ratio (b_{wat}) was given by Eq. (3.6), with the parameters set utilizing our field measurement data and referring to paper by Kobatake et al. (1997).

$$b_{wat} = 0.6 + 0.4\left(1 - \exp\left(-1.783\left(h - 0.1\right)\right)\right). \tag{3.6}$$

Sensible and latent heat fluxes in Eq. (3.4) were determined by applying the Monin-Obukhov similarity theory to the surface layer above the river. They were estimated from the bulk expression of the similarity theory as defined in Eqs. (3.7)-(3.9).

$$\frac{\rho_a}{E} k u_* \left(q_s - q\right) = \int_{\zeta_q}^{\zeta_z} \frac{\phi_e(\zeta)}{\zeta} d\zeta \equiv \Psi_e\,, \tag{3.7}$$

$$\frac{c_{pa}\rho_a}{H} k u_* \left(\theta_s - \theta\right) = \int_{\zeta_T}^{\zeta_z} \frac{\phi_h(\zeta)}{\zeta} d\zeta \equiv \Psi_h\,, \tag{3.8}$$

$$\frac{1}{u_*} kU = \int_{\zeta_0}^{\zeta_z} \frac{\phi_m(\zeta)}{\zeta} d\zeta \equiv \Psi_m\,, \tag{3.9}$$

where ρ_a: air density, c_{pa}: specific heat of the air, u_*: friction velocity of air, k: Karman's constant (=0.4), E: flux of water vapor at the surface, θ, θ_s: potential temperature of air and at the water surface, $\zeta_z = z/L$, $\zeta_q = z_q/L$, $\zeta_T = z_T/L$, ϕ_e, ϕ_h, ϕ_m: universal functions for the vertical gradient of specific humidity, air temperature and wind velocity, respectively, Ψ_e, Ψ_h, Ψ_m: integrated universal functions for specific humidity, air temperature and wind velocity. The universal functions can take the forms of Eqs. (3.10)-(3.12). For unstable conditions ($-1<\zeta<0$), Eqs. (3.10) and (3.11) are applied, for stable conditions ($\zeta>0$), Eq. (3.12) is assumed.

$$\phi_m = \left(1 - 16\xi\right)^{-1/4}\,, \tag{3.10}$$

$$\phi_h = \phi_e = (1-16\zeta)^{-1/2}, \tag{3.11}$$

$$\phi_m = \phi_h = \phi_e = 1+7\zeta, \tag{3.12}$$

The Monin-Obukhov stability length L is defined as follows.

$$L = \frac{{u_*}^2\theta}{kgT_*} = -\frac{c_{pa}\rho_a {u_*}^3\theta}{kgH}, \tag{3.13}$$

where T_*: temperature scale. The roughness heights of momentum, latent and sensible heat transports z_0, z_q, z_T were assumed to be given by Eq. (3.14) (Brutsaert, 1982),

$$z_0 = 0.135\nu/u_*, \quad z_q = 0.624\nu/u_*, \quad z_T = 0.395\nu/u_*, \tag{3.14}$$

where ν: kinematic molecular viscosity of air. These equations were used in the model, giving the air temperature, relative humidity and wind velocity measured over the water surface.

Heat exchange between the stream and sediment was modeled by the advection-dispersion equation (Eq. (3.15)), assuming the thermal equilibrium between sediments and water, and no transversal heat advection in the ground (Constantz et al., 2002).

$$[\phi C_w + (1-\phi)C_s]\frac{\partial T_g}{\partial t} = \lambda_{eff}\frac{\partial^2 T_g}{\partial z^2} - Q_g C_w \frac{\partial T_g}{\partial z}, \tag{3.15}$$

where T_g: temperature of water in the sediment pore (equals to the sediment temperature at the same location), C_s: heat capacity of sediment material, ϕ: porosity, z: vertical distance from the water-sediment interface (positive downward), λ_{eff}: effective thermal conductivity, Q_g: the vertical velocity of groundwater (positive for recharging water).

In Eq. (3.15), the groundwater flows through the sediment were assumed to be one dimensional in the vertical direction so that the horizontal (lateral and longitudinal) flows were neglected in this study. However, a number of recent studies show that the hyporheic exchange, where surface water enters the shallow subsurface (channel bed, banks or morphological features) and then reemerges back into the main stream, works as an important flow path of surface water (Kasahara and Wondzell, 2003) and thus plays a key role in the thermal dynamics of some streams (Story et al., 2003; Johnson, 2004). Acuna and Tockner (2009) investigated the thermal patterns controlled by surface-subsurface water exchange for four alluvial reaches in the Tagliamento River (Italy). Their study revealed that as much as 21% to 52% of the water flows through the hyporheic compartment; more importantly, the hyporheic exchange flows were found to shape the surface temperature and reduce the temperature extremes, which created potential local thermal refugia for aquatic

biota. Burkholder et al. (2008) demonstrated that in summer, the hyporheic discharge comprised a small fraction (<<1%) of mainstream discharge along a 24-km reach of the lower Clarkamas River (U.S.), which resulted in small river-cooling effects (0.012°C).

As the hyporheic flow paths can have different temperatures and chemical conditions relative to the groundwater flow paths (Fanelli and Lautz, 2008), there arises a need recently to distinguish between groundwater and hyporheic components of groundwater-surface water interactions (Jones and Mulholland, 2000). However, it was also reported that in some stream reaches, due to the shared pressure distribution, the predominantly vertical groundwater flux worked to suppress the shallow hyporheic exchange flow (Wondzell and Swanson, 1996; Cardenas and Wilson, 2007). For example, Binley et al. (2013) quantified the vertical and horizontal water fluxes at the groundwater-surface water interface along a 200 m reach by coupling Darcian flow estimates with in-stream piezometer tracer dilution tests. They found that in the upper section of the reach, the hyporheic exchange was suppressed at locations with localized connectivity to the regional groundwater; whereas in the further downstream section, the hyporheic exchange appeared to contribute more to the subsurface flow due to the reduced groundwater upwelling. In addition, Bhaskar et al. (2012) showed that the magnitude of hyporheic and groundwater fluxes are largely independent until the groundwater fluxes exceed hyporheic fluxes by orders of magnitude (100- to 1000-fold) using a one-dimensional heat transport model. They suggested that the incorporation of both hyporheic and groundwater fluxes can be achieved by conceptualizing the bed form-scale hyporheic flow as enhanced thermal dispersion. Following their study as well as those by Healy and Ronan (1996), Hatch et al. (2006) and Hopmans et al. (2002), λ_{eff} in the present study is used to represent the combined effects from conduction in the bulk sediment and thermal dispersion of groundwater, and is formulated by Eq. (3.16) neglecting the dispersion in the direction perpendicular to z.

$$\lambda_{eff} = \lambda_0 + C_w \beta_L \left| Q_g \right| = (1-\phi)\lambda_s + \phi\lambda_w + C_w \beta_L \left| Q_g \right|, \tag{3.16}$$

where β_L: longitudinal dispersivity, λ_0: bulk sediment thermal conductivity, λ_s, λ_w: thermal conductivity of sediment materials and water. The third term on the right side of Eq. (3.16) represents the increase in effective thermal diffusivity caused by hydro-dynamic dispersion. If there is no interaction between stream water and groundwater, the effect of dispersion disappears and λ_{eff} equals the bulk thermal conductivity λ_0.

The heat balance on the riverbed surface is written by Eqs. (3.17a) and (3.17b). When Q_g>0 (recharging to groundwater),

$$S_b + C_w Q_g T = G + H_{bed} + C_w Q_g T_g\big|_{z=0} = -\lambda_{eff}\frac{\partial T_g}{\partial z} + K(T_g\big|_{z=0} - T) + C_w Q_g T_g\big|_{z=0}, \quad (3.17a)$$

When Q_g<0 (outflowing to the stream),

$$S_b - C_w Q_g T_g\big|_{z=0} = G + H_{bed} - C_w Q_g T = -\lambda_{eff}\frac{\partial T_g}{\partial z} + K(T_g\big|_{z=0} - T) - C_w Q_g T, \quad (3.17b)$$

where G is heat flux into the ground modeled by the Fick's law, H_{bed} is assumed to be linearly related to the difference of temperatures between the sediment surface and stream water with constant K. S_b: incident solar radiation absorbed by the riverbed which is expressed as

$$S_b = (1 - al_{bed})(1 - b_{wat})(1 - al_{bed})S_d, \quad (3.18)$$

To evaluate relative agreement between the simulated results and the observations, the root mean square error (RMSE) will be used, which is given by

$$RMSE = \sqrt{\frac{\sum_{i=1}^{N}(O_i - S_i)^2}{N}} \quad (3.19)$$

where N: number of 10-miniute stream temperature observations, O_i: observed water temperature, S_i: simulated water temperature.

3.4.2 Model application

In this chapter, we primarily applied this model to the reach between S4 and S6 (**Figure 3.1**) possessing a purpose to calibrate the model with data collected during intensive field measurements. Although the time duration was relatively short, the detailed measurements on surface and subsurface water temperatures, stream flow rate as well as meteorological conditions were considered sufficient and accurate for calibrating the model parameters.

For simulating river flow and heat transport in the stream reach, a time step of 10 second (further integrated into 10 minute values) and a space increment of 100 m were adopted. A sensitivity analysis of the importance of the time step indicated that no significant differences in the accuracy of the solution is obtained for 1 second, 10 second and 1 minute settings. Therefore, considering the time cost and accuracy of the simulation, the time step of 10 second was adopted to run the heat transport model.

The basic equations above need to be solved numerically with the given boundary conditions. Following the work by Kinouchi and Kawahara (1998), a finite difference approach using a four-point scheme and a double sweep method was employed. A weighting factor was set at 0.75.

To run the deterministic model, there are large amount of data required as listed in **Table 3.3**. The downstream boundary condition was specified by the water level recorded at the downstream ends. The measured flow rate at upstream site was used for upstream boundary condition. Measured stream temperatures at S4 were used as an upstream boundary condition of Eq. (3.3). Weather conditions recorded at Met. site were utilized as the atmospheric forcing of the model.

The lateral inflows (Eq. (1)) considered in this chapter were from wastewater and tributary (only one major tributary was considered as marked by 'Tri.2' in **Figure 3.1**). Since no continuous records on tributary temperature were available in winter, they can be estimated by correlating to the air temperature. For this reason, a relationship between air and water temperatures was established for this tributary by plotting the monthly measured temperatures versus the instantaneous air temperatures recorded by MLIT (**Figure 3.9**). Data were selected for February individually from the year 1990 to 2013. With this relationship, it is able to estimate the continuous tributary water temperature from the air temperature recorded at M4 (see **Figure 1.**2 for site).

The real cross–section shape at intervals of 200 m along the mainstream, after being modified, was used. The bottom slope was obtained from the map issued by the MLIT local office.

Space increment for the heat advection-dispersion in the sediment was set to 1cm. As noted by Caissie and Giberson (2003), the temperature of groundwater below 100-cm depth is considered to remain constant during a certain period but vary seasonally. Therefore for each individual simulation period, a constant sediment temperature at 2m–deep was given as the bottom boundary condition of Eq. (3.15), the value of which was determined partially by referring to the measured stream and air temperatures but mainly by model calibration process. This value was then regarded as constant over space and time (within each individual simulation period).

The groundwater velocity through the sediment is assumed to be one dimensional in the vertical direction and that the flux is constant over space and time (within each individual simulation period). For each period, the flow gains from, or losses to groundwater in the stream was determined by water budget analysis, in which the groundwater flux was calculated as a residual from the monthly measured flow rates at the upstream and downstream ends and at tributaries (from MLIT), and the discharge volume from WWTPs. The groundwater flow was assumed to be evenly distributed over the length of the river. A similar way can be found in Younus et al. (2000), in which the subsurface flow was

computed by subtracting the measured upstream flow from the downstream flow. The temperature of groundwater outflows to stream was determined as the simulated sediment temperature at the riverbed surface, whereas the temperature of groundwater recharge was equated with stream temperature.

Parameters used for river flow and thermal properties were summarized in **Table 3.4**. The effect from water withdrawal was not considered, since no measurements were available and the flow alteration resulted from this process along our simulation reach was found negligible according to the official report.

3.4.3 Simulated results

Model performance results are presented in **Figures 3.10 and 3.11** for summer and winter cases respectively. Basically, this model was applied to the reach between S4 and S6; while in winter season, instead of S4, Keio was used as the upstream boundary due to the malfunction of stream temperature at S4. In this case, it is able to calibrate the model by the observed surface temperatures at Keio, Met. and S6 (Met. and S6 in winter), as well as the subsurface temperature at Met. site.

During the attempts to calibrate the model to observed temperatures, it became clear that the results are determined predominantly by five factors. They are the longitudinal dispersivity (β_L), the flux of groundwater Q_g, the sediment temperature at 2-m depth, the heat transfer coefficient K along with the longitudinal dispersion coefficient D_L/u_*h. Results showed a satisfactory agreement between the observed and simulated stream temperatures, with the root mean square error (RMSE) calculated on average at 0.43 °C for surface temperature and 0.34 °C for sediment temperature for both seasons. The explicit RMSE values for each case were included in the corresponding figures. Tributary was counted as one of the lateral inflows in the model so that the monitored (in summer) and estimated (in winter) tributary temperatures have been plotted in the figures showing temperatures at S6 as reference.

The setting of parameters (**Table 3.4**) was determined by model calibration as well as by referring to the literatures as discussed below.

(1) Manning's roughness coefficient n ($s/m^{1/3}$): for an open channel with gravel bottom, the typical manning's n is suggested at 0.020 ($s/m^{1/3}$) for concrete side, at 0.023 ($s/m^{1/3}$) for mortared stone side and at 0.033 ($s/m^{1/3}$) for riprap side (Chow et al., 1988), so that in the case of the Tama River, which has relative coarse sediments with fractions of sand, gravel and stone, the value of 0.025 ($s/m^{1/3}$) lies within the proper range.

(2) Dispersion constant $D_L/(u_*h)$: dispersion is known as the interaction of turbulent diffusion with velocity gradients caused by shear forces in the water body that causes a greater degree of mixing (Schnoor, J.L., 1996). A longitudinal dispersion coefficient is applied to model this process. However, Fischer et al. (1979) reported that this parameter in real streams varies widely, which reflects its site-specific nature. After calibration, $D_L/(u*h)$ was set to 1000 in this study that lies within the acceptable range indicated by Fisher et al.(1979).

(3) Bulk sediment thermal conductivity λ_0(W/m/K): is a function of mineral type and geometrical arrangement of various phases, as well as the water content. For a sand channel this value is likely to vary between 1.0 and 2.0 W/m/K (Constantz et al., 2002).

(4) Porosity ϕ: the porosity stands for the ratio of the volume of voids to the total volume of the porous medium, ranging from 25 to 40 (%) for gravel and 25 to 50 (%) for sand (Chow et al., 1988).

(5) Heat capacity of sediment C_s ($J/m^3/K$) can be determined from the specific heat and density of the sediment constituent. Hopmans et al. (2002) used a similar value of 1.92E+6 for sandy sediment.

Once the model parameters were physically fixed or calibrated as shown in Table 3.3, the same values of the parameters will be applied throughout all seasons for the further study regarding diurnal and seasonal stream temperature simulation (in Chapter 4). Note that the groundwater flux and sediment temperature at 2-m deep were the only two exceptions to this rule, both of which vary with seasons; thus these two parameters will be specifically calculated or calibrated for each individual simulation period.

3.5 Sensitivity analysis

As the accuracy and reliability of model behavior are highly dependent on input data and setting of parameters, a further investigation on sensitivity analysis was carried out to understand how the simulation results would behave in response to variations of input data and parameters.

When carrying out sensitivity analysis, typically one model parameter or input data type is varied at a time, usually by a fixed percentage of a state variable while all the others remain unchanged. Among those listed in **Tables 3.3** and **3.4**, seven items were targeted, including tributary, evaporation, groundwater flux (Q_g), sediment temperature at 2m-depth

($T_g \mid_{z=200}$), longitudinal dispersivity (β_L), heat transfer coefficient (K) and longitudinal dispersion constant ($D_L/(u*h)$).

The sensitivity test was conducted for reach S4 to S6 and Keio to S6 for the summer and winter intensive measurement periods, respectively. As discussed above, the model performance was firstly evaluated by adjusting the calibration parameters and by comparing model results against the observations. Once the best performance was achieved (e.g. RMSE at S6 was 0.25°C for summer and 0.10°C for winter), the parameters assigned in **Table 3.4** and the resulting simulations at S6 in **Figures 3.10** and **3.11** were regarded as the benchmark for comparison. A sensitivity parameter SP was introduced which is defined as the ratio of change in criteria over change in target parameter (Schnoor, 1996),

$$SP = \frac{\Delta RMSE / RMSE}{|\Delta P / P|} \times 100\% \tag{3.20}$$

where $\Delta RMSE$: change of RMSE at S6, $RMSE$: $RMSE$ under reference condition, P is the target parameter being assessed, ΔP: change of parameter value, P: parameter value under reference condition.

3.5.1 Sensitivity to input data

(1) Tributary effect

Due to a lack of data on continuous tributary temperature, the sensitivity test was carried out to assess the effects of tributary inflows on stream temperature. Results were compared between cases with and without considering tributary. As shown in **Table 3.5**, the RMSE increased at a rate of 0.04 °C and 0.10 °C, when tributary effects were eliminated for summer and winter seasons, respectively. Moreover, the SP values were calculated at 19% and 10%, suggesting that the simulated stream temperature was not that sensitive to tributary effects.

As a result, it is acceptable to use the estimated tributary temperature when suffering from data scarcity in our further study.

(2) Evaporation

River evaporation as latent heat has been recognized as an important heat loss factor in river water temperature modeling (Maheu et al., 2013). However, water loss due to evaporative process, which might alter the stream flow rate and further affect heat capacity, has been neglected both for water balance analysis and for temperature modeling in this study. In this chapter, the effect of evaporation was examined by applying the mass transfer

method in Eq. (2.11).

As shown in **Figure 3.12,** the rate of evaporation displayed a diurnal variation basically following the wind velocity and saturated vapor pressure, which accounts for a rate at 0.01 m^3/s of water loss over the reach S4 to S6 for both seasons. Compared with other flow elements indicated in **Figure 3.7**, the water loss through evaporation explained such a small amount in water balance that could be assumed as negligible in our further study.

(3) Downward longwave radiation

In the historical analysis (Chapter 2), downward longwave radiation from the atmosphere was calculated using Eqs. (2.6)–(2.8); while these equations were originally proposed to obtain the daily mean values (Brutsaert, 1982). In contrast, methods for estimating downward longwave radiation in a shorter interval, e.g. 10 minutes, have been rarely specified in the literature. Therefore, the same method will be applied to obtain the 10-minute downward longwave radiation for temperature modeling purpose in our further study. Once the actual on-site data were collected during the intensive field measurements, comparisons could be made in order to validate this calculation method.

One point worth noticing, when calculating the 10-minute data, was that during the night time, sunshine duration in Eq. (2.8) are recorded as none, which is thus no longer an effective index reflecting the cloud cover condition; instead, the fractional cloud cover (m_c) was introduced to obtain an index equivalent to N_c (fraction of sunshine hours) using the following correlation (Brutsaert, 1982).

$$aN_c + bm_c = 1 \tag{3.21}$$

where a=1.11 and b=0.78 were derived by Kondo (1967) from data in Japan. The cloud cover fraction (m_c) was recorded at M1 (**Figure 1.2**) by Japan Meteorological Agency.

Figure 3.13 showed the comparison results between the observed and calculated downward longwave radiations with 10 minutes interval. In general, good agreements were observed between the observed and calculated data, especially during the summer period. However, slightly larger gap was found in winter period approximately from the noon time of February 8 to the midnight, with an overestimation at about 40 W/m^2.

Furthermore, the resulting effect on stream temperature, by applying the calculated downward longwave radiation as an alternative of the observed data, was quantified. As shown in **Figure 3.14**, results indicated rather minor differences in the simulated temperatures by using the observed and calculated downward longwave radiations as input. This is applicable to both seasons, with the changes in RMSE at 0.01 °C for summer and

0.07 °C for winter (RMSE between observed and simulated temperatures are indicated in the **Figure 3.14** legend), respectively. As a result, the slight underestimation/overestimation of downward longwave radiation has resulted minor error of simulated water temperature, which was considered as negligible in this study.

3.5.2 Sensitivity to parameters

Sensitivity of simulated temperature were analyzed independently for a fixed change (e.g. ±10%, ±30%, ±50%, ±100% and +500%) of several target parameters, i.e. groundwater flux Q_g, sediment temperature at 2m-depth ($T_g \mid_{z=200}$), longitudinal dispersivity (β_L), heat transfer coefficient (K) and longitudinal dispersion constant ($D_L/(u*h)$).

Results were summarized in **Tables 3.6** to **3.10** for five parameters, respectively. In each table, the reference condition, as indicated by 0% changes of parameters, has the smallest RMSE value between the observed and simulated stream temperatures. The setting of parameters after increasing or reducing a certain percentage, as well as its resulting average water temperature, RMSE, and SP compared with the reference case were also included. We found that the sediment temperature at 2-m depth ($T_g \mid_{z=200}$) was the most sensitive parameter (**Table 3.7**), with SP greater than 1000 (%) for its ±10% and ±30% variations in both seasons.

Comparatively, the groundwater flux (Q_g) and longitudinal dispersivity (β_L) were the next group, with SP ranging from 0 to about 200 (%) (**Tables 3.6** and **3.8**). These two parameters were both determinant for the thermal dispersion caused by groundwater flows as indicated in Eq. (3.16), therefore can have an influence on the heat transport through water-streambed interface.

Other parameters were found insensitive, such as heat transfer coefficient (K) and longitudinal dispersion constant ($D_L/(u*h)$), as indicated by SP lower than 10 (%) (**Tables 3.9** and **3.10**). Notably, an exception was observed for both seasons when K was set to zero (**Table 3.9**), i.e. RMSE increased a lot and SP reached more than 200 (%). The reason was that in the model, the heat convection at the riverbed surface (H_{bed}) would totally disappear when K equals to zero, while the advective heat by groundwater flow and radiant heat absorbed by riverbed become the only heat sources from the sediment. As a result of less influenced by heat from the sediment, the simulated water temperature changed significantly.

3.6 Summary

In this chapter, the intensive field measurements were conducted in summer and winter seasons to collect more elaborate and continuous data on surface and subsurface water temperatures, stream flow rates, radiant fluxes and meteorological conditions. Comparing to historical analysis, consistent results were obtained through the intensive study, e.g. tendency of spatial variation of stream temperature and flow rate, and water and heat budgets. Therefore, the accuracy and reliability of historical analysis were confirmed by the present-day intensive measurements.

To predict water temperature and quantify heat flux, we developed a 1-D deterministic model for river flow and heat transport interacted with the sediment and anthropogenic heat input. The groundwater flows and heat transport through the sediment were assumed as 1-D (vertical direction) processes in our model, although, in fact, we may have mixed flows of groundwater recharge, groundwater outflows (into stream) and hyporheic flow (horizontal direction). Our assumption can be reasonable because some studies have proven that the 1D vertical model is able to represent hyporheic flow effects, e.g. by the enhanced effective thermal conductivity (Bhaskar et al., 2012).

This model was primarily applied to the middle to downstream reach (S4-6) of the Tama River and was calibrated using the observed surface and sediment water temperatures. A variety of parameters relating to the river flow and heat transports in the mainstream and the sediment were calibrated; the values of which will be used in the further temperature simulation regarding long-term diurnal and seasonal variations (Chapter 4).

Moreover, the sensitivity analysis in this chapter has provided a reference base for the further parameterization in modeling stream temperature. Results suggested that the sediment water temperature as a boundary condition was the most important in controlling the water temperature; while groundwater flux (Q_g) and longitudinal dispersivity (β_L) were the next group. Others were not sensitive as indicated by SP bounded within 10%.

Table 3.1 Summary of intensive field measurements in summer and winter seasons.

Measurement	Season	Location	Time	Interval
Radiant fluxes; Meteorological conditions; Sediment temperature; Heat conduction into the ground	summer	Met.	2012/8/2 10:00-2012/8/3 16:00	1 min
	winter	Met.	2013/2/7 12:00-2013/2/9 12:00	1 min
Stream temperature	summer	S1, Ozku, S2, S3, S4, Keio, Met.[a)], S6, S8, Tri.2	2012/8/2 00:00-2012/8/7 00:00	10 min
	winter	S3, S4, Keio[b)], Met., S6, S8	2013/2/7 12:00-2013/2/9 12:00	10 min
Flow rate	summer	S1, S2, S3, S4, Keio, Met., Tri.2	once in 2012/8/2 or 8/3	—
	winter	S3, S4, Keio, S5	once in 2013/2/8	—

[a)]Stream temperature at Met. in summer was measured from 2012/8/2 10:00 to 2012/8/3 16:00
[b)]Stream temperature at Keio in winter started from 2013/2/7 18:00.

Table 3.2 Values of daily total heat flux gains and losses to the river water (at Met. site) during the intensive measurement period.

	Summer (MJ m^{-2} day^{-1}) 2012.8.2 12:00 to2012.8.3 12:00			Winter (MJ m^{-2} day^{-1}) 2013.2.7 12:00 to 2013.2.9 12:00		
	In	Out	Balance	In	Out	Balance
Solar radiation	24.7	1.1	23.6	11.9	1.1	10.8
Longwave	35.2	40.1	-4.9	22.2	31.3	-9.1
Latent	—	3.9	-3.9	—	5.7	-5.7
Sensible	0.3	0.1	0.2	—	3.4	-3.4
Sediment	0.001	0.08	-0.08	0.003	0.047	-0.04

Table 3.3 List of main input data used in the model.

Category	Recorded (R)/Calculated (C)/ Calibrated (C*)
Upstream flow rate	R
Downstream water level	R
Cross-section shape	R
Bottom slope	R
Meteorological condition	R
Upstream water temperature	R
Wastewater temperature and volume	R
Tributary temperature and volume [a)]	R, C
Groundwater flux	C
Sediment temperature at 2m deep	C*

[a)]Tributary temperature was only recorded in summer

Table 3.4 Setting of major parameters.

River flow	Manning's n ($s/m^{1/3}$)	0.025
	Groundwater Q_g (m/s)[a)]	summer: 1.79E-6 winter: 2.68E-6
Stream temperature	Dispersion constant $D_L/(u*h)$	1000
	Heat transfer coefficient K ($W/m^2/K$)	1000
Sediment	Porosity ϕ	0.3
	Bulk thermal conductivity λ_0 (W/m/K)	1.35
	Heat capacity of sediment C_s ($J/m^3/K$)	1.84E+6
	Longitudinal dispersivity β_L (m)	9
	Sediment temperature at 2-m deep (°C)	summer: 23.5 winter: 9.0

[a)]Q_g is positive/negative when groundwater recharge/outflow to stream occurred.

Table 3.5 Sensitivity of stream temperature (S6) to tributary effect.

	Summer 2012.8.2 0:00 to 2012.8.8 12:00			Winter 2013.2.7 18:00 to 2013.2.9 12:00		
	T_M(°C)[a)]	RMSE (°C)	SP(%)	T_M(°C)	RMSE (°C)	SP(%)
With tributary	26.92	0.25	—	12.25	0.11	—
Without tributary	26.96	0.29	19	12.42	0.21	10

[a)] T_M is the mean value of simulated temperature (S6) during each period.

Table 3.6 Sensitivity of stream temperature (S6) due to ±10%, ±30%, ±50% and ±100% changes in groundwater flux (Q_g).

	Summer 2012.8.2 0:00 to 2012.8.8 12:00				Winter 2013.2.7 18:00 to 2013.2.9 12:00			
	Q_g (10^{-6}m s^{-1})	T_M(°C)[a)]	RMSE (°C)	SP(%)	Q_g (10^{-6}m s^{-1})	T_M(°C)	RMSE (°C)	SP(%)
-100%	0.00	27.48	0.85	239	0.00	12.13	0.36	237
-50%	0.89	27.18	0.37	91	1.34	12.27	0.16	106
-30%	1.25	27.08	0.29	51	1.88	12.27	0.13	66
-10%	1.61	26.98	0.25	5	2.41	12.26	0.11	22
0%[b)]	1.79	26.92	0.25	—	2.68	12.25	0.10	—
+10%	1.96	26.87	0.26	41	2.95	12.23	0.11	44
+30%	2.32	26.77	0.31	75	3.48	12.23	0.13	80
+50%	2.68	26.70	0.36	86	4.02	12.22	0.16	105
+100%	3.57	26.50	0.52	108	5.36	12.20	0.25	135

[a)] T_M is the mean value of simulated temperature (S6) during each period.
[b)] 0% represents the reference case as indicated in **Table 3.4**.

Table 3.7 Sensitivity of stream temperature (S6) due to ±10% and ±30% changes of sediment temperature at 2m-depth ($T_g \mid_{z=200}$).

	Summer 2012.8.2 0:00 to 2012.8.8 12:00				Winter 2013.2.7 18:00 to 2013.2.9 12:00			
	T_g (°C)	T_M(°C)[a)]	RMSE (°C)	SP(%)	T_g (°C)	T_M(°C)	RMSE (°C)	SP(%)
-30%	16.4	25.55	1.40	1518	7.7	11.57	0.68	1784
-10%	21.2	26.47	0.52	1081	9.9	12.02	0.24	1272
0%[b)]	23.5	26.92	0.25	—	11.0	12.25	0.10	—
+10%	25.8	27.38	0.52	1062	12.1	12.47	0.26	1406
+30%	30.6	28.29	1.39	1506	14.3	12.93	0.70	1834

[a)] T_M is the mean value of simulated temperature (S6) during each period.
[b)] 0% represents the reference case as indicated in **Table 3.4**.

Table 3.8 Sensitivity of stream temperature (S6) due to ±10%, ±30% and ±50% changes of longitudinal dispersivity (β_L).

	Summer 2012.8.2 0:00 to 2012.8.8 12:00				Winter 2013.2.7 18:00 to 2013.2.9 12:00			
	β_L (m)	T_M(°C)[a)]	RMSE (°C)	SP(%)	β_L (m)	T_M(°C)	RMSE (°C)	SP(%)
-50%	4.5	27.28	0.45	158	4.5	12.35	0.20	163
-30%	6.3	27.14	0.33	104	6.3	12.31	0.14	106
-10%	8.1	26.98	0.26	26	8.1	12.26	0.11	24
0%[b)]	9.0	26.92	0.25	—	9.0	12.25	0.10	—
+10%	9.9	26.86	0.26	51	9.9	12.22	0.11	58
+30%	11.7	26.74	0.32	94	11.7	12.18	0.15	123
+50%	13.5	26.63	0.40	122	13.5	12.15	0.19	146

[a)] T_M is the mean value of simulated temperature (S6) during each period.
[b)] 0% represents the reference case as indicated in **Table 3.4**.

Table 3.9 Sensitivity of stream temperature (S6) due to ±50%, ±100% and +500% changes of heat transfer coefficient (K).

	Summer 2012.8.2 0:00 to 2012.8.8 12:00				Winter 2013.2.7 18:00 to 2013.2.9 12:00			
	K (W m^{-2} K^{-1})	T_M(°C)[a)]	RMSE (°C)	SP(%)	K (W m^{-2} K^{-1})	T_M(°C)	RMSE (°C)	SP(%)
-100%	0	27.4	0.82	224	0	12.14	0.36	230
-50%	500	26.94	0.26	4	500	12.24	0.11	1
0%[b)]	1000	26.92	0.25	—	1000	12.25	0.10	—
+50%	1500	26.92	0.25	0	1500	12.25	0.11	2
+100%	2000	26.91	0.25	0	2000	12.25	0.11	2
+500%	6000	26.91	0.25	0	6000	12.25	0.11	1

[a)] T_M is the mean value of simulated temperature (S6) during each period.
[b)] 0% represents the reference case as indicated in **Table 3.4**.

Table 3.10 Sensitivity of stream temperature (S6) due to -50%, ±100% and +500% changes of longitudinal dispersion constant ($D_L/u_* h$).

	Summer 2012.8.2 0:00 to 2012.8.8 12:00				Winter 2013.2.7 18:00 to 2013.2.9 12:00			
	$D_L/(u_* h)$	T_M(°C)[a)]	RMSE (°C)	SP(%)	$D_L/(u_* h)$	T_M(°C)	RMSE (°C)	SP(%)
-100%	0	26.90	0.25	0	0	12.23	0.11	1
-50%	500	26.91	0.25	1	500	12.24	0.11	1
0%[b)]	1000	26.92	0.25	—	1000	12.25	0.10	—
+100%	2000	26.95	0.26	2	2000	12.27	0.11	4
+500%	6000	27.04	0.31	5	6000	12.32	0.14	8

[a)] T_M is the mean value of simulated temperature (S6) during each period.
[b)] 0% represents the reference case as indicated in **Table 3.4**.

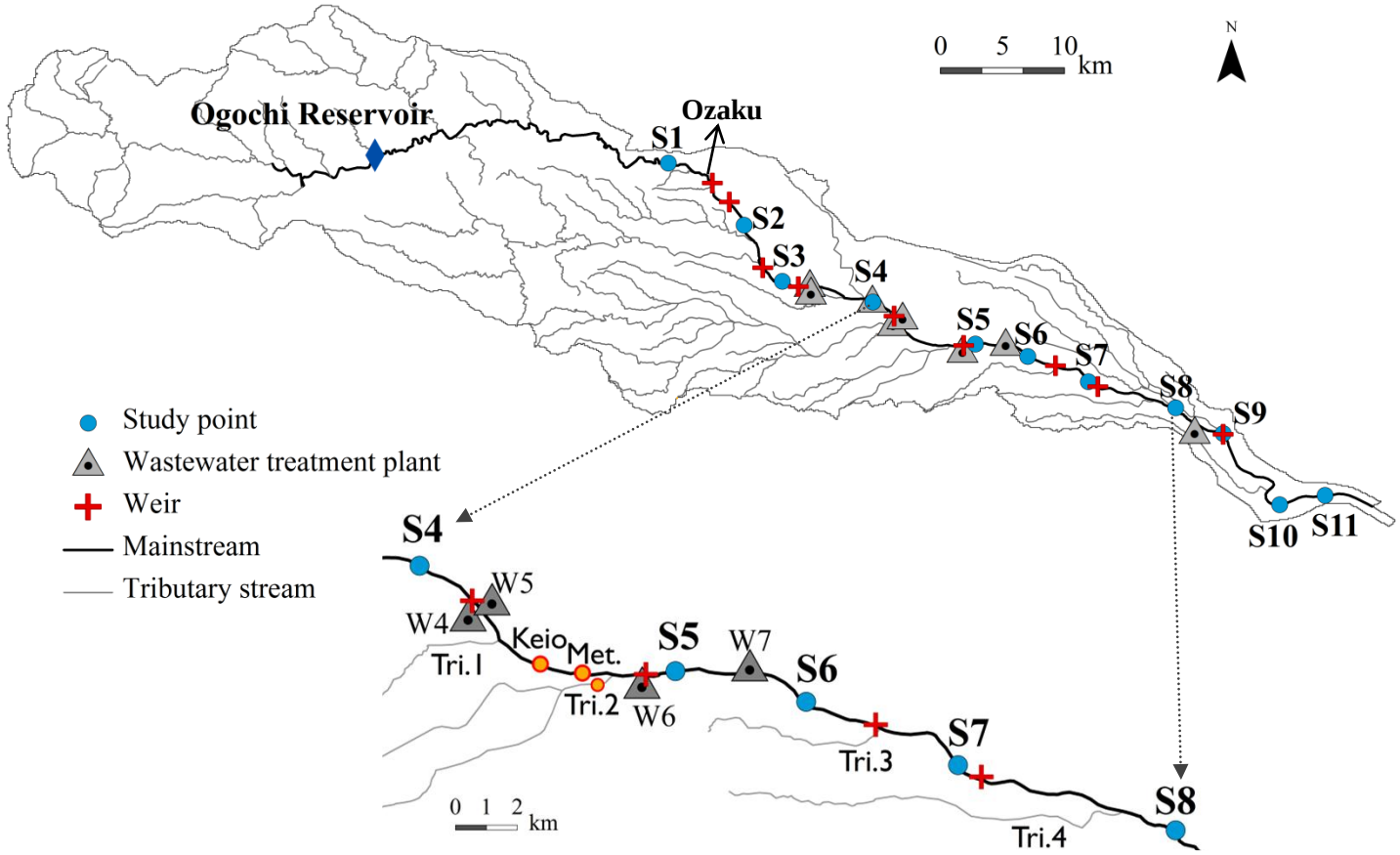

Figure 3.1 Study map indicating the locations of field measurements.

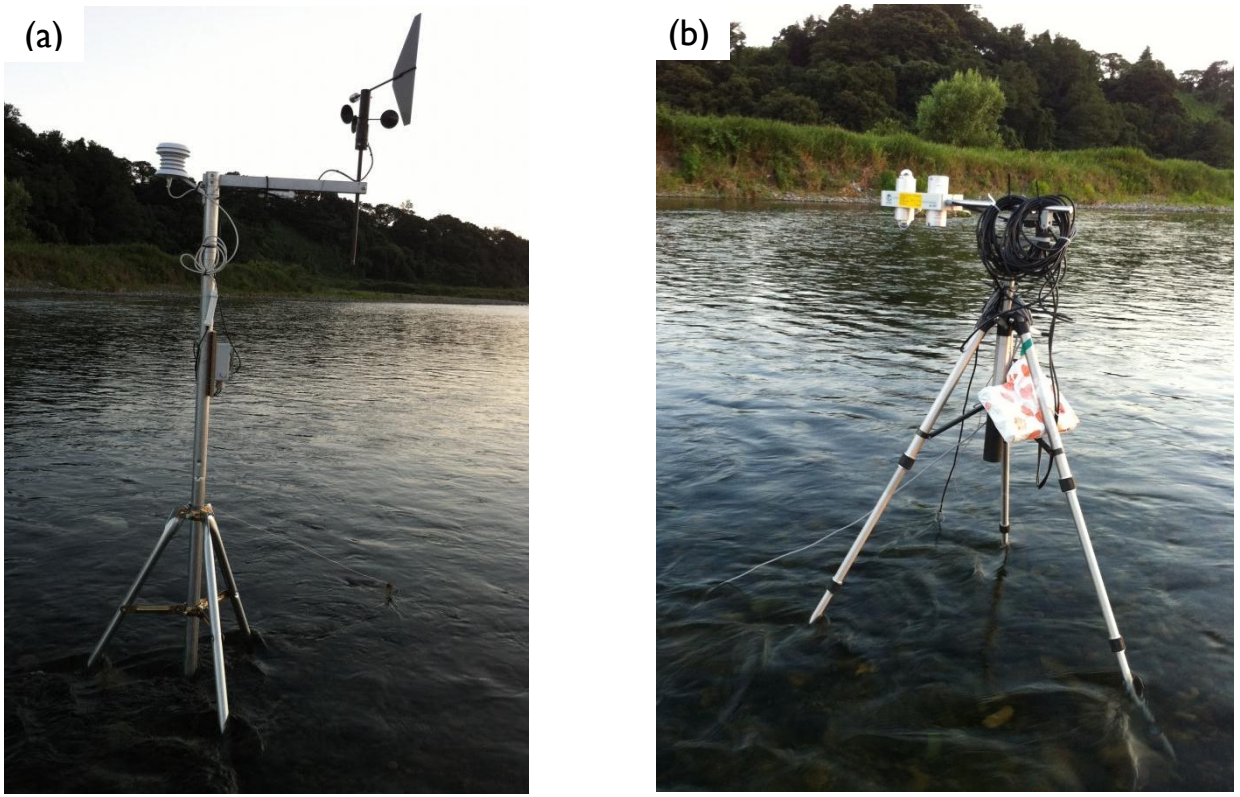

Figure 3.2 Equipment installed at Met. site for (a) meteorological conditions and (b) radiant fluxes during intensive measurements.

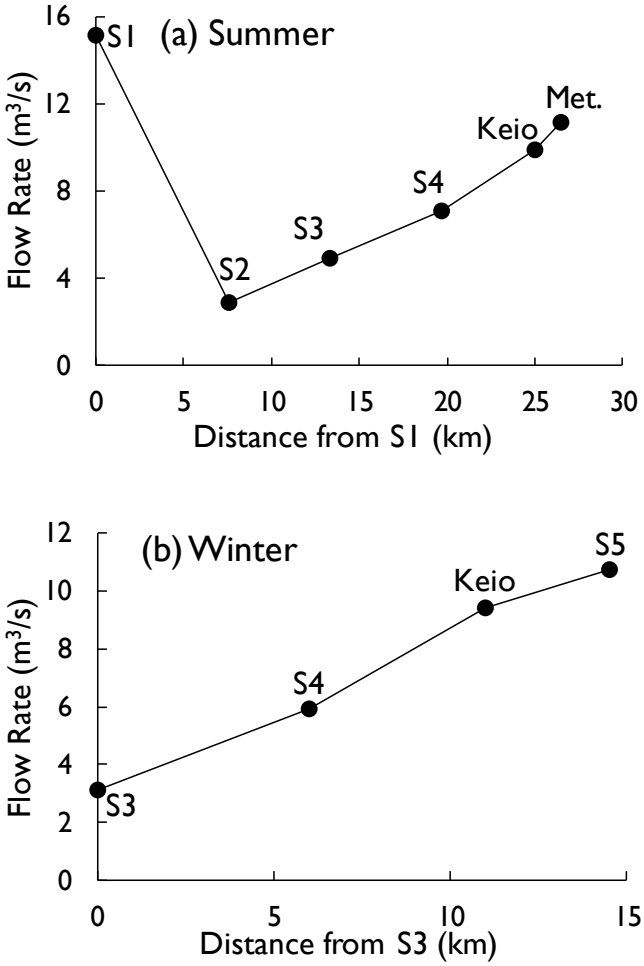

Figure 3.3 Measured stream flow rates in (a) summer and (b) winter seasons.

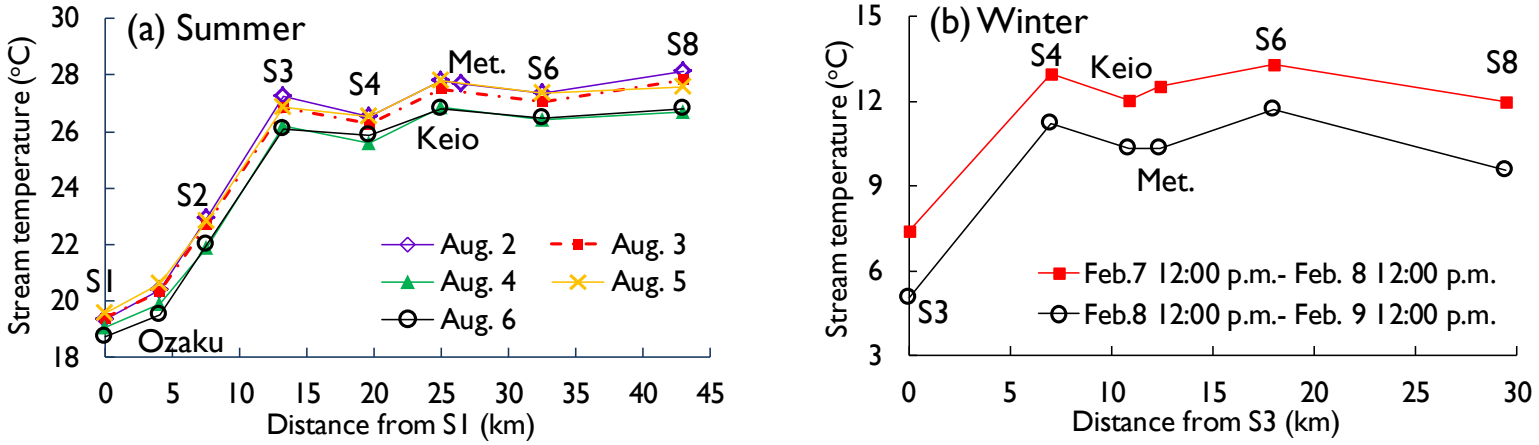

Figure 3.4 Measured daily mean stream temperatures in (a) summer and (b) winter seasons.

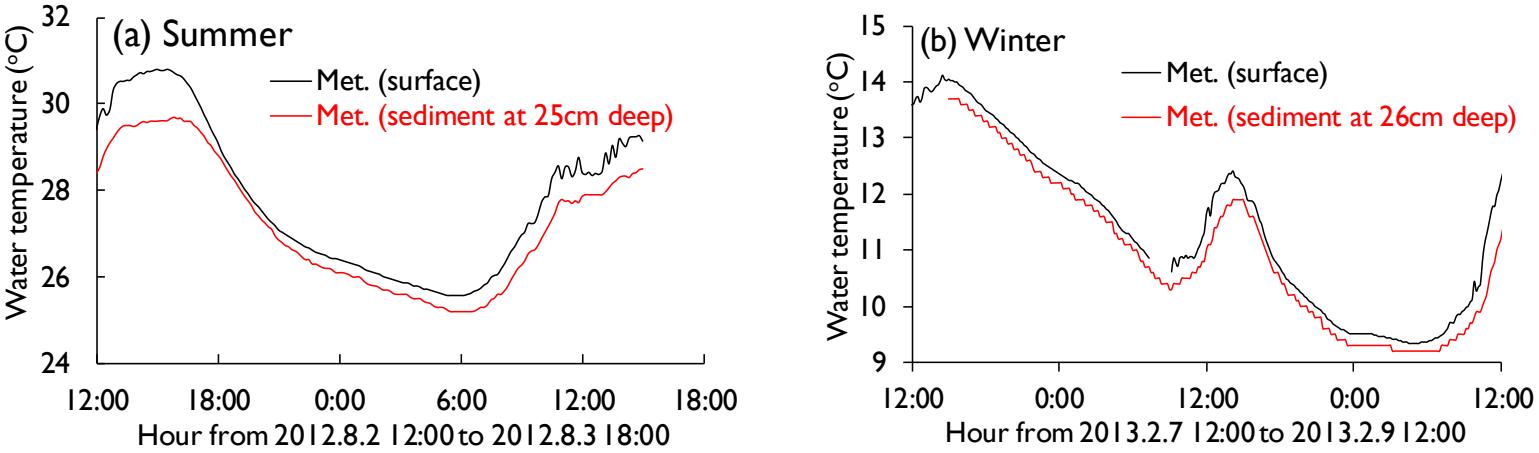

Figure 3.5 Comparison of monitored surface and sediment temperatures at Met. site in (a) summer and (b) winter.

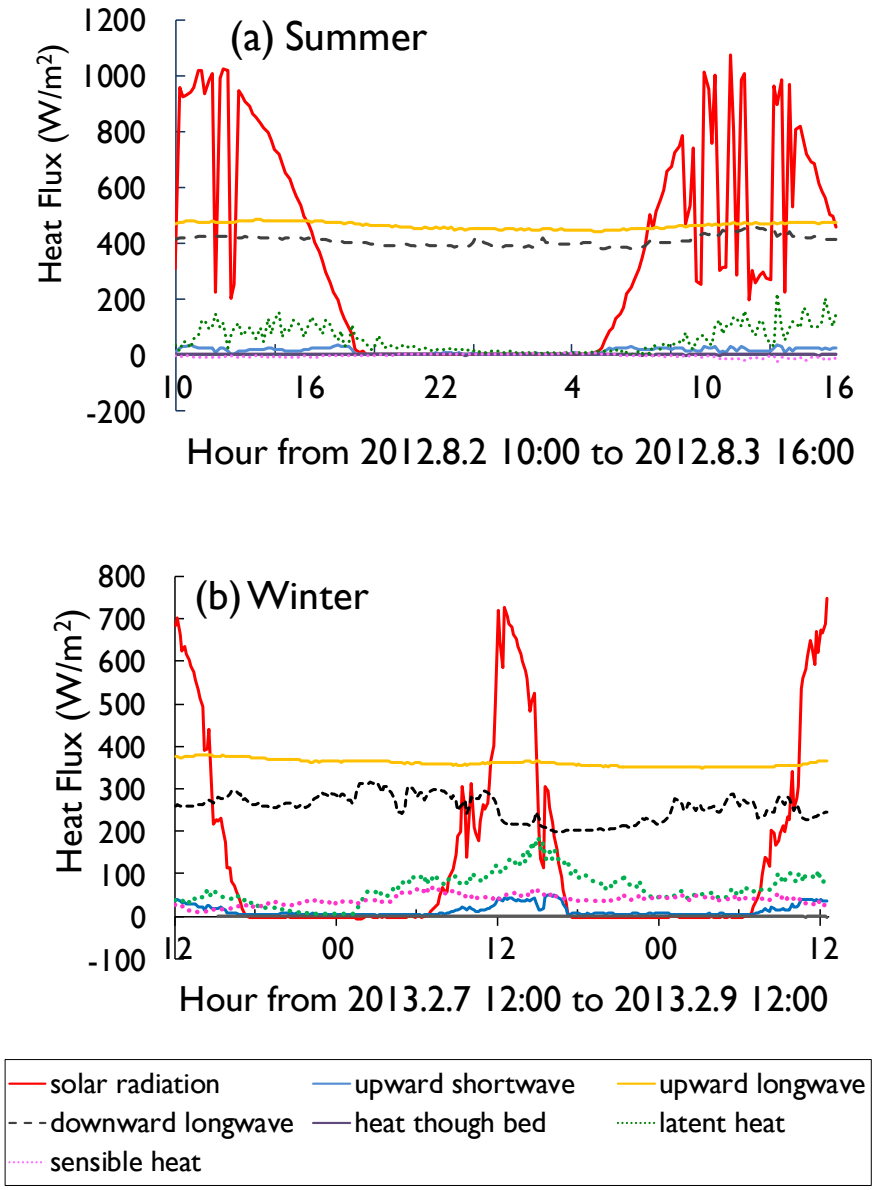

Figure 3.6 Time series of measured and calculated heat fluxes at the air-water and streambed-water interfaces in (a) summer and (b) winter.

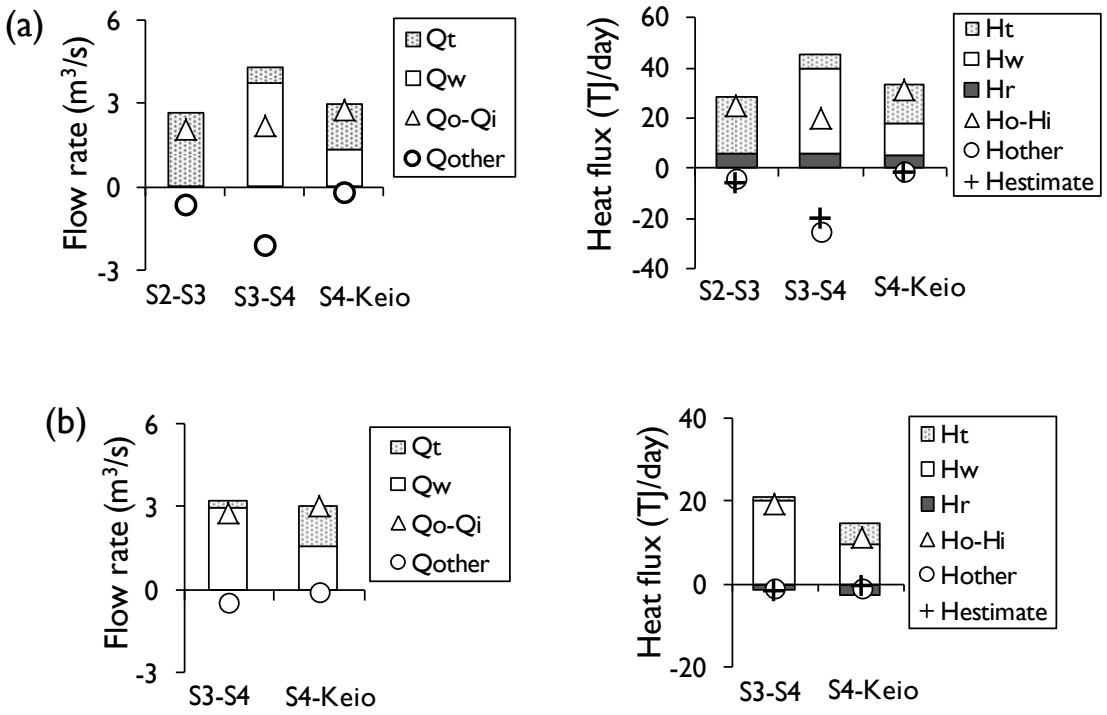

Figure 3.7 Water and heat budgets for during intensive measurements in (a) summer and (b) winter (notations are the same as defined in Eqs. (2.1), (2.2) and (2.17)).

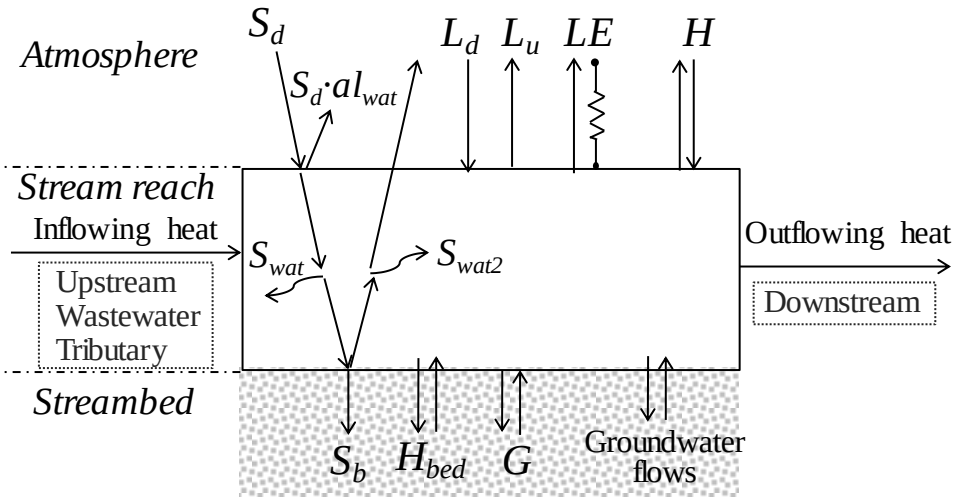

Figure 3.8 Schematic of heat transport processes considered in the model for a stream reach. (notations are the same as described in section 3.4.1. S_d: global solar radiation, al_{wat}: albedo of water surface, S_{wat}, S_{wat2}: incident solar radiation absorbed by the stream water before and after reaching the streambed, L_d, L_u: downward and upward longwave radiation, *LE, H*: latent and sensible heat fluxes, S_b: incident solar radiation absorbed by the riverbed, H_{bed}: convective heat flux transported from the riverbed surface to the stream, *G*: heat flux into the ground)

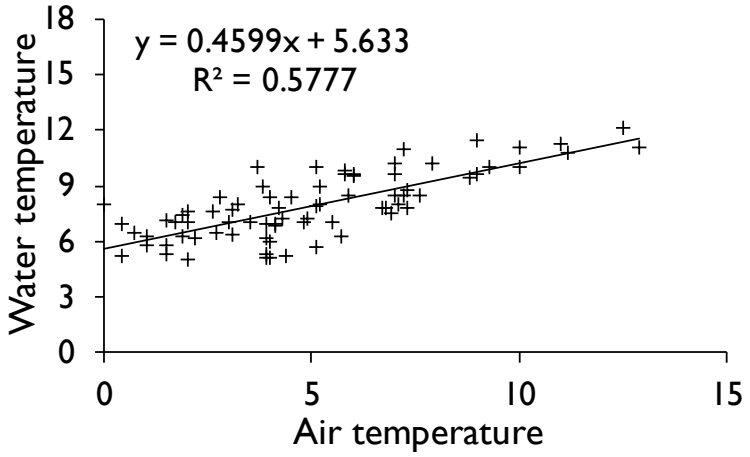

Figure 3.9 Regression relationship between water and air temperatures in February for the tributary considered in the model.

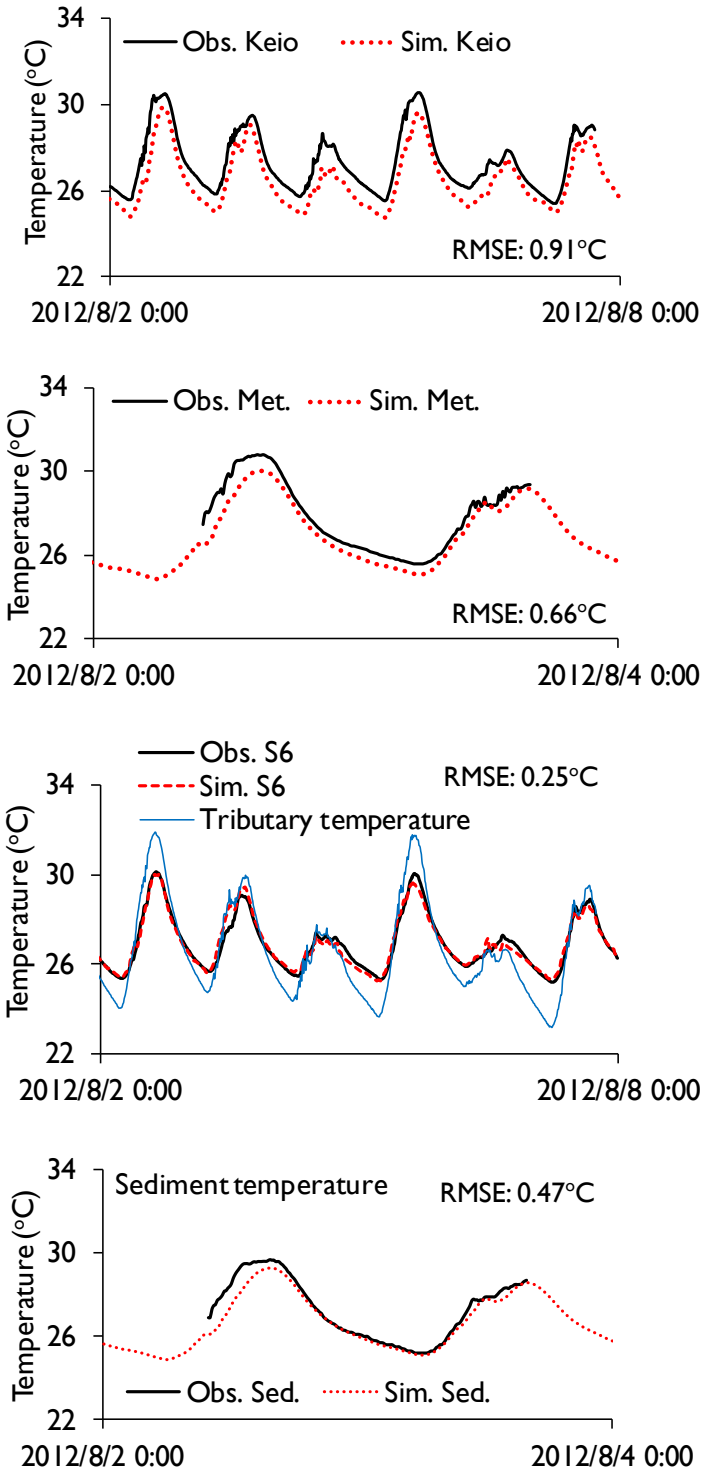

Figure 3.10 Simulation results of stream (at Keio, Met. and S6) and sediment (25cm-depth at Met.) temperatures during summer period. Observed tributary temperature was plotted in figure showing temperatures at S6 as reference. RMSE between observed and simulated values for each case was indicated in the figures.

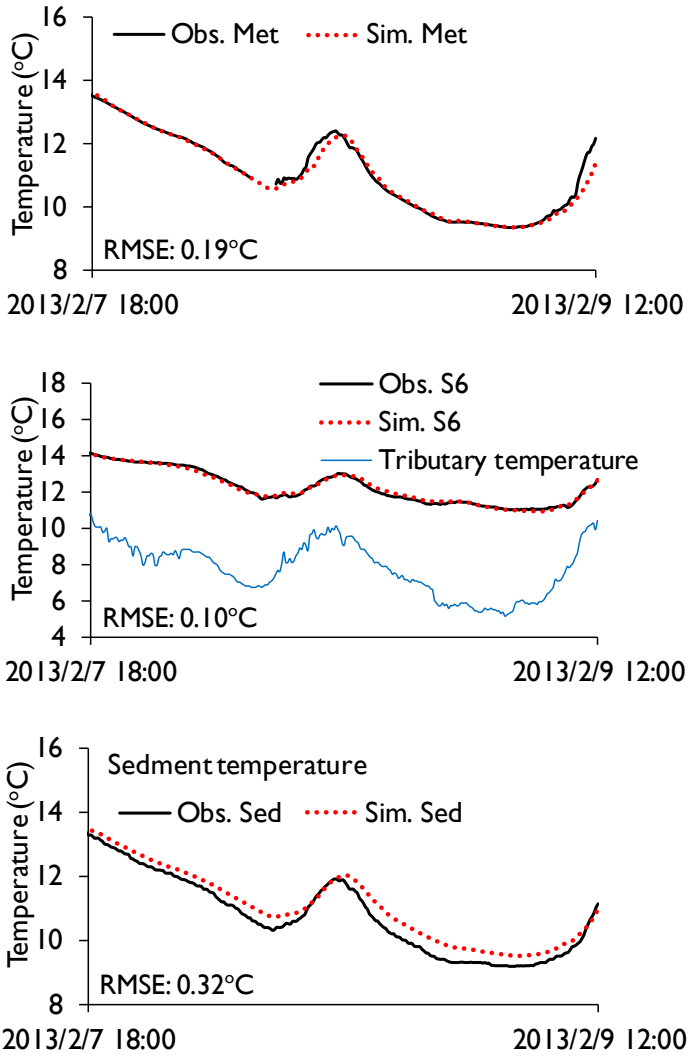

Figure 3.11 Simulation results of stream (at Met. and S6) and sediment (26cm-depth at Met.) temperatures during winter period. Estimated tributary temperature was plotted in figure showing temperatures at S6 as reference. RMSE between observed and simulated values for each case was indicated in the figures.

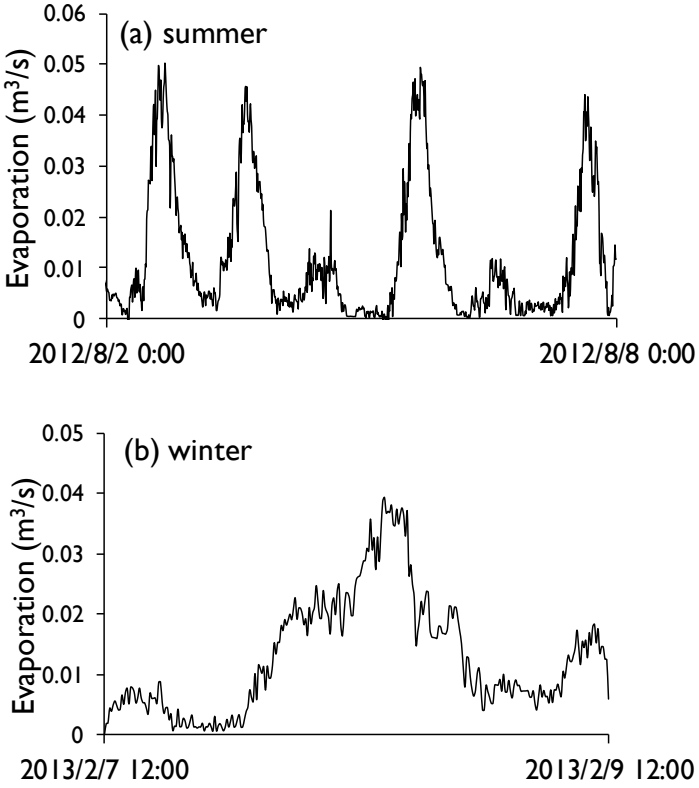

Figure 3.12 Rates of evaporation on 10-minute basis averaged over reach S4 to S6 for (a) summer and reach Keio to S6 for (b) winter.

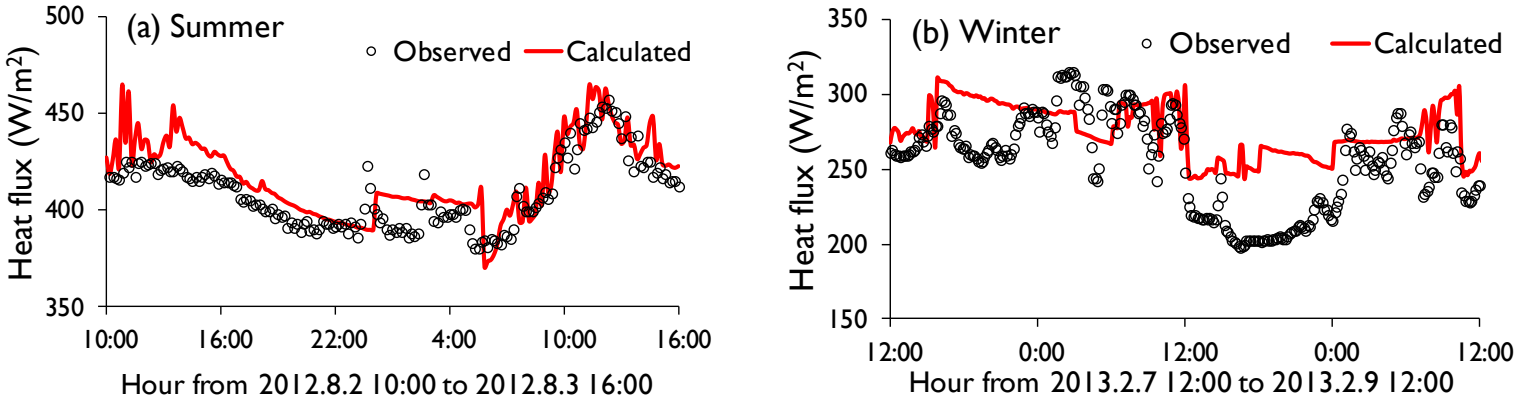

Figure 3.13 Comparisons with observed downward longwave radiation from intensive measurements conducted in (a) summer and (b) winter.

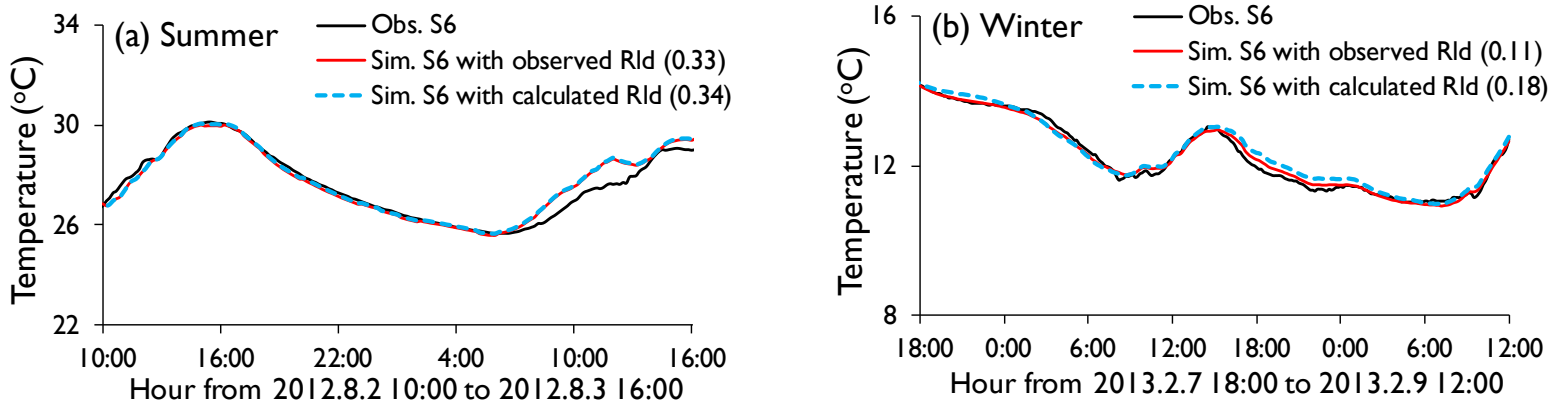

Figure 3.14 Comparisons of simulated stream temperatures (S6) derived from the observed and calculated downward longwave radiation (Rld) as input, for (a) summer and (b) winter seasons. Values in the legend denoted the RMSE between simulated and observed temperatures in each case.

References

Bhaskar, A.S., Judson, W.H., Henry, E.J., 2012. Resolving hyporheic and groundwater components of streambed water flux using heat as a tracer. Water Resources Research, 48, W08524, doi: 10.1029/2011WR011784.

Binley, A., Ullah, S., Heathwaite, A.L., Heppell, C., Byrne, P., Lansdown, K., Trimmer, M., Zhang, H., 2013. Revealing the spatial variability of water fluxes at the groundwater-surface water interface. Water Resources Research, 49, 1-15.

Brutsaert, W., 1982. Evaporation into the atmosphere. Kluwer, The Netherlands.

Burkholder, B.K., Grant, G.E., Haggerty, R., Khangaonkar, T., Wampler, P.J., 2008. Influence of hyporheic flow and geomorphology on temperature of a large, gravel-bed river, Clackamas River, Oregon, USA. Hydrological Processes, 22, 941-953.

Caissie, D., Giberson, D.J., 2003. Temporal variation of stream and intragravel water temperatures in an Atlantic salmon (Salmo salar) spawning area in Catamaran Brook (New Brunswick). Canadian Technical Report of Fisheries and Aquatic Sciences 2464, 26p .

Cardenas, M.B., Wilson, J.L., 2007. Exchange across a sediment-water interface with ambient groundwater discharge. Journal of Hydrology, 346, 69-80.

Chow, T.V., Maidment, D.R., Mays, L.W., 1988. Applied hydrology. McGraw-Hill Book Company, Singapore.

Constantz, J., Stewart, A.E., Niswonger, R., Sarma, L., 2002. Analysis of temperature profiles for investigating stream losses beneath ephemeral channels. Water Resources Research, 38, 1316, doi:10.1029/2001WR001221.

Deacon, E.L., 1970. The derivation of Swinbank's long-wave radiation from clear skies, Quarterly Journal of the Royal Meteorological Society, 96, 313-319.

Evans, E.C., Mcgregor, G.R., Petts, G.E., 1998. River energy budgets with special reference to river bed processes. Hydrological Processes, 12, 575-595.

Fanelli, R.M., Lautz, L.K., 2008. Patterns of water, heat , and solute flux through streambeds around small dams. Ground Water, 46, 671-687.

Fischer, H. B., List, E. J., Koh, R. C. Y., Imberger, J., Brooks, N. H., 1979. Mixing in Inland and Coastal Waters. Academic Press.

Harvey, J.W., Wagner, B.J., Bencala, K.E., 1996. Evaluating the reliability of the stream tracer approach to characterize stream-subsurface water exchange. Water Resources Research, 32, 2441-2451.

Hatch, C.E., Fisher, A.T., Revenaugh, J.S. Constantz, J., Ruechl, C., 2006. Quantifying surface water-groundwater interactions using time series analysis of streambed thermal records: Method development. Water Resources Research, 42, W10410, doi:10.1029/2005WR004787.

Healy, R.W., Ronan, A.D., 1996. Documentation of computer program VS2DH for simulation of energy transport in variably saturated porous media-modification of the U.S. Geological Survey's computer program VS2DT, U.S. Geological Survey, Water-Resources Investigations Report 96-4230.

Hopmans, J. W., Simunek, J., Bristow, K.L., 2002. Indirect estimation of soil thermal properties and water flux using heat pulse probe measurements: geometry and dispersion effects. Water Resources Research, 38, 1-14.

Johnson, S.L., 2004. Factors influencing stream temperatures in small streams: substrate effects and a shading experiment. Canadian Journal of Fisheries and Aquatic Sciences, 61, 913-923.

Jones, J., Mulholland, P.J., 2000. Streams and Ground Waters, Academic, San Diego, Calif.

Kasahara, T., Wondzell, S.M., 2003. Geomorphic controls on hyporheic exchange flow in mountain streams. Water Resources Research, 39, 1005, doi: 10.1029/2002WR001386.

Kinouchi, T., Kawahara, Y., 1998. Measurement and modeling of stream temperatures under tidal variation in Tokyo District.

Kobatake, S., Shioda, T., Kawauchi, S., 1997. Effect of absorption of light on river water temperature. Annual Journal of Hydraulic Engineering, JSCE, 41, 599-604. (in Japanese)

Kondo, J., 1967. Analysis of solar radiation and downward long-wave radiation data in Japan. Sci. Rep. Tohoku Univ., Ser. 5, Geophys., 18, 91-124.

Kondo, J., 1994. Meteorology of the water environment. Asakura, Tokyo (in Japanese).

Maheu, A., Caissie, D., St-Hilaire, A., EI-JIabi, N., 2013. River evaporation and corresponding heat fluxes in forested catchments. Hydrological Processes, doi: 10.1002/hyp.10071

Schnoor, J.L., 1996. Environmental modeling: fate and transport of pollutants in water, air, and soil. Wiley, New York.

Story, A, Moore, R.D., Macdonald, J.S., 2003. Stream temperatures in two shaded reaches below cutblocks and logging roads: downstream cooling linked to subsurface hydrology. Canadian Journal of Forest Research, 33, 1383-1396.

Wondzell, S.M., Swanson, F.J., 1996. Seasonal and storm dynamics of the hyporheic zone of a 4th order mountain stream. : Hydrologic processes. Journal of the North American Benthological Society, 15, 3-19.

Younus, M., Hondzo, M., Engel, B.A., 2000. Stream temperature dynamics in upland agricultural watersheds. Journal of Environmental Engineering, 126, 518-526.

Chapter 4
Model Application for All Seasons: Quantification of Factors Significant for Temperature Regime

4.1 Review and purpose

Deterministic model has been a particularly efficient tool that contributes to the explanation of physical forcing heat exchanges between river water and its surrounding environment. However, a significant drawback of this model group is the large amount of data required (i.e. geometry, hydrology and meteorology) and the use of data from a remote meteorological station rather than site-specific data. The in-stream data has been shown to be important, especially for forested ecosystem (Brosofske et al., 1997; Chen et al., 1999). Benyahya et al. (2010) showed that microclimate (near stream) conditions can be highly variable depending on streamside forest vegetation, e.g. the solar radiation and wind speed were found the most variable between near stream and remote meteorological stations in relation with topography and canopy closure. Therefore, a question that how well the remote meteorological station data capture the in/near stream condition, is important to consider when studying stream temperatures.

In this chapter, we firstly aimed to characterize and compare the meteorological conditions at the near stream and remote stations thereby yielding new insights into the situations of an urban river with less shading and sheltering by riparian vegetation. Three data sources were available for this purpose: (1) in-stream data (Met. Site in **Figure 3.1**) obtained during the intensive field measurements (see details in sections 3.2 and 3.3.2), (2) near-stream meteorological station installed at S6 (**Figure 3.1**), (3) remote stations at M1 (for solar radiation and relative humidity) and M3 (for air temperature and wind velocity) (**Figure 1.2**).

Another purpose of this chapter was to predict river water temperature and quantify the relevant heat fluxes by applying the 1D physical model introduced in Chapter 3. As reviewed in Chapter 1, considerable efforts have been devoted to field measurement as well as to formulation of deterministic models. However, most previous studies dealt with water temperature modeling have limitations either by short-term durations, i.e. data collected in a specific season of the year, or by site-specific location, i.e. temperature varied with time.

In this chapter, the longitudinal variations of water temperature and corresponding heat fluxes due to natural (i.e. heat exchanges at air-water and streambed-water interfaces and through tributary) and anthropogenic impacts (wastewater effluents) were considered. Besides, as the biological behaviors vary with seasons and are very sensitive to their living temperatures, the seasonal and diurnal characteristics of stream temperature were studied owing to the continuous field measurement throughout the 2 year cycles. Consideration of all processes that significant in modeling water temperature enables the further assessment and quantification of factors that affect stream water temperature, thereby providing a better understanding of the thermal regimes in an urban river.

4.2 Field monitoring results

4.2.1 Monitoring of stream and wastewater temperatures

In order to collect accurate and continuous data for analysis, this study conducted field measurements of stream temperatures during the course of 2 years (April 2011 to March 2013) for four sites from the upstream to the downstream, i.e. Ozaku, S4, S6 and S8. There are two main reasons of site selection. On one hand, natural structures that are suitable for fixing the devices are available at these sites. On the other hand, historical data showed that temperature increased abruptly before S4 and thereafter reached the highest values at S6 in winter season; besides, Ozaku was located in the very upstream area so that the measurements were not affected by the wastewater effluent; S8 was selected to represent a further downstream situation that suited far away from the wastewater discharge. The logging interval for temperature records was 10 minutes. All measurements were implemented using HOBO Water Temp Pro v2, with its sensor placed approximately 0.5–1 m (in the middle of the water depth) below the water surface in the main flowing area so that no lateral differences were expected due to the well mixed nature of the river.

Temperatures and volumes of the dam-released water from Ogochi Dam that forms the Ogochi Reservoir (see **Figure 1.2**), were provided on an hourly basis by Bureau of Sewerage, Tokyo Metropolitan Government from April 2011 to March 2012.

Meanwhile, as wastewater effluents have previously been proven to exert remarkable impacts on surface water temperature in our study reach, the temperatures of wastewater that drained into the mainstream were monitored at six wastewater treatment plants (W1, W2 and W4 to W7, see **Figure 1.2** for site information) from July 2011 to March 2013.

4.2.1.1 Seasonal and longitudinal variations of stream temperature

Figure 4.1 displays the daily mean stream temperatures integrated from 10-minute database over the monitoring period. The dam-released water temperatures integrated from hourly records, as well as the site-averaged wastewater temperatures were plotted together for comparison. The temperature pattern of wastewater and its potential effects on stream temperatures will be discussed later in detail (section 4.2.1.2).

Some gaps were present in the stream temperature data series because of two main reasons: the accidental device loss that happened to S4 and S8, and the exposure to the air due to water level decrease by weir operation that happened to Ozaku. As indicated in **Figure 4.1**, stream water temperatures followed the annual cycle of variation at Ozaku, S4, S6 and S8. Peak values were recorded either in June or August and minimum values in January. A marked gap in temperature between the upstream site Ozaku and middle to downstream sites i.e. S4, S6 and S8, was clearly observed throughout the whole study period. The overall mean temperatures for these two groups were calculated at 13.4 °C and 17.7 °C, respectively. The reason was that since Ozaku, stream water was warmed as a result of integrated effects from atmosphere, streambed as well as wastewater. Comparing records among the middle and downstream sites at S4, S6 and S8, a strong temperature difference was evident for late autumn to winter seasons, during which temperatures at S6 were found much higher than the other sites, while this was not pronounced for the rest of warmer seasons.

When comparing the wastewater temperature with stream temperature (only for S4, S6 and S8 that are affected by wastewater), two points were noticeable. Firstly, the temperature of wastewater was much higher than that of stream water from September to next June; whereas for the rest seasons of the year, the temperature magnitudes of wastewater and stream water were comparable (**Figure 4.1**). For example, the average temperatures of stream water and wastewater from all treatment plants were 16.4 °C and 22.5 °C, through a one-year cycle from July 2011 to June 2012. Secondly, the annual fluctuation reflected by the difference between annual maxima and minima, was on average 19.5 °C for stream water temperature compared to 11.6 °C for wastewater temperature, suggesting a very much less annual variability in wastewater temperature.

Although the effect of dam-release on upstream water temperature was not explicitly quantified in this study, historical analysis had proven that the dam release effect exists to the upstream site of S3 due to the differences in temperature patterns between dam-released water and upstream water. Solid evidence can also be found from **Figure 4.1**, which shows that the temperature of dam-released water was relatively lower than the upstream Ozaku

during warmer seasons, but the reverse was true for winter seasons. For example, temperatures were calculated at 12.6 °C and 15.4 °C for dam-release water and Ozaku during March to November, while at 6.4 °C and 6.0 °C during December to February. In addition to the temperature effects, it was found from **Figure 4.2** that the water discharged from the Ogochi Dam (under normal condition) was the primary stream flow source at S1. The differences in flow rates indicated the inflows from other natural sources which may mitigate the effects of dam release on the upstream temperature regime.

Longitudinal temperature varied along the mainstream in the study reach. **Figure 4.3** presented the spatial variations of stream temperature by four seasons, in which the averaging periods regardless of years, were from March to June for spring, from July to September for summer, from November to December for autumn and from December to next February for winter. Results showed a marked temperature increase from the upstream Ozaku to S4, whereafter a continued increase until S6 during autumn and winter months whereas a slight drop in spring and summer. The temperature changes from S4 to S6 presented in **Figure 4.3** were -0.4 °C, -0.4 °C, 0.8 °C and 1.1 °C for spring, summer, autumn and winter periods, respectively. When looking at the further downstream site at S8, a slight decrease in stream temperature can be observed in most seasons, with the exception of summer during which there was a temperature increase in response to thermal loads from the ambient atmosphere. Generally, the main trend of spatial variations agreed well with the patterns in historical (**Figure 2.2**) and intensive studies (**Figure 3.4**).

4.2.1.2 Monitoring results of wastewater temperature

Figure 4.4 presented the monitored wastewater temperatures from six WWTPs based on daily mean values. The annual cycle approximated a sinusoidal curve in wastewater temperature following the annual variations of supply water temperature and air temperature (Kinouchi, 2007). The magnitudes of effluent temperatures from six WWTPs were comparable over the study period, although slight higher records can be observed at W6, especially during warmer periods.

The contrast in fluctuating magnitudes of temperatures between stream and wastewater was evident for the daily amplitude. For illustration purpose, the hourly mean temperatures of stream water at S4, S6 and S8 along with those of wastewater averaged from W4 to W7 (between S4 and S6), were presented for two extreme periods that are in summer (from August 19, 2012 to September 1, 2012) and winter (from January 2, 2013 to January 14, 2013).

As shown in **Figure 4.5**, patterns were very different between summer and winter seasons. In summer, wastewater possessed an average temperature of 27.7 ºC, which was comparable to that of stream water at S4 (26.8 ºC), S6 (27.6 ºC) and S8 (27.9 ºC). However, compared to those of stream water, hourly temperatures of wastewater were extremely stable with fairly minor fluctuations within a daily cycle. For example, the diurnal variation, represented by the daily maxima minus the minima, were on average 0.3 ºC for wastewater, and 5.1 ºC, 3.9 ºC and 3.9 ºC for stream water at S4, S6 and S8, respectively in summer. Comparison of records between S4 and S6 (**Figure 4.5 (a)**) indicated that the daily maxima were very close in most cases, although receiving strong solar radiation in summer; whereas the daily minima showed a few degrees higher at S6 than S4. This suggested that the presence of wastewater effluent moderated the daily variability at downstream S6, primarily by depressing the daily maxima in summer. The magnitude of disturbance by wastewater progressively diminished as it goes further to the downstream S8, where the overall temperature slightly increased in response to the atmospheric heating.

When looking at the winter season (**Figure 4.5 (b)**), it was noted that the temperature of wastewater was in a considerable higher magnitude than that of the stream water; the average temperatures over the study period in **Figure 4.5 (b)** were calculated at 19.3 ºC for wastewater and 11.6 ºC, 12.6 ºC and 11.0 ºC for stream water at S4, S6 and S8 respectively. By comparing the stream temperature records, it is reasonable to conclude that the presence of wastewater with high temperature degrees enhanced the downstream temperatures at S6 in winter; further, as this effect diminished with distance, the temperature at S8 reduced in a more natural way in response to the heat gain/loss through atmosphere and riverbed.

4.2.2 Characterization of meteorological patterns

To capture the microclimate (in/near-stream) data for analysis, a meteorological station was installed at the river bank of S6, recording solar radiation, air temperature, wind velocity, and relative humidity. The instrument deployment is illustrated in **Figure 4.6**. Sensors were installed approximately 5.1 m above the water surface for air temperature and humidity, and 5.5 m for wind velocity and solar radiation. All measurements were sampled at every one minute and the 10-minute average was then calculated and stored in the data logger. The meteorological records started in March, 2012 and ended in February, 2014.

Figures 4.7 and **4.8** displayed the monthly and daily means, respectively, of on-site observed data, including solar radiation, air temperature, wind velocity, and relative humidity, which demonstrated the meteorological conditions throughout the 2-year period

in our study reach. A gap was observed in **Figure 4.8** for a few days in May, 2012 because of the missing data due to instrument malfunctioning. As shown, both solar radiation and air temperature represented an obvious seasonal pattern with relatively larger amount of solar radiation received in August for 2012 (monthly mean of 205.6 W/m^2) and in May for 2013 (monthly mean of 201.8 W/m^2); whereas peak values were always recorded in August for air temperature (monthly means of 28.4°C (2012) and 28.6 °C (2013)) with minimum values in January (monthly means of 4.5 °C for both).

Time series of wind velocity and relative humidity also showed variability depending on seasons, although the pattern was not obvious from **Figures 4.7** and **4.8**. For example, wind velocity presented lower values (**Figure 4.7**) and lower variability (**Figure 4.8 (a)**) in late autumn and winter, while the reverse was true for spring and summer. Also noted from these two figures was that the relative humidity was comparatively high and stable in the period from July to September; whereas during the rest seasons of the year, it became lower and more variable.

4.2.3 Uniformity of surface water temperature

Deterministic modeling is most often carried out as a one-dimensional problem where the temperature is simulated along the river's principal axis. This is because water temperature in rivers is relatively uniform both in transverse and vertical directions (Caissie, 2006). However in fact, the cross-sectional temperature gradients are sometimes observed at the confluence with other rivers or tributaries (Clark et al., 1999). Therefore, in this study, the localized variations in stream water temperatures were examined by a thermal infra camera at several transections from bank to bank. Two sites of S4 and S6 were selected for this analysis because they were both affected by wastewater discharge and were considered representative for modeling. Measurements were conducted specifically during the evening time of February 26, 2013.

Results were plotted in **Figure 4.9**, showing three-time trials of temperatures detected at several transections along the river width at S4 and S6. The temperature distributions from the left to right bank were generally uniform as represented by the standard deviations on average at 0.15 °C and 0.14 °C for S4 and S6, respectively. Therefore, it can be concluded that the river water was naturally well-mixed at both sites although suffering from wastewater discharge.

Although the measurement was done on a specific day of February 26, 2013, there are two reasons explaining that the measurement was representative enough. On one hand, this

day represents a winter case so that the transverse inhomogeneity, if exists, is most likely to occur due to the considerable distinction between stream water and wastewater temperatures. Besides, it was on a typical day when the meteorological condition was normal and stable, and also the flow was under normal condition. This can be concluded from **Figure 4.10** which showed a relatively stable air temperature trend and no precipitation within a few days prior to the measurement.

4.3 Data verification

4.3.1 Comparison of continuous and instantaneous stream temperatures

As noted previously in historical analysis (Chapter 2), given the scarcity of frequently sampled stream temperature data for long term periods, temperatures from instantaneous measurements which were carried out two to four times on a specific day each month (from MLIT), were utilized for the period from 1990 to 2013. In this case, bias may arise in terms of the calculation of mean daily/monthly water temperature because of the time and date of measurements (Prats, 2007). Therefore, the accuracy of instantaneous data as an alternative measure of daily/monthly mean temperature was checked in this chapter.

Comparisons were made based on three data types: (1) instantaneous average, which was calculated by averaging the two to four times measurements on a specific day each month; (2) daily mean, which was calculated based on the 10-minute dataset of our monitoring on the day of instantaneous measurement; (3) monthly mean, which was calculated based on the 10-minute dataset of our monitoring over the month of instantaneous measurement. The site and date selected for this analysis were based on data availability of our continuous measurement.

As shown in **Figure 4.11**, in most cases, the instantaneous average agreed well with either daily mean or monthly mean, or both. However, exceptions can be observed in several events when the instantaneous average over/underestimated the daily/monthly means, such as 20120801, 20121212 for S4; 20110519, 20121212, 20130214, 20130306 for S6 and 20130214, 20130306 for S8. With these events being excluded, the average differences in absolute terms, between instantaneous average and daily/monthly mean were 0.50 °C for S4, 0.42 °C for S6 and 0.57 °C for S8. Moreover, the instantaneous data were often collected within the former ten days in each month, which can minimize the bias when considering the long term temperature trends.

4.3.2 Comparison of meteorological conditions

Suffering from the scarcity of in/near-stream meteorological data for long term periods, those collected at remote stations (M1 to M4) were used for our historical analysis (Chapter 2). Therefore, once the in/near stream data were obtained, comparisons could be made in order to have a better knowledge of meteorological patters from different scales. **Figure 4.12** showed the comparison results with a 10-minute interval, including solar radiation, air temperature, relative humidity and wind velocity. For each pattern, data from three sources were available: (1) in-stream data monitored at Met. Site (see **Figure 3.1** for site information) during the intensive field measurements (Chapter 3); (2) near-stream data by meteorological station at S6, as introduced previously in this chapter and (3) remote stations at M1 (for solar radiation and relative humidity) and M3 (for air temperature and wind velocity) of AMeDAS (see **Figure 1.2** for site information). The analyzing period was limited by the intensive measurements which lasted for a relatively shorter duration. The in-stream data, i.e. air temperature, relative humidity and wind velocity from intensive measurements, were only available until 7:20 in the morning of February 8, 2013 due to the accidental malfunction of the instrument thereafter.

Since solar radiation at the remote site M1 was provided on hourly total basis, it was further downscaled linearly into 10-minute series, which as a result exhibited less fluctuated especially during the peak times. As indicated in **Figure 4.12 (a)**, solar radiation from all sites showed a consistent diurnal pattern and was equally effective due to the very similar values. Although slight differences can be observed, the overall means were 365.1 W/m^2 (in-stream), 310.2 W/m^2 (near-stream) and 371.3 W/m^2 (remote station) for summer period, and 156.6 W/m^2 (in-stream), 138.9 W/m^2 (near-stream) and 147.0 W/m^2 (remote station) for winter period, respectively. The good relations were primarily due to the nature of less sheltered by riparian vegetation in our study reach.

As shown in **Figure 4.12 (b)**, air temperature showed relatively good agreements among sites, except for the higher values recorded sometimes at the near-stream site compared to those at the in-stream and remote sites. For example, the over means were calculated at 29.0 $^oC^2$ (in-stream), 30.2 ^oC (near-stream) and 29.7 ^oC (remote station) during summer period, and at 3.2 ^oC (near-stream) and 2.7 ^oC (remote station) during winter period, respectively.

Results of relative humidity showed better correlations between in-stream and near-stream data, with slightly lower values recorded at the remote station M3 (**Figure 4.12 (c)**). For example, the overall mean values were 70.5% (in-stream) and 68.3% (near-stream) compared to 63.2% at remote site during summer period, and were 36.1% (near-stream) compared to 29.6% at remote site. This was primarily because that the humidity can be

supplied locally by the stream evaporation (Brosofske et al., 1997).

Gaps in wind velocity were quite evident between the in-stream and near-stream sites for a certain period in both seasons (**Figure 4.12 (d)**), which was reflected by the higher values recorded at the near-stream site; during this period, data at the remote site were approaching to the in-stream site in winter and to the near-stream site in summer. A better correlation was observed at relatively lower wind velocity ranges, particularly in winter. The reason of high records at near-stream site could be attributed to its measurement height of 5.5 m compared to the in-stream site of 1.8m, which made the former less affected by the resistance due to near-surface stratification. This difference due to measurement height has been corrected in our modeling processes as explained in Eqs.(3.7) to (3.9) in last chapter.

4.4 Model application: data and parameters

The 1D physical model introduced in Chapter 3 was applied to reach between S4 and S8 (**Figure 3.1**) considering all the heat transport processes as specified in **Figure 3.8**. For simulating river flow and heat transport in the mainstream, a time step of 10 second (further integrated into 10 minutes values) and a space increment of 100 m were adopted.

The model parameters for simulating river flow, stream temperature and sediment transport, after being calibrated previously in Chapter 3, were also used in this chapter (see **Table 3.4** for setting of parameters). However, there are two exceptions to the previous setting. One is the groundwater velocity and the other is the sediment temperature at 2m-deep, both of which vary with seasons. The setting of these two parameters for each individual period will be explained in later details.

To reflect the normal hydrological condition, twelve periods (see **Table 4.2** and **Figure 4.17** for periods) throughout the 2-year duration (from April 2011 to March 2013) were selected to verify the model; whereas four periods covering four seasons of the year, i.e. 2012.8.19-8.31, 2012.10.8-10.16, 2012.12.9-12.14 and 2013.3.8-3.17, were exemplified to demonstrate the comparisons of latent and sensible heat fluxes (section 4.5), the impacts from influencing factors (section 4.7), and heat budgets (section 4.8). There are two main rules of period selection. On one hand, data at all sites are available during this period of time. On the other hand, there was no precipitation and the stream flow was under normal condition.

As listed in **Table 3.3**, there are lots of data required when applying the physical model.

(1) Hydrological data

Continuous flow rates at upstream boundary (S4) were not available during the long term period, which, therefore were calculated following the two steps. At first, flow gains from, or losses to groundwater in the stream was determined by applying the water balance method between reach S4–S6, in which the groundwater flux was calculated as a residual from the monthly measurements (measured 2 to 4 times on a specific day each month) of stream flow rates at S4, S6 and two tributaries between them, as well as the total discharge volume from four WWTPs. As a second step, by assuming groundwater flux to be constant over each discrete period, the continuous (hourly in this study) flow rates at S4 can be obtained by the hourly flow rates recorded at S6 and at the two tributaries between S4 and S6 from MLIT, as well as the wastewater discharge volumes downscaled from the daily total volume provided by the Bureau of Sewerage, Tokyo Metropolitan Government.

Water level recorded on an hourly basis by MLIT was given at downstream ends (S8). The real cross–section shape at every 200-meter distance along the mainstream, after being modified, was used. As illustrated in **Figure 4.13**, the complicated river channel shapes were simplified basically by maintaining the cross sectional area. The bottom slope was obtained from the map issued by MLIT.

(2) Meteorological data

The meteorological data, including solar radiation, air temperature, relatively humidity and wind speed recorded by the meteorological station at S6, was utilized as the atmospheric forcing of the model.

Methods for calculating net radiant fluxes, i.e. upward longwave radiation (Eq. (2.9)), downward longwave radiation (Eqs. (2.6)-(2.8)), and latent and sensible heat fluxes (Eqs. (3.7)-(3.14)), have been discussed in the previous chapters.

(3) Stream temperature and temperature and volume of lateral inflows

Measured stream temperature at S4 was used as the upstream boundary condition, and those at S6 and S8 were used to verify and to validate the stream temperature model.

Considering the characteristics of simulation reach, three types of lateral advections were included in this study: wastewater discharges, tributary inflows and groundwater flows. As illustrated above, temperatures of wastewater effluents from WWTPs were monitored every 10 minute, and the daily total discharge volumes were provided by the Bureau of Sewerage, Tokyo Metropolitan Government.

Continuous flow rates on an hourly basis were available for the two tributaries between

S4 and S6, whereas for those between S6 and S8, only the monthly measurements (measured 2 to 4 times on a specific day each month) were available which were then assumed as constant over each individual period for simulation.

In addition, temperatures of tributary inflows were not continuously recorded in practice and, therefore have to be estimated. Suffered from poor data availability, simple linear regressions were established between monthly measured tributary temperatures versus the instantaneous air temperatures. Relationships were obtained for individual months based on data from December, 1989 to March 2013 for Tri.1 and Tri.2, and from April, 2000 to March 2013 for Tri.3 and Tri.4 (see **Figure 3.1** for tributary information). **Table 4.1** summarized the slope and intercept of regression lines of water on air temperatures for four tributaries between S4 and S8. The slope was generally steeper for warmer month, while the relatively flatter slope in winter months indicated less variability in water temperature in response to air temperature. Correlations computed for individual months were relatively higher in warmer seasons, whereas scatter tended to increase in regressions for winter months with r^2 values less than 0.6. Similar regression trends have been reported between the monthly mean water and air temperatures by Webb and Nobilis (1997). Since sensitivity analysis suggested that the simulated temperature was not that sensitive to tributary effects (section 3.5.1), these simple linear regressions were further used in this study.

The groundwater flux and temperature are explained in the following part.

(4) Data for sediment (groundwater flux and sediment temperature at 2-m deep)

Space increment for the heat advection-dispersion in the sediment was set to 1cm.

Considering the flow-related data availability, spatially varied groundwater fluxes were given over the simulation reach from S4 to S8 as discussed below.

For each simulation period, the groundwater flux between reach S4 and S6 was determined as a residual from the monthly water balance, which was based on the monthly measured flow rates (in the same month as the simulation period) at the upstream (S4) and downstream (S6) ends and at tributaries (Tri.1 and 2 in **Figure 3.1**) (from MLIT), as well as the discharge volumes from WWTPs (W4-W7). This value was then regarded as constant over reach S4 to S6 during this specific simulation period.

Similarly, the groundwater flux for reach S6 to S8 for each simulation period was calculated as a residual from the monthly measured flow rates (the same month as the simulation period) at the upstream (S6) and downstream (S8) ends and at tributaries (Tri. 3

and 4 in **Figure 3.1**). This value was then regarded as constant over reach S6 to S8 for this selected simulation period.

Note that the groundwater velocity through the sediment is assumed to be one dimensional in the vertical direction and that the fluid is constant over time for a certain simulation period. The setting of groundwater flux for each individual period was summarized in **Figure 4.14**.

The temperature of groundwater outflows to stream was determined as the simulated sediment temperature at the riverbed surface, whereas the temperature of groundwater recharge was equated with stream temperature.

As explained previously in Chapter 3, a constant sediment temperature at 2m–deep at both spatial and temporal scales, was given for each individual period as the bottom boundary condition of Eq. (3.15). For each simulation period, this value was determined mainly by model calibration process. The setting of sediment boundary temperatures for each simulation period was summarized in **Figure 4.15**. The period-average of water and air temperatures have been plotted together as reference. The thermal and hydraulic properties of the sediments and fluid are assumed to be constant in both space and time (i.e. do not vary with depth or as a function of diurnal variations in surface water temperature), which has been proven to be practicable by Mitchell et al. (1990).

4.5 Latent and sensible heat fluxes

To testify the accuracy of latent and sensible heat fluxes simulated from the model method by applying the Monin-Obukhov similarity theory (Eqs. (3.7)-(3.9)), results were compared with those calculated from the bulk aerodynamic approach as described in Eqs. (2.10) and (2.11). **Figure 4.16** illustrated the time series of spatially averaged (over S4 to S6) heat fluxes for four periods covering all seasons of the year. Results from two different methods showed very good agreements; and the instantaneous fluxes were fairly well correlated for both latent and sensible heat fluxes. The RMSE between simulated (Monin-Obukhov similarity) and calculated (bulk aerodynamic) values for latent and sensible heat were 17.7 W/m^2 and 1.2 W/m^2 in summer, 15.4 W/m^2 and 1.7 W/m^2 in autumn, 13.3 W/m^2 and 3.4 W/m^2 in winter, and 23.3 W/m^2 and 17.4 W/m^2 in spring, respectively.

Since these comparisons indicated reasonable confidence in the fluxes simulated by Eqs. (3.7)-(3.9) in the model, latent and sensible heat transfers based on these equations were employed further in this study.

4.6 Model performance

Model performance results are presented in **Figure 4.17**, showing the comparisons between observed and simulated stream temperatures at S6 and S8 for twelve individual periods. As the tributary flow and wastewater discharge were included in the model as major lateral inflows, the estimated tributary temperature (averaged from Tri.1 to Tri.4) as well as the measured wastewater temperature (averaged from W4 to W7 between S4 and S6) were also displayed in **Figure 4.17** as reference.

In general, the agreements were satisfactory. The RMSE between observed and simulated temperatures at S6 and S8 for each period were summarized in **Table 4.2**. As shown, the agreements were better at S6 than S8, with the average RMSE calculated at 0.40 °C at S6 and 0.54 °C at S8. In particular, the smaller diurnal variation at S6 compared to S4, which was mainly attributed to the lower wastewater temperature range, was successfully produced. These indicate that this model is capable of simulating seasonal and diurnal water temperature variations in the study reach considering various natural and anthropogenic processes.

However, it can be observed that the simulated results sometimes could not capture the instantaneous temperature variations, particularly during the late afternoon in colder seasons when the warmer wastewater imposed strong effects on stream temperature. The possible reason was that in the model, the continuous data on wastewater volume, e.g. 10 minutes or hourly, were not available; as a compromise, a constant volume of wastewater, which is downscaled from the daily total value, was used instead at each time step throughout the day.

Currently, the observed solar radiation was used as inputs in the model, but the observed values of other heat elements, were not available for the model verification and validation. Therefore, stream temperatures at multiple stations along the mean stream were the only information that could be used currently to validate the model. For this reason, the potential error of heat flux was examined by comparing the residual heat fluxes that are equivalent to the temperature differences between simulated and observed values with other heat components. Two examples were given for summer (2012.8.19 to 2012.9.1) and winter (2012.12.9 to 2012.12.15) seasons in **Figure 4.18**, showing the residual heat flux, heat fluxes at the air-water and streambed-water interfaces, and from tributary and wastewater effluetns. The residual of heat flux was calculated by $C_p\rho \times Q \times (T_{sim}-T_{obs})$, converting the temperature differences between the simulated (T_{sim}) and observed (T_{obs}) temperatures into

the equivalent heat flux. Results indicated that the residual heat flux was in a very small magnitude compared with other heat components. Therefore the residuals are considered to lie within the uncertainty of the inputs, which may be neglected in this study.

4.7 Impacts of wastewater and surface-groundwater interaction

With reasonable and satisfactory simulation results obtained, this model was further employed to quantify the impacts of wastewater effluents and surface-groundwater interaction on surface stream temperature. As shown in **Figure 4.19**, changes in stream temperatures at S6 were simulated by solely eliminating the wastewater effluents as well as by solely eliminating groundwater flows between S4 and S6; whereas changes at S8 were simulated only for the case without groundwater flows between S6 and S8.

Comparing the simulated temperatures with and without wastewater impacts at S6, it can be concluded that in summer, the existence of wastewater helped to moderate the downstream temperature at S6 which was reflected by the suppressed daily maxima and the reduced daily amplitude. This was likely due to the lower diurnal ranges and the close daily means of the wastewater temperatures compared to stream temperature (**Figure 4.5 (a)**). Besides, it is apparent from these figures that in other colder seasons, stream temperatures have been greatly influenced by wastewater. For example, the temperature could be reduced at 1.16 ºC in autumn, 2.72 ºC in winter and 1.65 ºC in spring when the wastewater effects were eliminated. Therefore, results suggested a notable warming effect of wastewater effluents on stream temperature in colder seasons because the temperature of the wastewater is much higher than that of the stream water (e.g. **Figure 4.5 (b)**).

On the other hand, regardless of seasons, stream temperatures at both S6 and S8 increased under the condition of no groundwater flows. In general, dispersion in the porous media is the macro-scale process arises from the tortuous flow in inhomogeneous pores in the sediment. Heat and contaminant are longitudinally dispersed due to this reason. If there is no groundwater flow, dispersion never occurs, and thermal conduction is the only process to diffuse heat into the ground. As a result, the net radiation along with the effluents from WWTPs became the dominant processes that control the variation in stream temperature.

When sediment diffusion disappeared, the remarkable temperature increases could be found mostly during the daytime in summer season, which was primarily attributed to the intensive atmospheric heating. While during other colder seasons, temperature increases at S6 could be observed all the time with even pronounced differences during the daytime. This reflected a continuous warming effect from wastewater throughout the day that

particularly jointed with atmosphere stress during the daytime.

Based on the discussions above, it can be concluded that the wastewater effluents and surface-groundwater interaction are two major factors responsible for the temperature variations in the downstream reach of Tama River. Particularly, the extensive alluvial floodplains within the region represent areas of intensive surface-groundwater interactions that have a moderating effect on stream temperatures.

4.8 Heat budget

Time series of accompanied heat flux on 10-minute basis from each energy component were generated by the model and were further integrated into daily total heat flux (**Figure 4.20**). Each term in the figure indicates the spatial average of heat fluxes from every 100-meter increment over reach S4 to S6. The heat from wastewater (H (wastewater)) was the major contributor of heat increases in all periods. On the contrary, heat exchanges through riverbed (H_{bed}) were found to act as energy sinks consistently throughout the year and are more influential in colder seasons than in warmer seasons. There was a general pattern of variation evident, whereby heat flux at air-water interface was positive in summer due to the fact that gaining energy outweighed losing ones, while the reverse was true for winter months with cross-over periods in autumn and spring.

4.9 Ecological implications

Temperature regime of the Tama River is of special concern because of its population of aquatic species, the biological behaviors of which are very sensitive to the stream temperature variations. The predicted changes in stream temperature patterns and seasonal characteristics under condition of no wastewater or surface-groundwater interaction would likely have major impacts on aquatic ecosystems in our study reach.

As has been proven in this study, the existence of wastewater enhanced the river temperature in colder season, which may inspire fish species to migrate from the ocean to the stream following the warm flow in the late winter and early spring. In addition, wastewater with a lower temperature range contributed to suppress the daily maximum temperature in summer, which is beneficial for aquatic species to survive during this hottest season of the year.

On the other hand, according to the hypothesis that the surface-groundwater interaction disappeared, our results predicted an increase in stream temperature by as much as 0.6 ^{o}C

at S6 and 1.3 °C at S8 on average during the summer period. This suggests an increasing summertime thermal stress and a major bottleneck especially for cold water fish. For such an urban river with very less shading shelters, the summer stream temperature without interacting with groundwater would be particularly critical and threatened for aquatic species.

4.10 Summary

In this chapter, monitoring results of water temperature indicated a higher magnitude (except for summer) and less fluctuated diurnal and annual variations in wastewater temperature compared to the stream temperature. Comparing the meteorological patterns collected at different sites, it can be concluded that the near-stream data correlated well with the in-stream data, which were considered reliable and representable.

The physical model introduced and calibrated in the previous chapter was applied to reach between S4 and S8 using monitored data on water temperature, hydrological and meteorological variables. The simulated stream temperatures at S6 and S8 for selected twelve periods showed satisfactory agreements comparing with the observed values, which proved this temperature model was well-suited for a complex river system receiving wastewater discharge, tributary inflow and interactions with sediment, etc.

Further, the model was applied to quantify the impacts of wastewater and surface-ground water interaction on stream temperature. Results showed that the presence of wastewater from WWTPs increased stream temperature by 2.7 °C during a winter period. Other effects due to wastewater discharge were the suppression in daily maxima and diurnal fluctuation in summer. Regardless of seasons, stream temperature without interaction between surface and groundwater would increase a lot. If there is no groundwater flow, dispersion never occurs. Consequently, the net radiation along with the effluents from WWTPs became the dominant processes that control the variation in stream temperature.

Heat budget analysis indicated that the heat from wastewater was the major contributor of heat increases in all periods. On the contrary, heat interacted with sediment was found to act as energy sinks consistently throughout the year. The assessment of water temperature change in response to the change in controlling factors in different seasons contains valuable information for the river water management as well as for better conservation of aquatic species.

Table 4.1 Linear regression relationships between monthly water and air temperatures of four tributaries (Tri.1-4 in Figure 3.1) for 12 individual months.

	Tri.1			**Tri.2**			**Tri.3**			**Tri.4**		
	slope	intercept	r^2	slope	intercept	r^2	slope	intercept	r^2	slope	intercept	r^2
Jan	0.326	8.142	0.56	0.390	5.548	0.49	0.218	6.678	0.34	0.236	6.368	0.29
Feb	0.285	8.046	0.32	0.460	5.633	0.58	0.386	6.019	0.41	0.270	6.886	0.42
Mar	0.396	8.454	0.76	0.407	7.030	0.56	0.582	5.842	0.81	0.454	6.605	0.70
Apr	0.432	9.296	0.75	0.517	7.252	0.78	0.483	8.430	0.82	0.426	9.406	0.76
May	0.546	8.868	0.80	0.618	7.544	0.66	0.481	9.834	0.77	0.358	12.631	0.62
Jun	0.554	9.141	0.69	0.534	10.232	0.51	0.421	12.606	0.67	0.314	14.99	0.43
Jul	0.588	8.320	0.75	0.529	10.565	0.58	0.483	11.010	0.64	0.482	11.54	0.61
Aug	0.560	9.676	0.79	0.595	9.513	0.71	0.500	11.530	0.71	0.380	15.825	0.62
Sep	0.433	12.841	0.65	0.617	8.769	0.72	0.541	9.407	0.72	0.465	12.027	0.70
Oct	0.415	11.322	0.75	0.439	10.935	0.61	0.398	11.070	0.81	0.402	11.334	0.69
Nov	0.324	11.665	0.65	0.508	8.176	0.70	0.298	11.186	0.55	0.483	8.588	0.66
Dec	0.290	10.303	0.48	0.411	7.342	0.59	0.284	9.460	0.30	0.303	8.514	0.45

Table 4.2 RMSE between observed and simulated stream temperatures at S6 and S8.

Period	RMSE (°C)	
	S6	S8
2011.10.27-11.04	0.27	0.47
2011.12.24-12.31	0.40	0.54
2012.01.03-01.18	0.48	0.49
2012.01.25-02.05	0.50	0.66
2012.07.26-08.13	0.36	0.66
2012.08.19-08.31	0.34	0.54
2012.09.07-09.16	0.28	0.47
2012.10.08-10.16	0.31	0.47
2012.12.09-12.14	0.37	0.42
2013.01.04-01.13	0.39	0.45
2013.02.21-02.26	0.53	0.57
2013.03.08-03.11 and 03.15-03.17	0.57	0.72

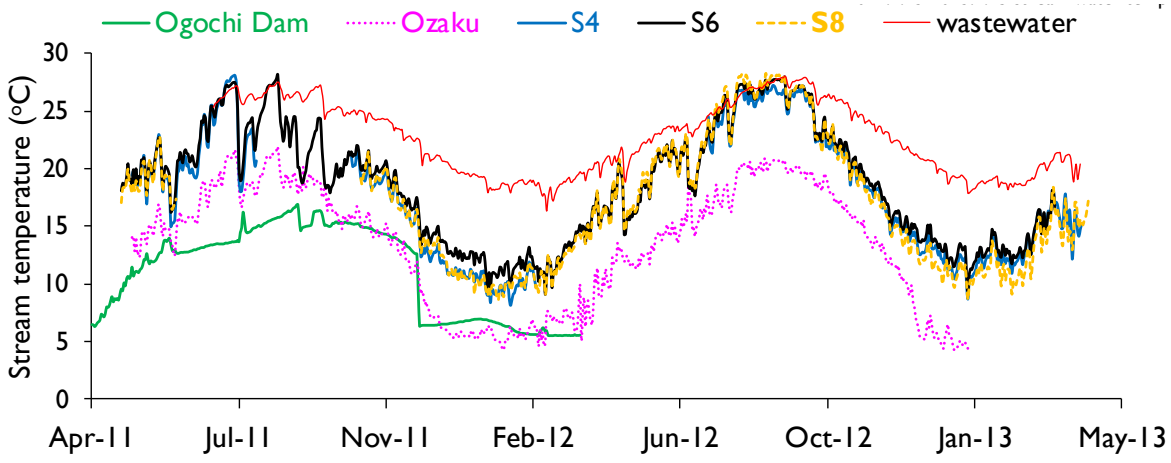

Figure 4.1 Daily mean water temperatures at Ozaku, S4, S6 and S8 over the monitoring period. The wastewater temperature averaged from six WWTPs (W1, W2 and W3 to W6) (red line), as well as the dam-released water temperature (green line) were plotted together as reference.

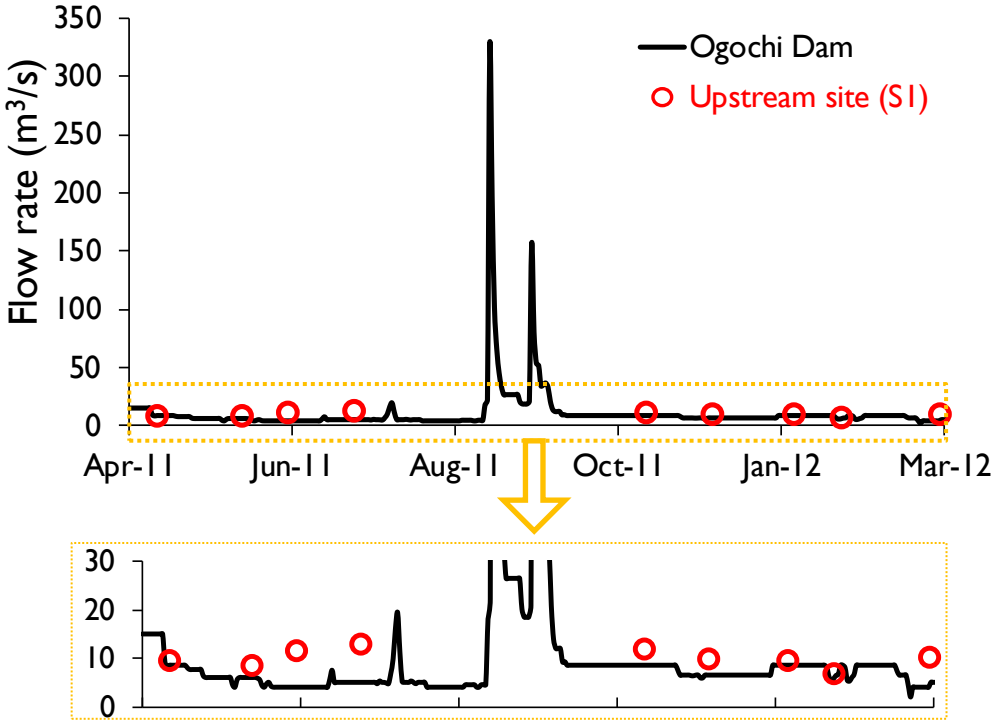

Figure 4.2 Comparison of dam-released flow with upstream (S1) flow from April 2011 to March 2012. The dam-released flow (black line) indicates the daily mean values and the upstream (S1) flow rate was based on the monthly measurement.

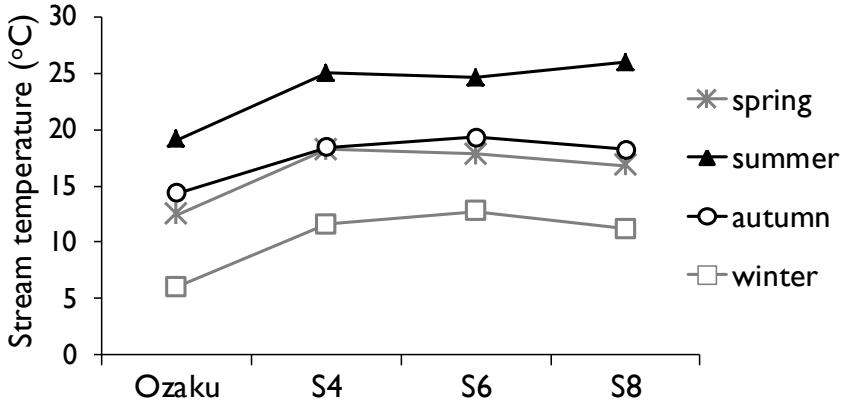

Figure 4.3 Longitudinal stream temperature variations by season. Each plot indicates a seasonal average of monitored data.

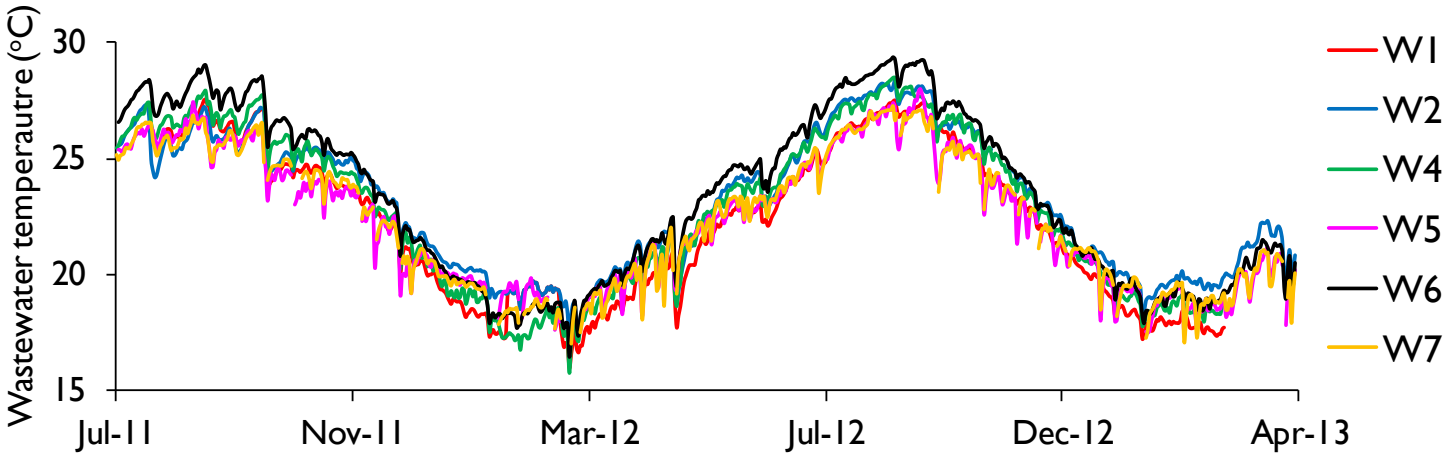

Figure 4.4 Daily mean temperatures of wastewater effluents from each WWTP over the monitoring period.

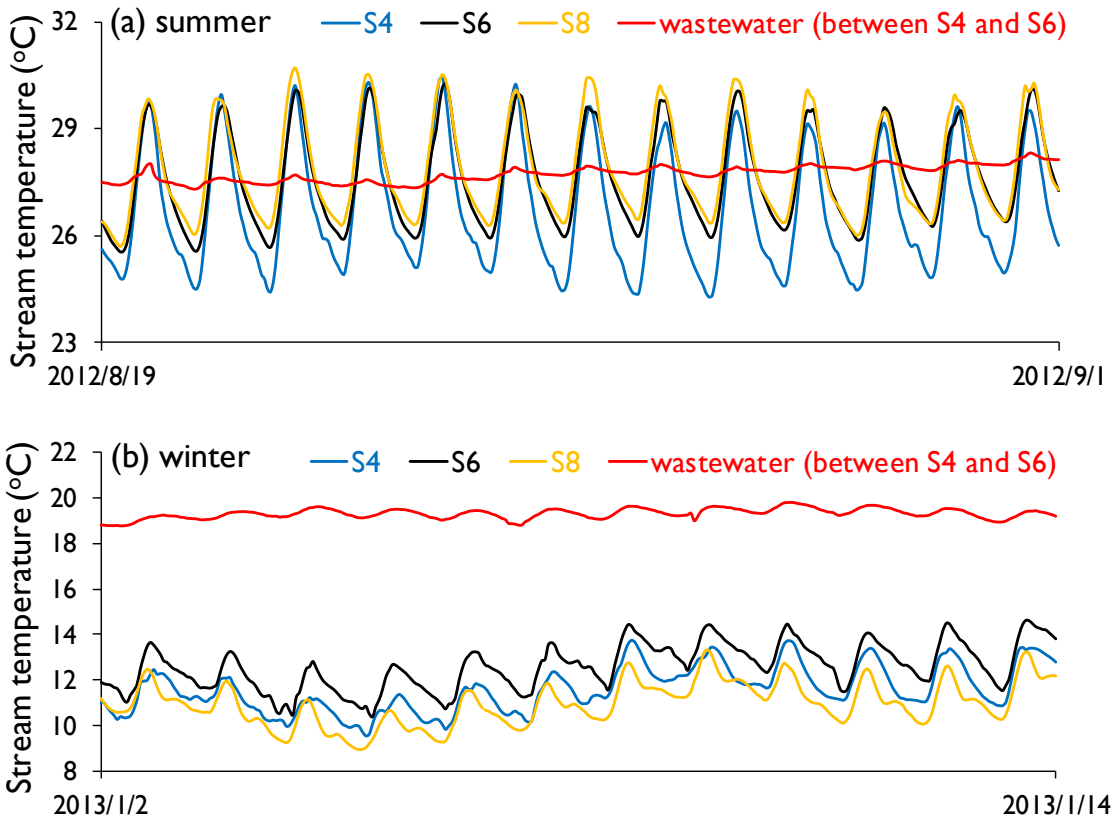

Figure 4.5 Daily variations of stream water and wastewater temperatures on an hourly basis for (a) summer and (b) winter periods.

Figure 4.6 Meteorological station installed at S6, recording solar radiation, air temperature, relative humidity and wind velocity.

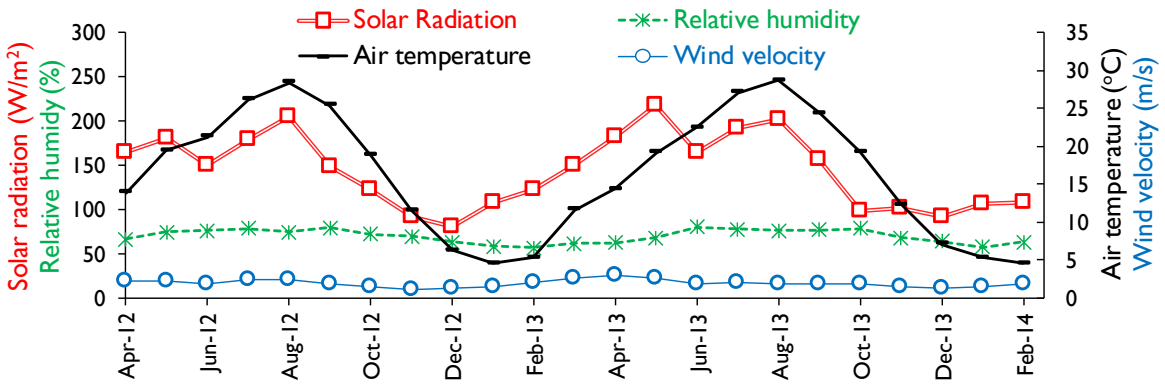

Figure 4.7 Seasonal variations in solar radiation, relative humidity, air temperature and wind velocity at S6 based on monthly mean values.

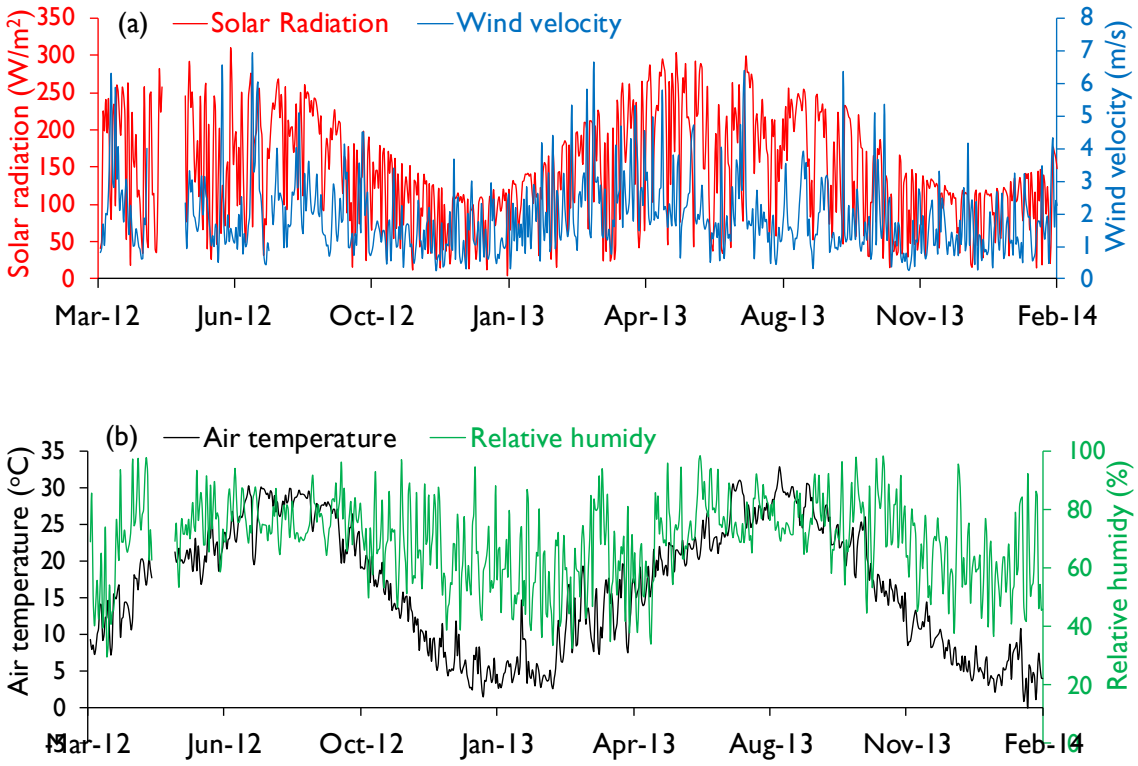

Figure 4.8 Daily mean (a) solar radiation and wind velocity, and (b) air temperature and relative humidity recorded by meteorological station at S6.

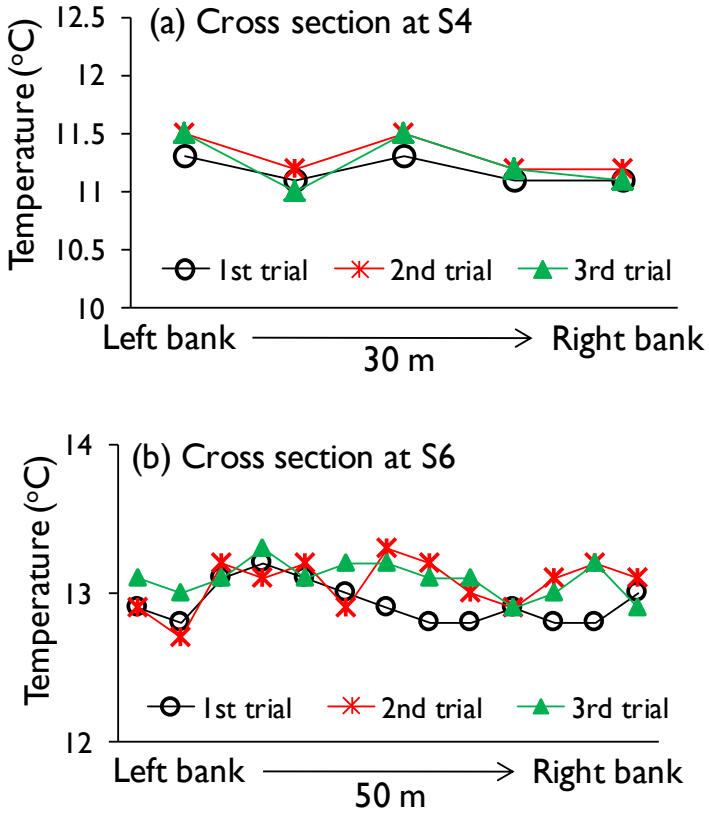

Figure 4.9 Transvers stream temperature variation at (a) S4 and (b) S6. The approximate widths were indicated below the horizontal axis.

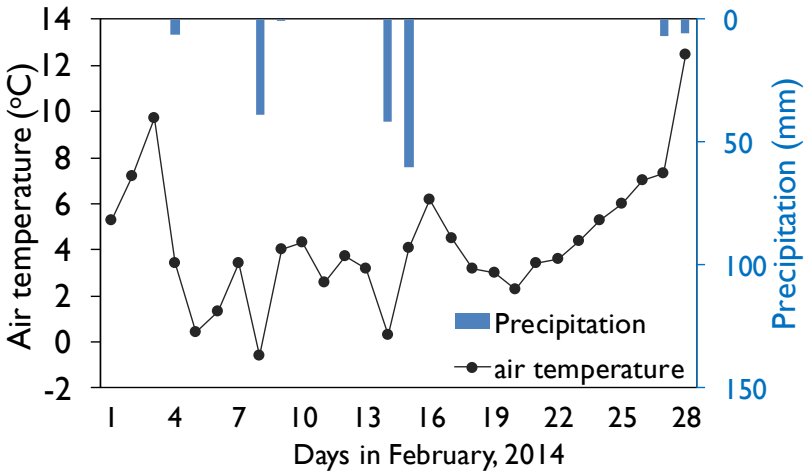

Figure 4.10 Meteorological conditions (air temperature and precipitation) before and after the measurement day of February 26, 2014.

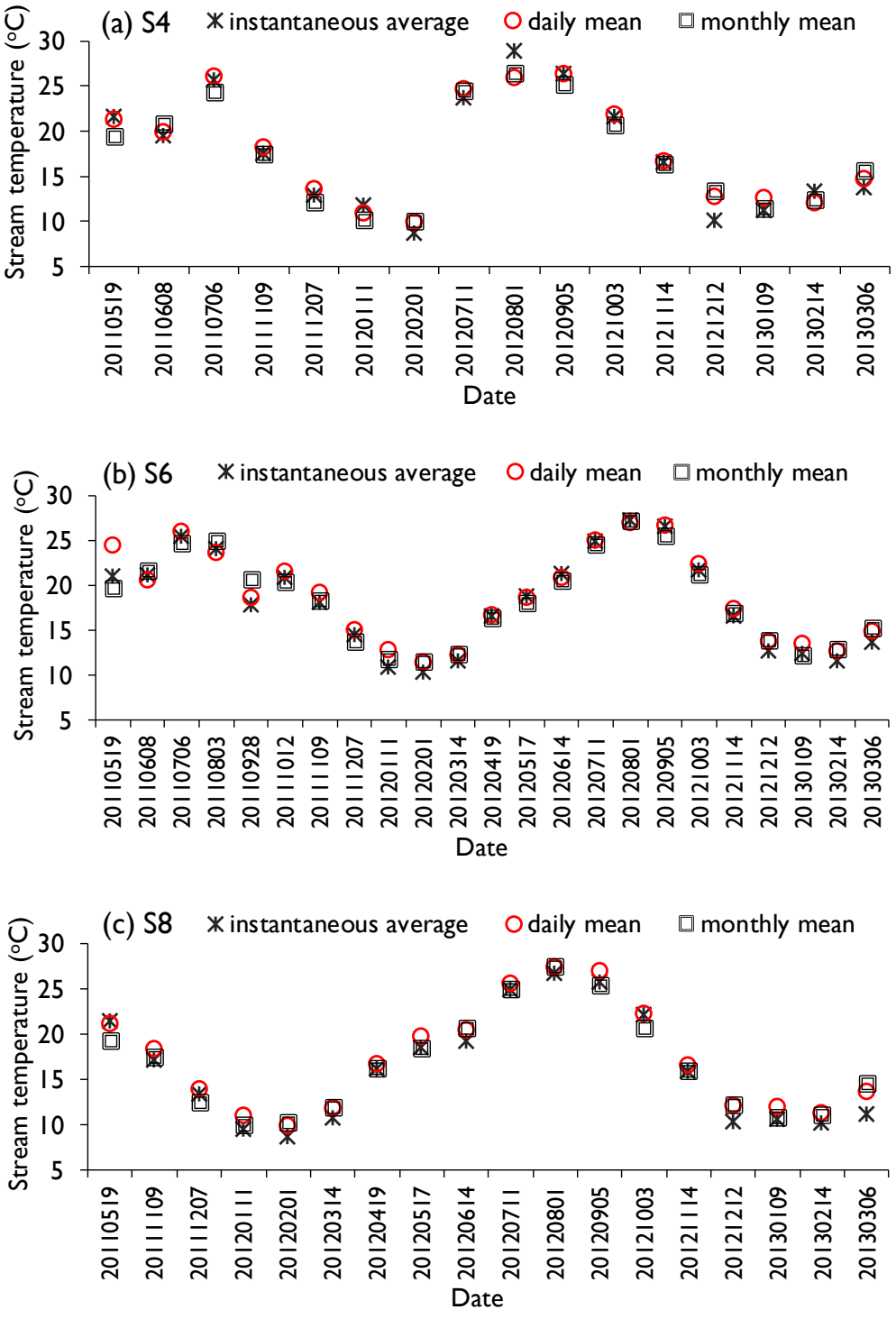

Figure 4.11 Comparisons of stream temperatures in instantaneous average, daily mean and monthly mean values at (a) S4, (b) S6 and (c) S8. Date below horizontal axis also denote the month over which monthly mean was calculated.

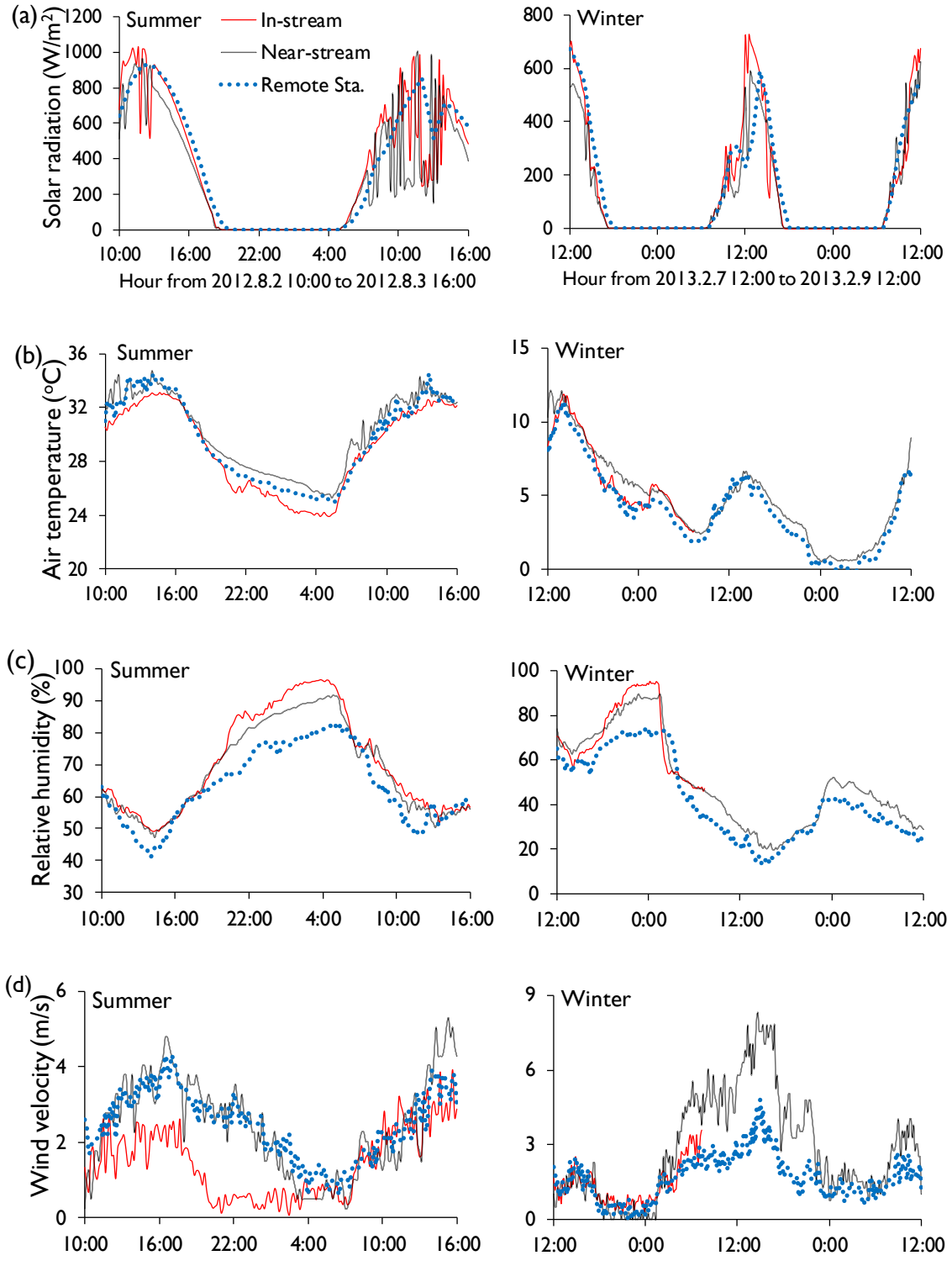

Figure 4.12 Comparisons of data from in-stream, near-stream and remote stations for (a) solar radiation, (b) air temperature, (c) relative humidity and (d) wind velocity. Figures on the left and right columns denoted to patterns in summer and winter periods, respectively.

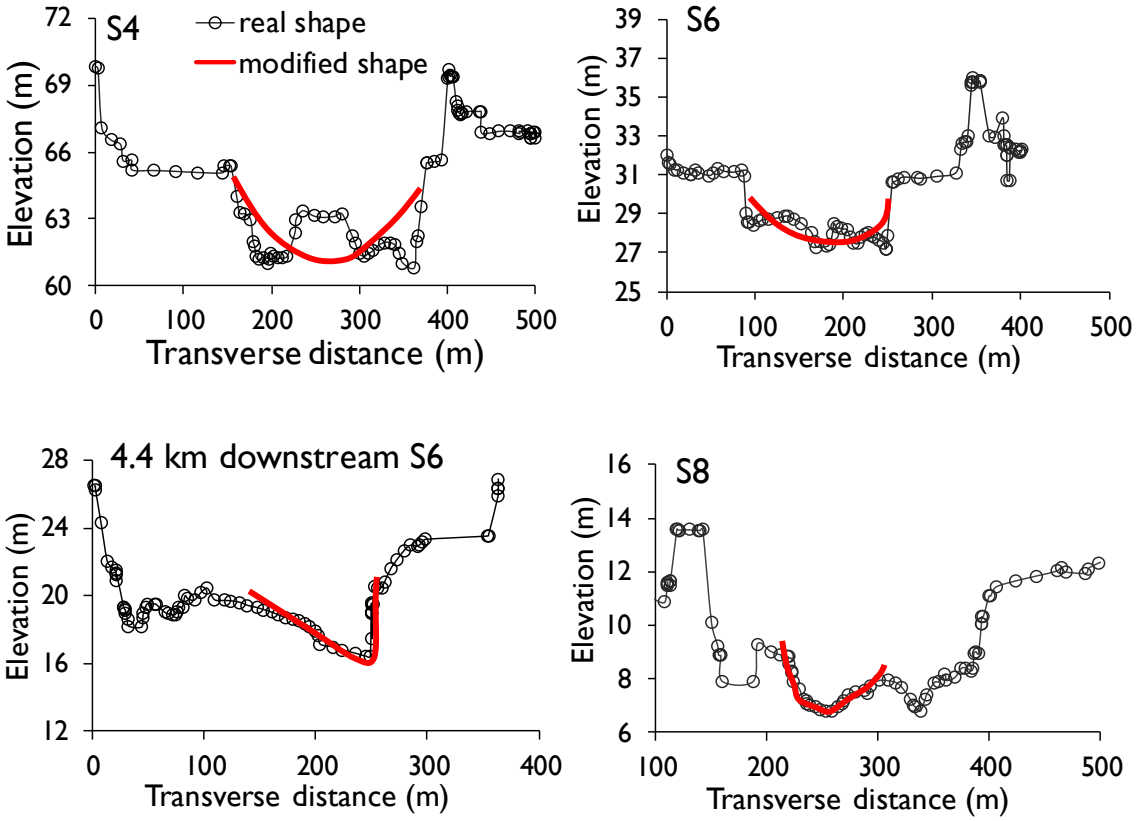

Figure 4.13 Modification of cross-sectional shape. Examples were given at four locations: S4, S6, 4.4 km downstream S6 and S8.

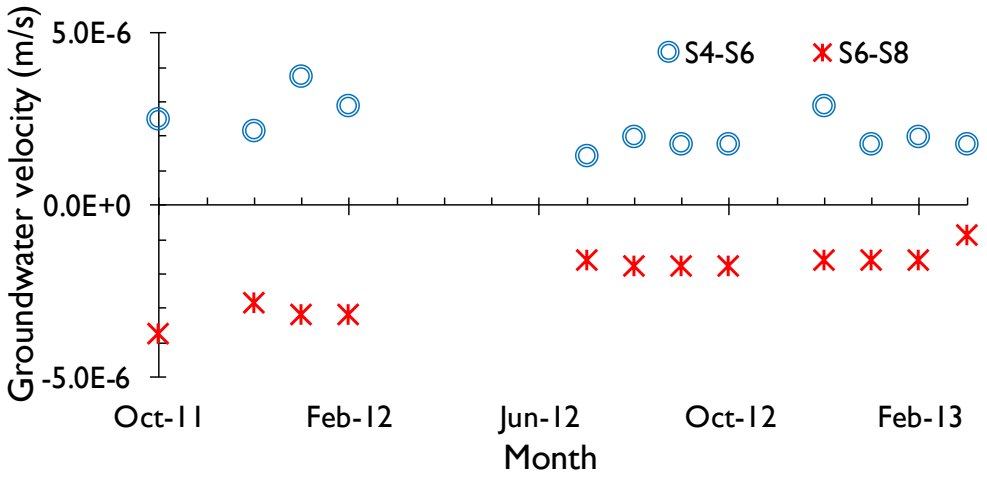

Figure 4.14 Setting of groundwater velocity for reaches S4 to S6 and S6 to S8 for each individual period (positive/negative values denote to groundwater recharge/outflow conditions).

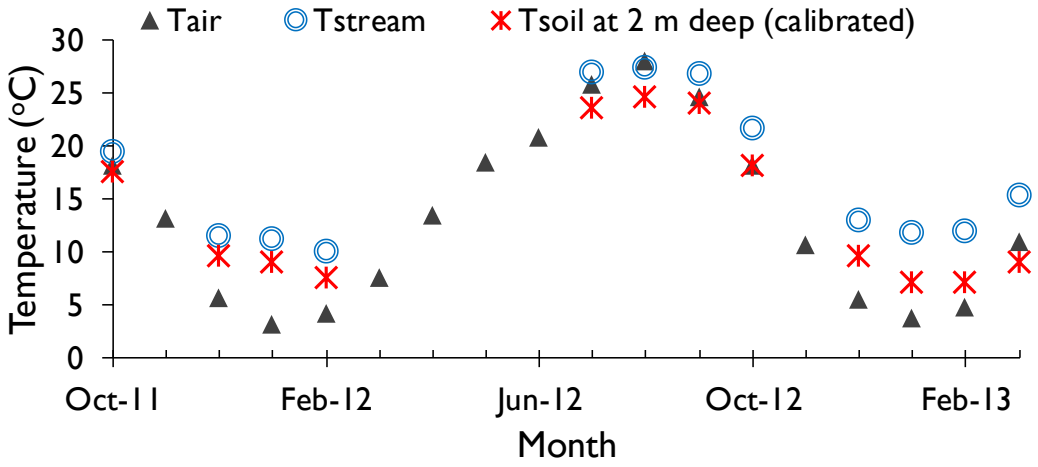

Figure 4.15 Setting of sediment temperature at 2-m deep after calibration for each individual period. The averages of air and stream temperatures were plotted as reference.

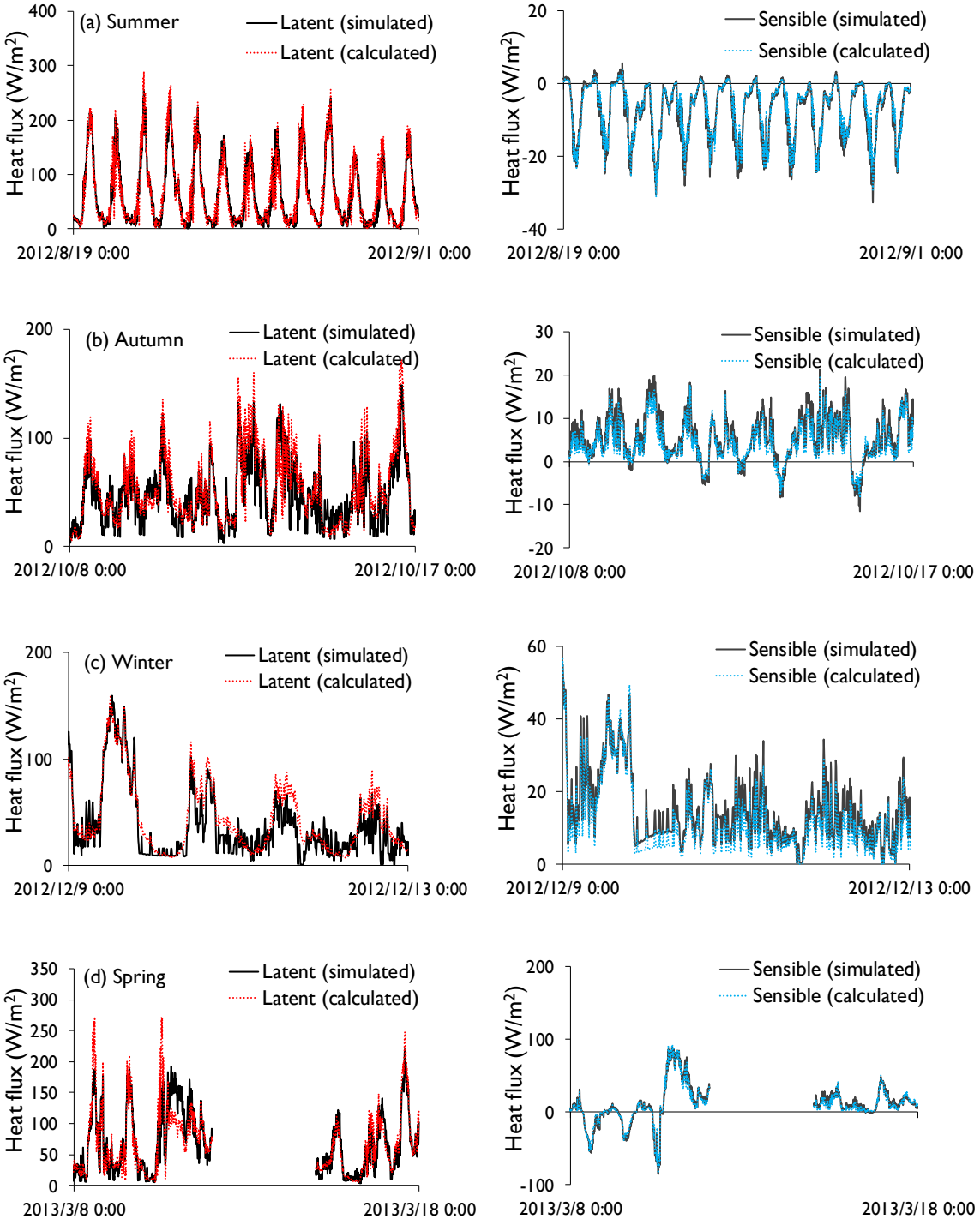

Figure 4.16 Comparisons between latent and sensible heat fluxes simulated by the model and those calculated based on measurements. Four periods in (a) summer, (b) autumn, (c) winter and (d) spring (gaps from 2013/3/12 to 2013/3/14 were due to rainfall events) seasons were illustrated.

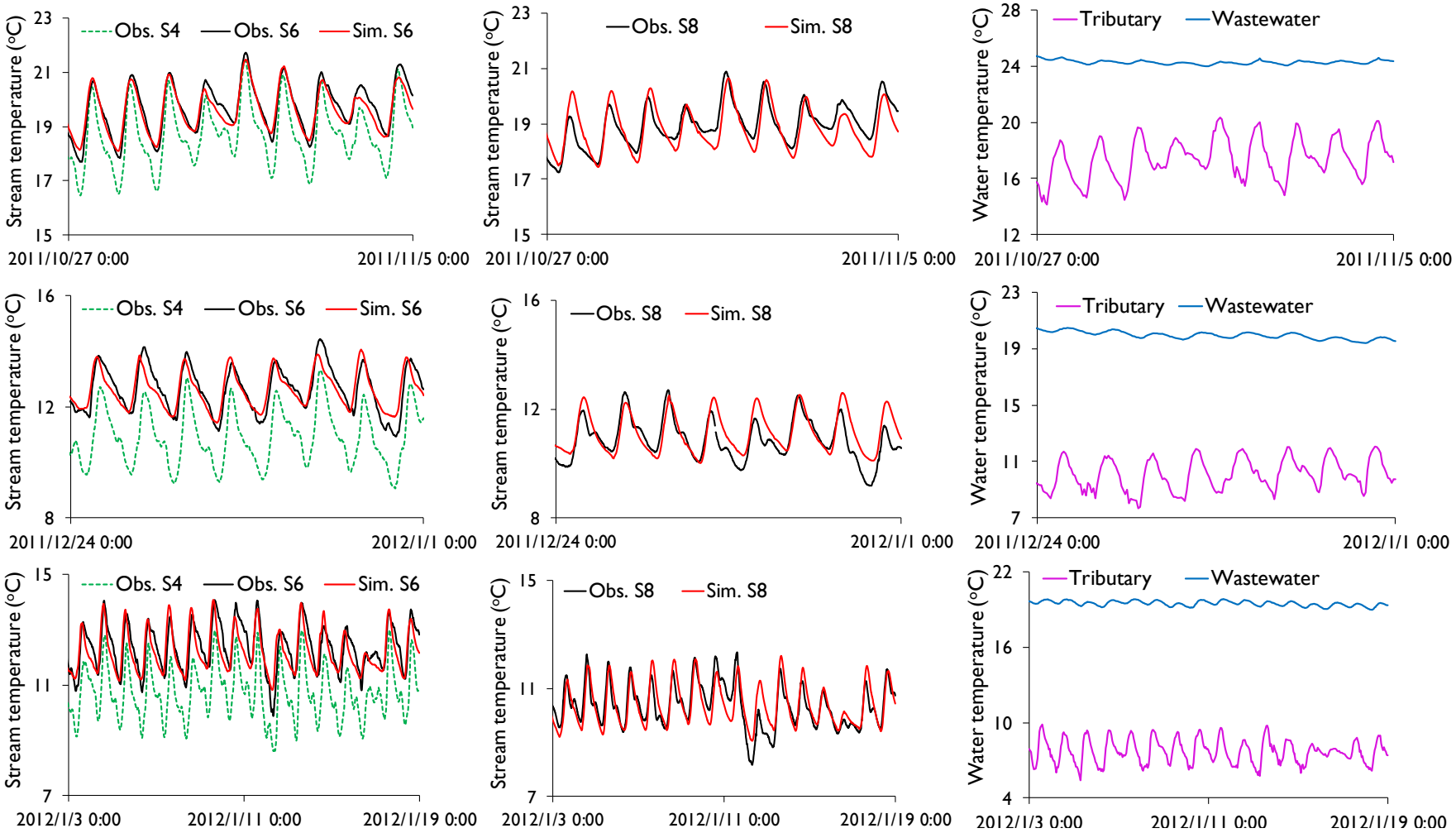

Figure 4.17 Comparisons between simulated stream temperatures and those measured at S6 and S8 for selected periods (see Table 4.2 for the corresponding RMSE for each figure). The average temperatures of tributaries from Tri.1 to Tri.4 (estimated) and those of wastewater from W4 to W7 (measured) were shown in the right column as reference.

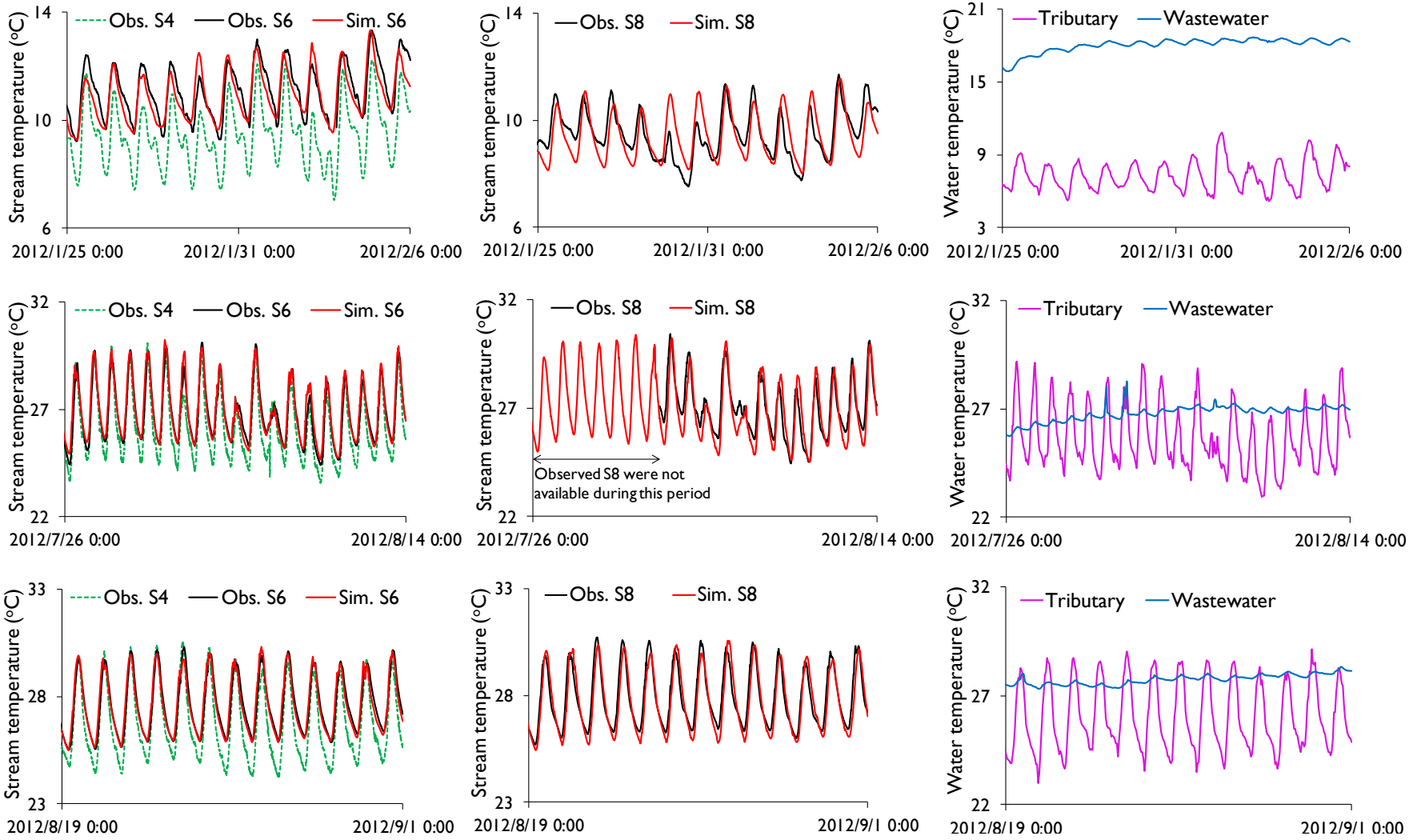

Figure 4.17 (Continued)

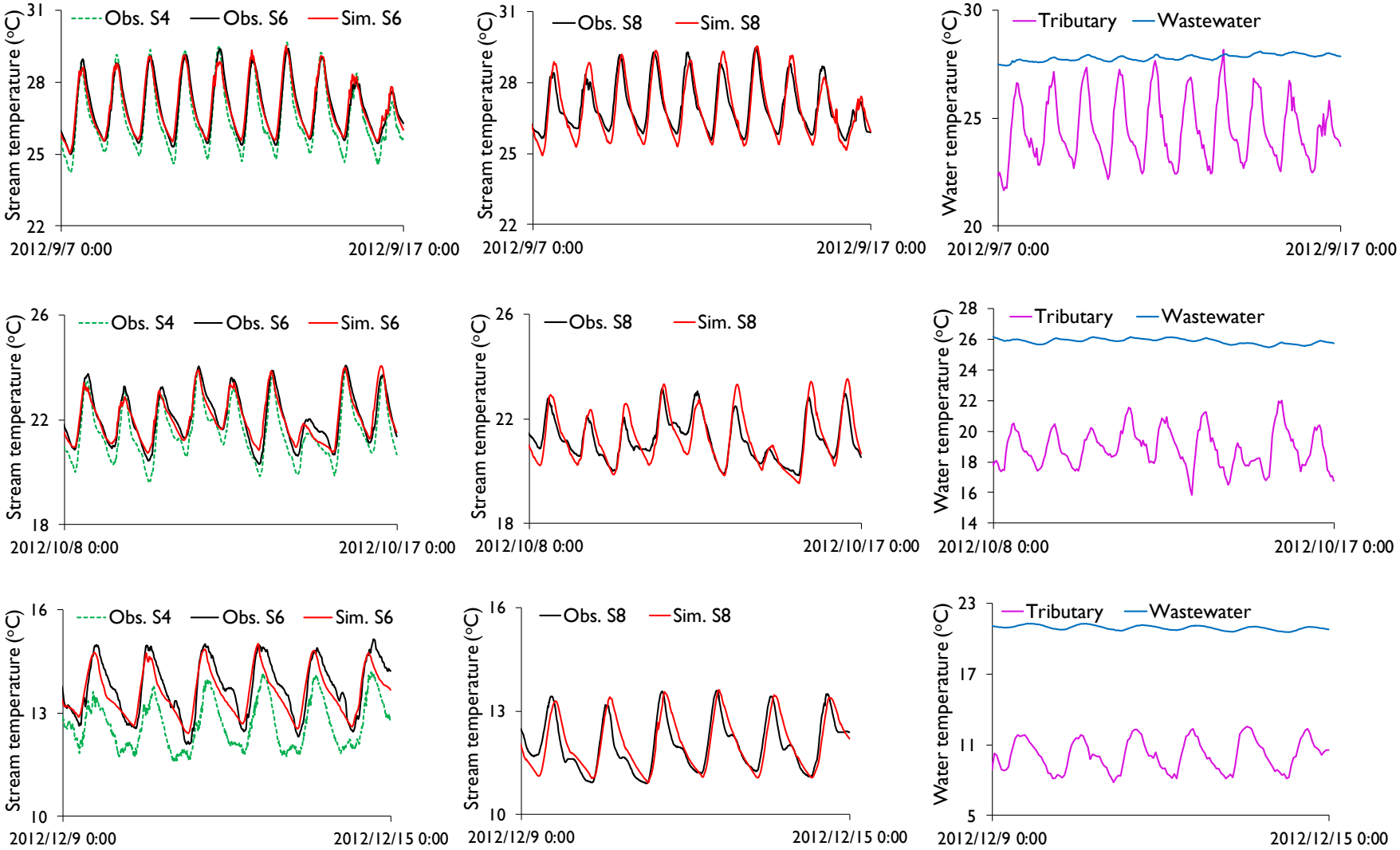

Figure 4.17 (Continued)

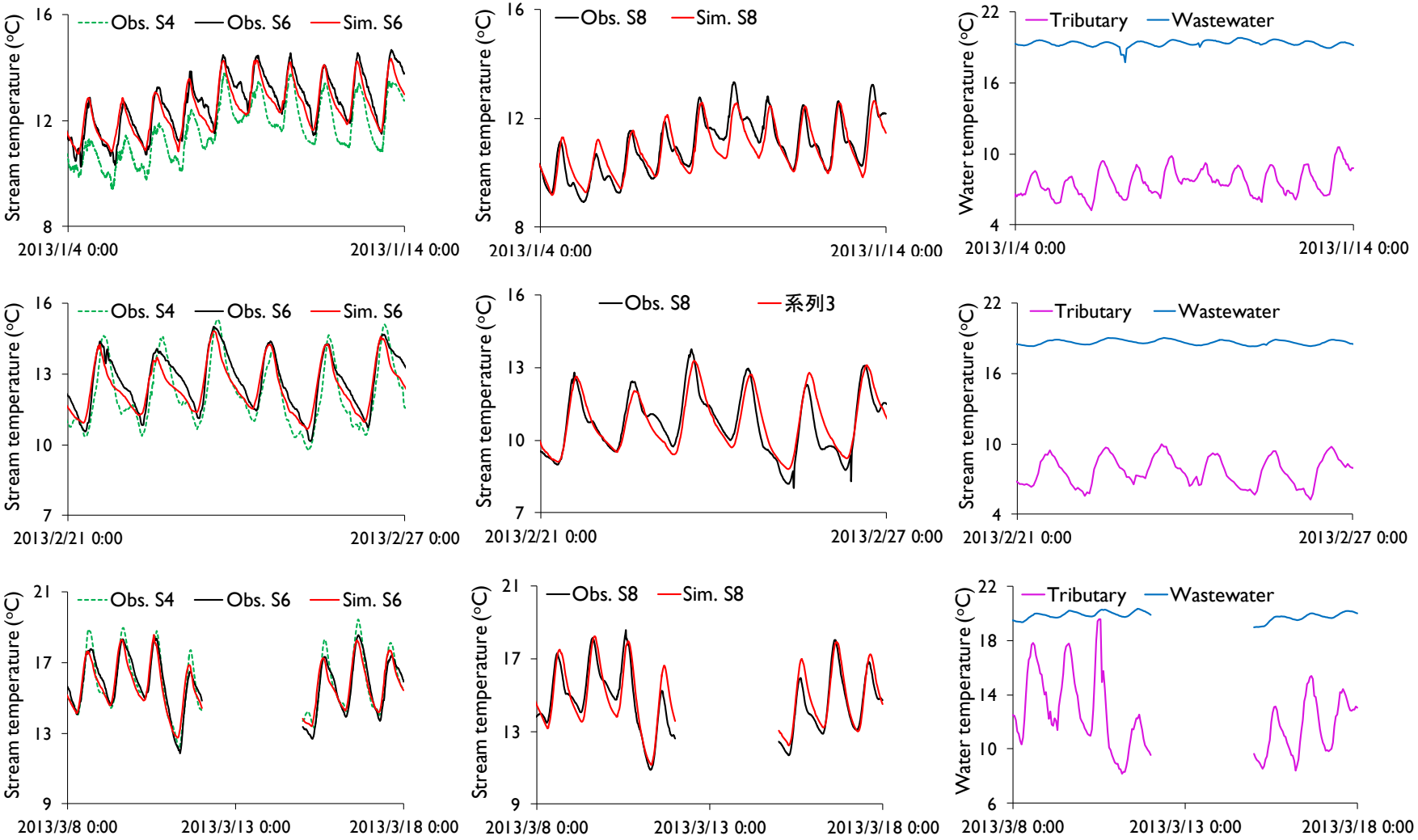

Figure 4.17 (Continued, gaps from 2013/3/12 to 2013/3/14 were due to rainfall events).

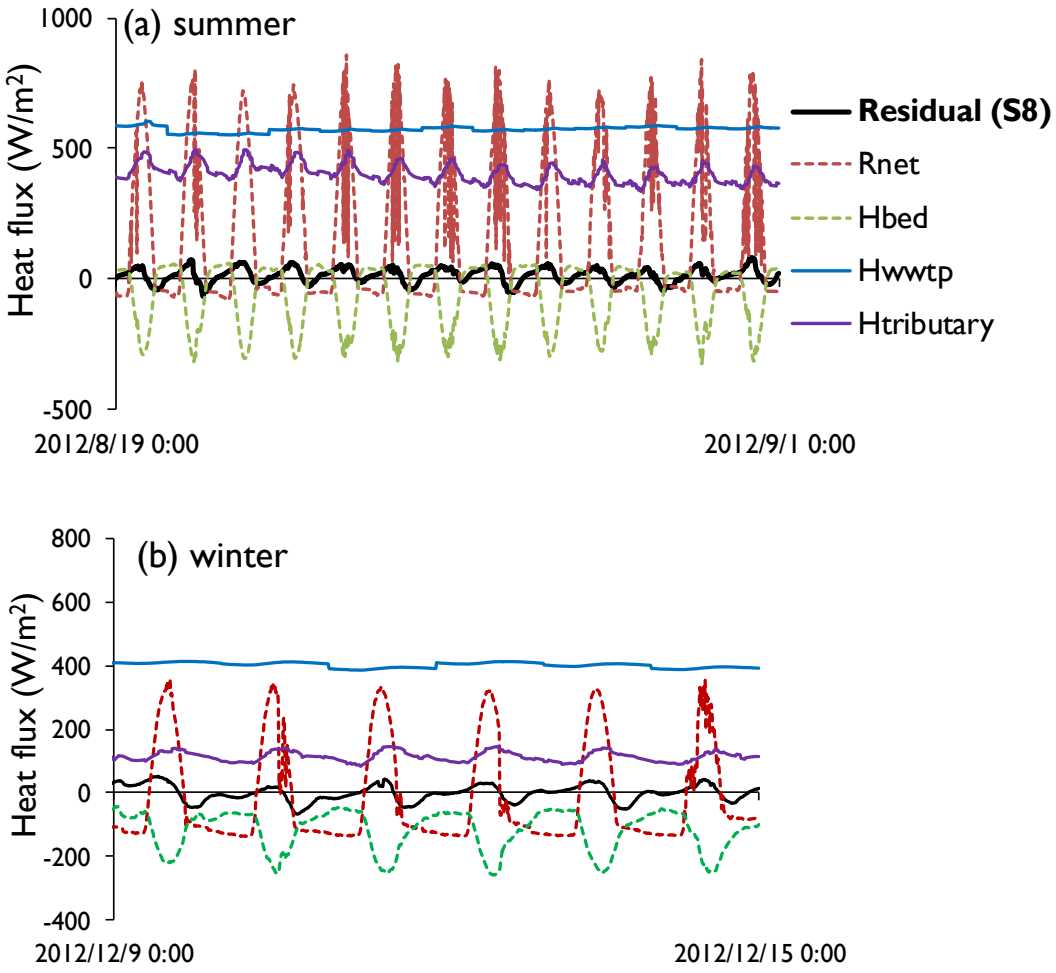

Figure 4.18 Residual heat flux at S8 compared with other heat components averaged over the reach S4-8 in (a) summer and (b) winter seasons.

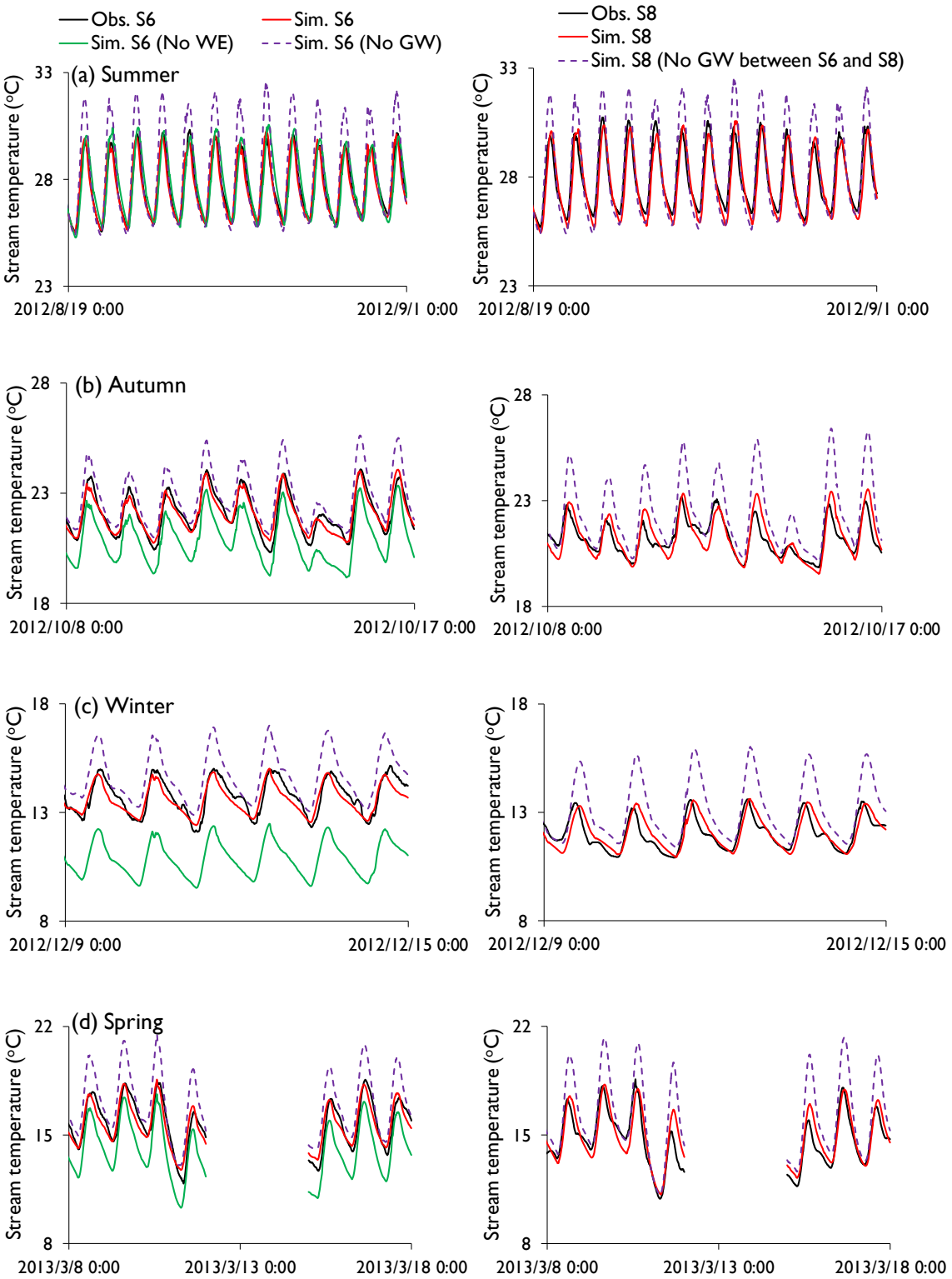

Figure 4.19 Simulated stream temperatures at S6 by eliminating wastewater effluents (WE), and those at S6 and S8 by eliminating groundwater (GW) flows. Four periods in (a) summer, (b) autumn, (c) winter and (d) spring were illustrated.

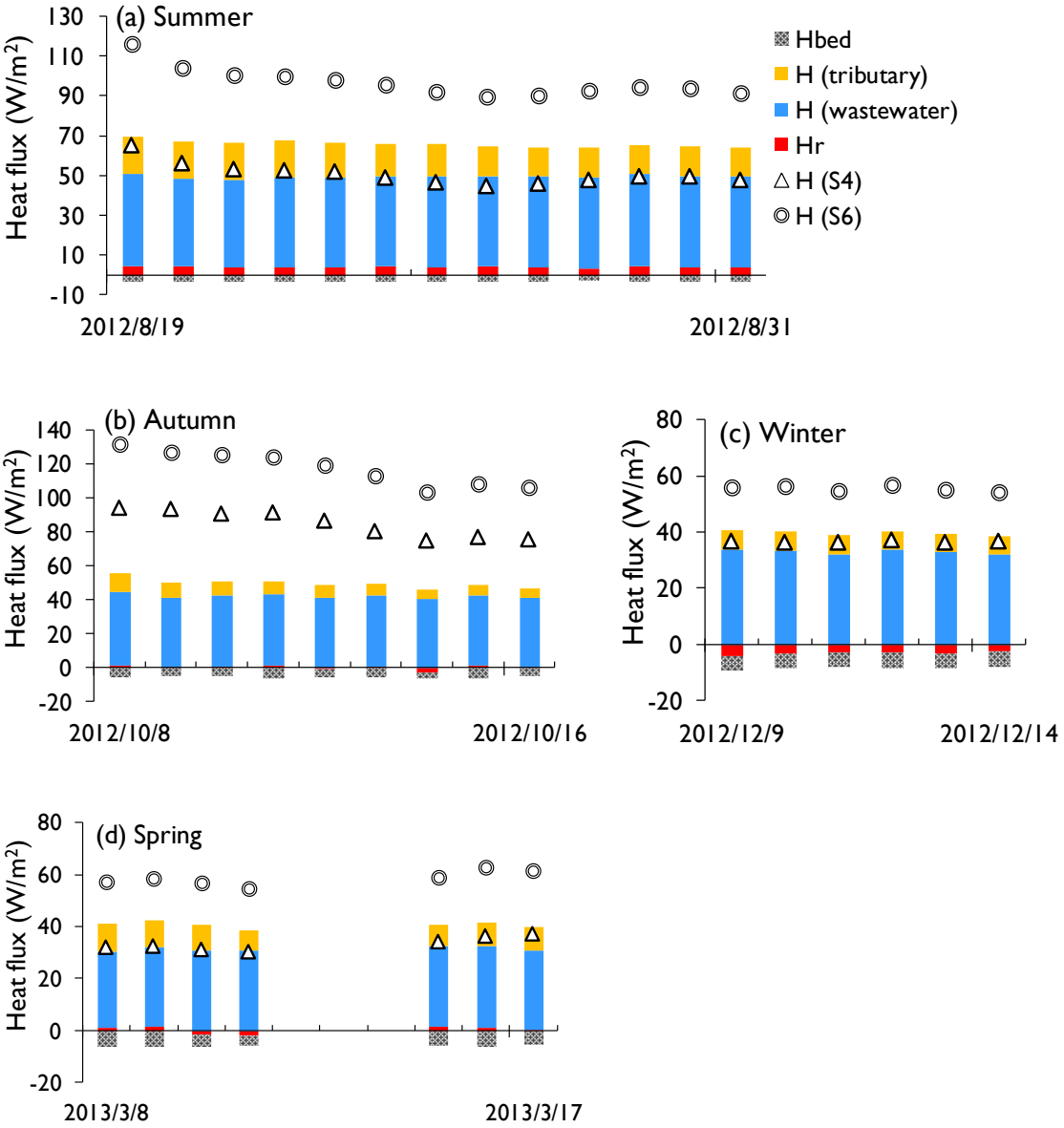

Figure 4.20 Daily total heat budgets (over S4 to S6) integrated from model results for four periods in (a) summer, (b) autumn, (c) winter and (d) spring, respectively. In each figure, H (S6) is the outflowing heat at S6, H (S4) is the inflowing heat at S4, H (tributary) is the heat inputs by tributaries, H (wastewater) is the total heat inputs by wastewater from WWTPs, Hbed is heat exchange at the streambed-water interface through convection, and Hr is heat exchange at the air-water interface.

References

Benyahya, 1., Caissie, D., EI-Jabi, N., Satish, M.G., 2010. Comparison of microclimate vs. remote meteorological data and results applied to a water temperature model (Miramichi River, Canada). Journal of Hydrology, 380, 247-259.

Brosofske, K.D., Chen, J., Naiman, R.J., Franklin, J.F., 1997. Harvesting effects on microclimatic gradients from small streams to uplands in western Washington. Ecological Applications, 7, 1188-1200.

Caissie, D., 2006. The thermal regime of rivers: a review. Freshwater Biology, 51, 1389-1406.

Caissie, D., Giberson, D.J., 2003. Temporal variation of stream and intragravel water temperatures in an Atlantic salmon (Salmo salar) spawning area in Catamaran Brook (New Brunswick). Canadian Technical Report of Fisheries and Aquatic Sciences 2464, 26p.

Clark, E., Webb, B.W., Ladle, M., 1999. Microthermal gradients and ecological implications in Dorset rivers. Hydrological Processes, 13, 423-438.

Chen, J., Saunders, S.C., Crow, T.R., Naiman, R.J., Brosofske, K.D., Mroz, G.D., Brookshire, B.L., Franklin, J.F., 1999. Microclimate in forest ecosystem and landscape ecology. Bioscience, 49, 288-297.

Kinouchi, T., 2007. Impact of long-term water and energy consumption in Tokyo on wastewater effluent: implications for the thermal degradation of urban streams. Hydrological Processes, 21, 1207-1216.

Mitchell, K.C., James, L.G., Elger, S., Pitts, M., 1990. Characterizing cyclic water-level fluctuations in irrigation canals. Journal of Irrigation and Drainage Engineering, 116, 261-272.

Prats, J., Val, R., Armengol, J., Dolz, J., 2007. A methodological approach to the reconstruction of the 1949-2000 water temperature series in the Ebro River at Escatrón. Limnetica, 26, 293-306.

Webb, B.W., Nobilis, F.,1997. Long-term perspective on the nature of the air-water temperature relationship: a case study. Hydrological Processes, 11, 137-147.

Chapter 5
Conclusions and Further Study

5.1 Conclusions of this study

In general, water temperature of streams and rivers is arguably one of the most important parameters that determine many aquatic habitat attributes and the general health of river ecosystems. Changes in temperature can influence the distribution, growth rate, production, habitat use and community dynamics of aquatic organisms. For stream that runs through highly urbanized area, water temperature can be affected by heat exchanges with atmosphere and with riverbed sediment as well as heat advections from tributary inflows, groundwater recharges/outflows and anthropogenic withdrawals/discharges. Therefore, it is essential to have a good understanding of river thermal processes for effective river management and aquatic resources conversation.

This study integrated data analysis, field measurement and modeling approach, and had a goal to provide insights of how human activities alter the stream temperature and heat budget of an urban river.

Chapter 2 revealed the long-term (from 1990 to 2013) and longitudinal (more than 50 km) variations of stream temperature in the mainstream of the Tama River. To identify the major factors that influenced these changes, the flow rate changes, the temperature and volume of wastewater effluents from WWTPs, as well as the relationships between air and stream temperatures were analyzed. Our analysis detected long-term stream temperature increases in the winter season at sites affected by intensive and warm effluents from WWTPs. In the summer season, a larger stream temperature increase was identified in the upstream reaches, which was attributable to the decreased flow rate due to water withdrawal. The relationship between air and stream temperatures indicated that stream temperatures at the upstream site (until S3) were likely to be affected by a dam release, while temperatures in the downstream reaches have deviated more from air temperatures in recent years, probably due to the increased impacts of effluents from WWTPs. Results of the water and heat budget analyses indicated that the largest contributions to water and heat gains were attributable to wastewater effluents, while other factors such as groundwater recharge and water withdrawal were found to behave as energy sinks, especially in summer. The inflow from tributaries worked to reduce the impacts of dam

release and the heat exchanges at the air–water interface contributed less to heat budgets in both winter and summer seasons for all river segments.

Chapter 3 conducted the present-day study on water temperature regime with the historical analysis as a reference condition. The accuracy and reliability of the historical results can be verified using the data collected from the intensive field measurements in both summer and winter seasons. Further, to predict river water temperatures and quantify heat fluxes, we developed a 1D deterministic model for simulating river flow and heat transports considering all processes significant in predicting stream temperature variations (e.g. lateral inflows/inflowing heat by tributary, wastewater and groundwater and water-streambed heat exchanges). This model was applied to the middle to downstream reach of the Tama River with data collected during intensive measurements. Major parameters relating to the river flow and heat transports in the mainstream and the sediment were calibrated. Moreover, sensitivity analysis was carried out to testify the sensitivity of simulation result to several input data and parameters, which has provided a reference base for the further parameterization in modeling stream temperature.

Chapter 4 dealt with the modeling of stream temperature for all seasons throughout a 2-year course by applying the model introduced in Chapter 3. Observed data on weather conditions, hydrodynamic variables and stream temperatures were used to run and to verify the model. In general, the agreements between the observed and simulated stream temperatures at two downstream sites were satisfactory. Further, this model was applied to assess the impacts of wastewater discharge and surface-groundwater interactions on stream temperature. Results suggested that the presence of wastewater helped to reduce the daily maximum temperatures in summer season; whereas in winter it enhanced the stream temperatures a lot. On the other hand, by assuming no groundwater flows, stream temperature would increase in all seasons. Heat budget analysis indicated that the heat from wastewater was the major contributor to heat gains in all periods; while heat interacted with sediment was found to act as energy sinks throughout the year. Finally, the findings of stream temperature change in response to changes in controlling factors in different seasons can to some extent provide biological implications for the river water management as well as for better conservation of aquatic species.

5.2 Implications for other urban river study

Although the discussion and analysis in this thesis concentrate on the Tama River in Japan, the ideas, methods and findings are also applicable to other rivers that have similar

characteristics to the Tama River in general. Basically, there are two main features of the Tama River. Firstly, it is an alluvial river that characterized by considerable surface-ground water exchange; therefore the temperature regime in the mainstream is greatly influenced by this process. Secondly, its middle to downstream reach runs through highly urbanized areas where thus suffered from considerable anthropogenic impacts, i.e. wastewater effluents from wastewater treatment plants.

Our findings can provide implications for new studies on other urban rivers over the world. For example, for an urban river that receives wastewater effluents, the stream temperature can be elevated by this process during the colder seasons whereas the extreme temperatures can be suppressed during the hot summer season. For rivers with alluvial sediments, it should be noted that the interaction between surface and groundwater can be a very important process that influence the thermal regime of surface water.

However, regarding a new study reach, the major factors being concerned will be different according to the characteristics of rivers. For example, for those with hard-rock riverbed, the groundwater is very hard to interact with the stream water; as a result this process can be ignored. For rivers that are affected by other human structures, e.g. water intake, nuclear power plants, these processes should be newly considered.

5.3 Suggestions for further study

Although this study combined the historical and present-day analysis on the temperature regime and heat transports of an urban river, and provided implications for ecological protection, there are three main aspects that could be improved in the further study.

Firstly, for modeling stream temperature, the hydro-thermal conditions in riverbed sediment (e.g. groundwater flux and sediment boundary temperature at 2 m deep) were currently regarded as constant over space during each simulation period. As such, the spatial variability (e.g. every 100 m in space) of these parameters can be considered to make better simulation of stream temperature in this study reach in further details. In addition, further measurements or verifications of the hydro-thermal conditions will be appreciated.

Secondly, the combination of river heat transport model with the hydrological model is strongly required in order to understand the instantaneous watershed-scale water and heat transport processes as well as its resulting effects on stream environment. In this case, the long-term impacts on water and heat transport processes may be able to be assessed under the projected future climate scenarios.

Thirdly, for better river ecological conservation, it is necessary to quantify the impacts of water environment change on biological behaviors using some index and criteria.